





University of Alberta  
Library  
Edmonton, Alberta  
T6G 2G1  
Canada



Digitized by the Internet Archive  
in 2019 with funding from  
University of Alberta Libraries

<https://archive.org/details/Butchart1965>











5716315  
1965  
#7

THE UNIVERSITY OF ALBERTA

TEST OF FOUR CONTINUOUS TWO-SPAN PRESTRESSED CONCRETE BEAMS

by

HAROLD TREMAYNE BUTCHART

A THESIS

SUBMITTED TO THE FACULTY OF GRADUATE STUDIES

IN PARTIAL FULFILMENT OF THE REQUIREMENTS FOR THE DEGREE

of

MASTER OF SCIENCE

DEPARTMENT OF CIVIL ENGINEERING

EDMONTON, ALBERTA

MAY, 1965

THE UNIVERSITY OF CHICAGO

THE CHICAGO SCHOOL OF THEOLOGY

CHICAGO, ILL.

1900

THE CHICAGO SCHOOL OF THEOLOGY  
CHICAGO, ILL.

1900

CHICAGO, ILL.

CHICAGO, ILL.

1900



UNIVERSITY OF ALBERTA  
FACULTY OF GRADUATE STUDIES

The undersigned certify that they have read, and recommend to the Faculty of Graduate Studies for acceptance, a thesis entitled TEST OF FOUR CONTINUOUS TWO-SPAN PRESTRESSED CONCRETE BEAMS submitted by Harold Tremayne Butchart in partial fulfilment of the requirements for the degree of Master of Science.





## ABSTRACT

The purpose of this investigation was to devise and execute methods for construction and testing continuous prestressed concrete beams.

Results are reported for load tests of two post-tensioned, and two pretensioned 6" x 12" prestressed concrete I-beams spanning continuously over two ten-foot spans. These beams were as similar to each other as was practical. The reinforcement percentage was .382% and the tendons were prestressed to 125 k.s.i. The loading consisted of a concentrated load applied at the centre of both spans. Midspan deflections, concrete strains, reactions, and horizontal movement of the end supports, were measured.

The measured deflections were generally found to be higher than predicted by calculation before flexural cracking, and lower thereafter. Failure of all beams occurred after yielding of the steel and full moment redistribution, and was mainly due to excessive flexural stresses.





## ACKNOWLEDGEMENTS

The successful completion of this investigation was made possible by the cooperation of many individuals. To all those who in any manner aided in the work, the author expresses his sincere thanks.

The author is especially grateful to Professor J. Longworth for his supervision and assistance in the investigation, and for his patience and constructive criticisms during the preparation of this thesis.

Thanks go to R. Brown and other members of the shop staff for their cooperation.

For typing, proofreading of the manuscript, and understanding, the author wishes to thank his wife, Gloria.



## TABLE OF CONTENTS

	Page
Title Page .....	i
Approval Sheet .....	ii
Abstract .....	iii
Acknowledgements .....	iv
Table of Contents .....	v
List of Tables .....	viii
List of Figures .....	ix
List of Symbols .....	xii
CHAPTER I INTRODUCTION	
1.1 General Remarks .....	1
1.2 Previous Investigations .....	1
1.3 Scope of Investigation .....	4
CHAPTER II STRENGTH AND DEFORMATION CHARACTERISTICS OF TWO-SPAN CONTINUOUS BEAMS	
2.1 Flexural Resistance at a Section .....	5
2.2 Inclined Cracking Resistance at a Section ...	6
2.3 Flexural-shear Resistance at a Section .....	7
2.4 Curvatures and Deflections .....	10
CHAPTER III TEST SPECIMENS	
3.1 General Description .....	15
3.2 Prestressing Steel Stresses .....	16
3.3 Prestressing Concrete Stresses .....	16





## TABLE OF CONTENTS (continued)

	Page
CHAPTER IV	INSTRUMENTATION AND LOADING EQUIPMENT
4.1	Deflection Measurements ..... 26
4.2	Concrete Strain Measurements ..... 26
4.3	Reaction Measurements ..... 27
4.4	Loading System ..... 28
CHAPTER V	EXPERIMENTAL PROCEDURE
5.1	Pre-test Preparation ..... 31
5.2	Test Procedure ..... 31
CHAPTER VI	MATERIAL PROPERTIES
6.1	Concrete and Grout ..... 33
6.2	Steel Reinforcement ..... 34
CHAPTER VII	TEST RESULTS
7.1	Deflections and Movements ..... 41
7.2	Reaction Measurements ..... 41
7.3	Strain Measurements ..... 42
7.4	Photographs ..... 42
CHAPTER VIII	DISCUSSION
8.1	Material Properties ..... 73
8.2	Predicted Behavior of the test Beams ..... 75
8.3	Evaluation of Test Results ..... 77
8.4	Suggestions for Future Investigations ..... 83
CHAPTER IX	CONCLUSIONS ..... 86





## TABLE OF CONTENTS (continued)

	Page
List of References .....	87
Appendix A Procedure for Construction of Beams .....	A1
Appendix B Casting Form .....	B1
Appendix C Loading Beam .....	C1
Appendix D Load Cells .....	D1
Appendix E Prestressing and Loading Jacks .....	E1
Appendix F Calculation of Prestress Loss in the Steel .....	F1
Appendix G Calculations for Predicting the Behavior of the Test Beams .....	G1



## LIST OF TABLES

Table		Page
III-1	Estimated Steel Stresses .....	18
III-2	Sectional and Material Properties .....	19
VI-1	Concrete and Grout Test Results .....	35
VIII-1	Significant Observed Loads and Deflections .....	85
E-4	Calibration of Load Jacks .....	E5





## LIST OF FIGURES

Figure		Page
2.1	Stress and Strain Distribution on a Beam Section at Ultimate Flexural Moment .....	11
2.2	Free Body Diagrams for a Section With an Inclined Crack .....	12
2.3	Curvature Distribution .....	13
2.4	Idealized Increase in Strain Relationship .....	14
3.1	Details of the Pretensioned Beams .....	20
3.2	Details of the Post-tensioned Beams .....	22
3.3	Design Diagrams of Beams .....	24
3.4	Initial Bending Moments .....	25
4.1	Instrumentation .....	29
4.2	Gage Plug Locations .....	30
6.1	Stress Versus Strain Graphs for Concrete .....	36
6.2	Stress Versus Strain for Prestressing Wires .....	40
7.1	Applied Load Versus Vertical Deflection at Midspans .....	43
7.2	Applied Load Versus Average Vertical Deflection at Midspan .....	47
7.3	Applied Load Versus Average Support Movement .....	48
7.4	Applied Load Versus One-half the Difference in Horizontal Movement of Supports .....	49
7.5	Applied Load Versus End Support Reactions .....	50
7.6	Applied Load Versus Centre Support Reaction .....	52
7.7	Applied Load Versus Vertical Support Ratio .....	54



## LIST OF FIGURES (continued)

Figure		Page
7.8	Applied Load Versus Concrete Strains at Midspans ...	55
7.9	Applied Load Versus Concrete Strains at Centre Support .....	59
7.10	Applied Load Versus Curvature at Midspans .....	61
7.11	Applied Load Versus Average Curvature at Midspans ..	63
7.12	Applied Load Versus Curvature at Centre Support ....	64
7.13	Applied Load Versus Difference in Strains .....	65
7.14	Photographs of Beams After Failure at Midspans and Centre Support .....	67
7.15	Photographs of Beams After Failure .....	71
A-1	Form Assembly for Pretensioned Beam .....	A4
A-2	Photographs of Casting Form Assembled for Pretensioned Beam .....	A5
A-3	Assembly of Casting Form for a Post-tensioned Beam .	A6
A-4	Photographs of Casting Form for a Post-tensioned Beam .....	A7
A-5	Photograph Showing Grouting of a Post-tensioned Beam .....	A8
B-1	Casting Form Pieces .....	B2
B-2	Casting Form Pieces for the Pretensioned Beam .....	B3
B-3	Casting Form Pieces for the Post-tensioned Beam ....	B4
C-1	Loading Beam Details .....	C2
C-2	Loading Beam Details .....	C3
D-1	Load Cell .....	D2





## LIST OF FIGURES (continued)

Figure		Page
D-2	Calibration Graph of Load Cells .....	D3
E-1	Prestressing Jack Attachments .....	E2
E-2	Calibration of Prestressing Jacks .....	E3
E-3	Loading Jack Attachment .....	E4
G-1	Idealized Stress Distribution for Concrete .....	G13
G-2	Calculated Bending Moment Diagrams at Various Stages of Loading .....	G14
G-3	Bending Moment and Shear Force Diagrams .....	G15
G-4	Calculated Strain Relationships .....	G16
G-5	Calculated Moment-Maximum Curvature Relationships .	G17
G-6	Calculated Curvature Distribution at Various Stages of Loading .....	G18
G-7	Calculated Load-deflection Relationship .....	G19



## LIST OF SYMBOLS

### CROSS-SECTIONAL CONSTANTS

- $A$  = total cross-sectional area of beam
- $A_s$  = total area of prestressed reinforcement
- $A_c$  = total area of concrete in compression
- $A_v$  = total cross-sectional area of one stirrup
- $a$  = length of shear span
- $b$  = width of rectangular beam or width of flange for flanged beam
- $b'$  = thickness of web for flanged beam
- $d$  = effective depth of the prestressed reinforcement
- $e$  = distance from the centroidal axis to the line of action of the total prestressing force
- $h$  = overall depth of the beam
- $I$  = moment of inertia of gross concrete section about the centroidal axis
- $Q$  = first moment of area above a horizontal section about the centroidal axis
- $x_h$  = horizontal projection of the inclined crack
- $y_b$  = distance from centroidal axis to the extreme fiber in tension
- $y_s$  = distance from centroidal axis to the centroid of steel
- $Z$  =  $I/y_b$  = section modulus

### LOADS

- $C$  = total compressive force in the concrete
- $C_1$  = total compressive force in the concrete above an inclined crack



- $C_2$  = total compressive force in the concrete below an inclined crack  
 $F_{se}$  = total prestressing force  
 $M$  = moment at any stage of loading  
 $M_{cr}$  = resisting moment at flexural cracking  
 $M_v$  = moment of the web reinforcement about the maximum moment section  
 $P$  = concentrated load applied at one midspan of the test beams  
 $P_d$  = self weight of test beams assumed to act as a concentrated load of 0.3 kips at each midspan  
 $P_t = P_d + P$   
 $T$  = total tensile force  
 $V$  = shear at any stage of loading  
 $V_c$  = computed inclined cracking shear  
 $V_f$  = computed initiating flexural cracking shear  
 $V_s$  = computed shear corresponding to web-shear cracking  
 $V_z$  = dowelling force  
 $V_1$  = shear carried by the concrete above an inclined crack at the maximum moment section  
 $V_2$  = shear carried by the concrete below an inclined crack at the maximum moment section  
 $V_3$  = vertical shearing force over section between the apex of the inclined crack and the maximum moment section  
 $H$  = horizontal shearing force over section between the apex of the inclined crack and the maximum moment section

## STRESSES

### Concrete

- $f_c$  = compressive stress at any stage of loading  
 $f'_c$  = compressive strength determined by 6" x 12" control cylinders





$f_{ca}$  = effective strength of the concrete in the compression zone of a beam at any stage of loading

$f_{cu}$  = effective strength of the concrete in the compression zone of a beam at ultimate

$f_r$  = modulus of rupture determined from 6 x 6 x 24 inch control beams loaded at the third points over an 18 inch span

$f_t$  = tensile strength of the concrete

$v$  = shear stress

$E_c$  = assumed modulus of elasticity of concrete

#### Reinforcement

$f_{se}$  = effective prestress

$f_{su}$  = stress in the prestressing reinforcement at failure

$E_s$  = modulus of elasticity of the reinforcement

### STRAINS

#### Concrete

$\epsilon_u$  = useful limit of strain in the compressed concrete

$\epsilon_c$  = concrete compressive strain

$\epsilon_{ca}$  = increase in the concrete strain in the compression fiber above that at transfer

$\epsilon_{ce}$  = strain at the level of the reinforcement due to effective prestress

$\epsilon_o$  = strain dividing the elastic and plastic ranges of idealized stress-strain curve for concrete

#### Reinforcement

$\epsilon_s$  = reinforcement strain

$\epsilon_{se}$  = effective prestrain corresponding to effective prestress

$\epsilon_{su}$  = strain the prestressing reinforcement at failure

$\epsilon_{sa}$  = increase in strain in the prestressing reinforcement beyond the strain at effective prestress



$\epsilon'_{sa}$  = increase in strain in the prestressing reinforcement beyond the strain at effective prestress neglecting the effects of  $\epsilon_{ce}$

### DIMENSIONLESS FACTORS

F = strain compatibility factor

k = ratio of neutral axis depth to effective depth

$k_u$  = ratio of neutral axis depth at failure to effective depth

$k_2$  = ratio of the depth of the compressive force to depth of the neutral axis

$k_3$  = factor relating the maximum stress in the beam to the 6 x 12 inch cylinder strength

p =  $A_s/bd$  = longitudinal reinforcement ratio

$m_1$  = ratio of length of internal lever arm to center of compression force above the inclined crack to the effective depth

$m_2$  = ratio of length of internal lever arm to center of compression force below the inclined crack to the effective depth

$m_3$  = ratio of length of internal lever arm to horizontal shear stress force along the section between the apex of the inclined crack and the maximum moment section to the effective depth

### MISCELLANEOUS

$\beta$  = angle of inclination of draped longitudinal reinforcement

$\phi_{cr}$  = curvature at flexural cracking

$\phi_u$  =  $\epsilon_u/k_u d$  = curvature at failure of the beam

$x_3$  = distance from maximum moment section to the line of action of the vertical shearing force over the section between the apex of the inclined crack and the maximum moment section

PE-1 and PE-2 - designations for the pretensioned beams

PO-1 and PO-2 - designations for the post-tensioned beams





## CHAPTER I

### INTRODUCTION

#### 1.1 GENERAL REMARKS

Prestressing of concrete structural members is a relatively new method of construction in the building industry of this province. To the author's knowledge the first prestressed structure in Alberta, a 60 foot span highway bridge crossing Ross Creek near Medicine Hat, was constructed in 1954. Since that time the prestressing industry has expanded so that at present precast beams, slabs, and bridge girders, compete vigorously with older methods of construction. However these members are generally statically determinate. The only major continuous prestressed structure built to date in Alberta is the Allowance Avenue railroad overpass which was constructed in Medicine Hat in 1962.

In Europe, where the industry is much older, continuity is common in prestressed structures. Research into the basic principles involved in design for continuity has been published mainly during the past ten years.

#### 1.2 PREVIOUS INVESTIGATION

The following summaries are, where indicated, reported by Hawkins (1)<sup>\*</sup>. In many cases the original papers were not available to

---

\* Numbers in parentheses refer to reference listed on page 87.



the author, or were written in a language in which the author is not conversant. The summaries are presented in chronological order.

- (a) Tests of Four Two-span Continuous Beams by Y. Guyon (2)  
Hawkins (1)

The author concluded that all the beams failed in flexure after full moment redistribution had taken place. In his reanalysis (3) Guyon presents a failure theory for continuous structures which takes into account the full or partial redistribution of moments, and the effects of shear on the ultimate flexural strength.

- (b) Tests of the Three-span Beam by G. Magnel (4), Hawkins (1)

The author concluded that moment redistribution followed immediately after flexural cracking under the load points.

- (c) Tests of Four Two-span Continuous Beams by T.Y. Lin (5)  
Hawkins (1)  
(The test is summarized and discussed by Guyon (2) in 1960)

The author concluded that full moment redistribution did not occur and that the degree of distribution depended on the type of failure.

- (d) Tests on Twenty-eight Two-span Continuous Beams by  
P.B. Morice and H.E. Lewis (6), Hawkins (1)

The main variable introduced into the investigation was the linear transformation of the profile of the prestressing tendon, up or down, from its concordant position. In all beams (except one) it was concluded that the ultimate load was unchanged due to the tendon transformations and that full moment redistribution had taken place whether one or both spans were loaded.



- (e) Tests of Three-span Continuous Beams by G. Macchi (7),  
Hawkins (1)

The author concluded that partial redistribution occurred before flexural cracking, and that redistribution was not complete when the beam failure in flexure.

- (f) Tests on Four Two-span Continuous Beams at the Imperial College, London (1951) and Tests on Seven Two-span Continuous Beams at the University of Leeds, England (1954) (8)

Little information concerning the results of these tests is given. Morice indicated that further investigations were being carried out at the time at the Imperial College.

- (g) Tests of Twelve Two-span Continuous Beams by I. Zekaria (9)  
Hawkins (1)

Six beams failed in flexure after the formation of hinges while six beams failed in shear. One conclusion was that an increase in the bending moment decreased the shear capacity.

- (h) Tests by A.H. Mattock and Paul Kaar (10), Hawkins (1)

Fifteen I-beams with a composite cast-in-place deck slab were tested. The negative moment was resisted by placing mild steel bars in the cast-in-place deck slab. In all cases the mode of failure was due to excessive principal tensile stresses in the web of the beam.

- (i) Strength and Behavior of Two-span Continuous Prestressed Concrete Beams by N.M. Hawkins, M.A. Sozen and C.P. Siess (1)

This investigation included the testing of twenty-four 6 x 12 inch rectangular and I-beams, which spanned continuously over two nine foot spans. The modes of failure were reported as follows:





- 6 beams - flexure failure
- 11 beams - shear failure
- 5 beams - transitional failures (i.e. a combination  
of shear and flexure)
- 2 beams - bond failure

In this paper a theory was developed which predicts the ultimate load and deflection characteristics of continuous prestressed concrete beams. Portions of this theory, where applicable to the present investigations are summarized in the following chapter.

### 1.3 SCOPE OF INVESTIGATION

The investigation described in this thesis was intended to:

- (a) Devise a method of constructing pretensioned and post-tensioned concrete test beams at this University.
- (b) Devise methods for testing these beams.
- (c) Design and test two pretensioned and two post-tensioned concrete beams.
- (d) Review previous investigations concerning continuous prestressed concrete beams.

The major portion of the investigation consisted of load tests on the two pretensioned and the two post-tensioned beams. All four beams were 6" x 12" I-beams that spanned continuously over two ten foot spans and were loaded by equal concentrated loads at each midspan. The steel percentage at points of maximum moment was 0.382% and the percentage of web reinforcement was 0.262%. The only variable deliberately introduced into the investigation was the method of prestress.



## CHAPTER II

### STRENGTH AND DEFORMATION CHARACTERISTICS

#### OF TWO SPAN CONTINUOUS BEAMS

##### 2.1 FLEXURAL RESISTANCE AT A SECTION

Before flexural cracking, the stresses and rotations of any section may be assumed to follow the laws of the classical elastic theory. The moment which produces flexural cracking may be computed using the following expression:

$$M_{cr} = \frac{I}{y_b} \left( f_r + \frac{F_{se}}{A} + \frac{F_{se} e y_b}{I} \right) \quad \text{Eq. (1)}$$

where  $f_r$  is the modulus of rupture of concrete. After cracking, at a section, there is an immediate loss in stiffness, and the strains in the concrete and steel increase more rapidly.

At flexural failure (assuming that the mode of failure is crushing of the concrete) the distribution of the stresses and strains, on a section of a beam, are assumed to be as shown in FIGURE 2.1. Summation of forces and moments, and the strain compatibility will yield the following expressions:

$$k_u = \frac{p f_{su}}{f_{cu}} \quad \text{Eq. (2)}$$

and



$$\epsilon_{su} = \epsilon_{se} + \epsilon_{ce} + F\epsilon_u \frac{(1 - k_u)}{k_u} \quad \text{Eq. (3)}$$

In this discussion the terms  $k_2$  and  $f_{cu}$  relate to the shape and volume of the compressive stress block, in the concrete, at limiting strain  $\epsilon_u$ , in the extreme fibre.  $F$  is a factor which takes into account the bond slippage and lack of bond of the longitudinal steel. Reasonable values for all the terms except  $k_u$ ,  $f_{su}$ , and  $\epsilon_{su}$  are known or may be assumed. As the relationship between  $f_{su}$  and  $\epsilon_{su}$  is defined by the stress-strain relationship of the reinforcing steel, a simultaneous, trial and error solution of equations (2) and (3) may be made to determine  $f_{su}$ . A more thorough discussion of this method is found in Reference 12.

## 2.2 INCLINED CRACKING RESISTANCE AT A SECTION

Inclined cracking falls into two main categories, termed by McGregor (11), (a) web-shear cracks, and (b) flexure-shear cracks. Web-shear cracks develop in the web of a beam, and are caused by excessive principal tension stresses due to the flexural and shear stresses at the section. If the principal stresses are calculated at the elastic centroid of the beam, the following expression is derived:

$$V_s = \frac{Ib'}{Q} f_t \sqrt{\left(1 + \frac{F_{se}}{A f_t}\right)} + A_{sd} f_{se} \sin \beta \quad \text{Eq. (4)}$$

Flexure-shear cracks may originate in the web of the beam because of, or may continue from, an initiating flexural crack. McGregor (11) suggests that the initiating flexural crack will occur a distance  $d$  from the point of maximum moment. The appearance of this crack may be predicted by the expression:





$$V_f = \frac{z}{a-d} \left( f_r + \frac{F_{se}}{A} + \frac{F_{se} e y_b}{I} \right) \quad \text{Eq. (5)}$$

where  $a$  = distance from the point of zero bending moment to the maximum moment section, and  
 $e$  = eccentricity of centroid of steel at distance  $d$  from the maximum moment section.

### 2.3 FLEXURAL-SHEAR RESISTANCE AT A SECTION

The inclined crack may proceed into the compression zone of the beam and cause a premature flexural failure. This type of failure is termed a shear-compression failure, (1) (11). Assuming that an inclined crack had developed, in a beam with a horizontal steel profile and having no web reinforcement, as in FIGURE 2.2(a) and considering the portion of the beam above the crack FIGURE 2.2(b) as a free body, the following expression may be derived:

$$\frac{a - x}{a} = \frac{f_{sx}}{f_{sw}} \frac{(d - k_2 k d)_x}{(d - k_2 k d)_w} \quad \text{Eq. (6)}$$

where the subscripts  $x$  and  $w$  indicate values at those sections. Summation of the forces on the portion of the beam below the crack (neglecting the doweling force) yields:

$$A_s f_{sx} = A_s f_{sw} = A_s f_{sz} \quad \text{Eq. (7)}$$

combining equations (6) and (7) gives:

$$(kd)_x = (k_u d)_w + \frac{x}{a k_2} (d - k_2 k_u d)_w \quad \text{Eq. (8)}$$



For beams with draped longitudinal reinforcement and web reinforcement a similar analysis shows:

$$(kd)_x = (k_u d)_w - \frac{x \tan \beta}{k_2} + \frac{x}{a k_2} (d - k_2 k_u d)_w - \frac{M_v}{A_s f_{sw}} (d - k_u d)_w \quad \text{Eq. (9)}$$

where  $M_v$  is the moment of the forces produced by the vertical web reinforcement, at yield stress, when taken about section w in FIGURE 2.2(c).

It is apparent when considering FIGURE 2.2(a) that, the total curvature, in the cracked portion of the beam, must be the same whether it is computed using the increase in steel strains or the increase in concrete strains. Mathematically this may be expressed as:

$$\int_{a-x_h}^a \frac{\epsilon_{ca}}{(k d)_x} dx = \int_{a-x_h}^a \frac{\epsilon_s - \epsilon_{se}}{(d - k d)_x} dx \quad \text{Eq. (10)}$$

From strain measurements, it has been found that the compressive strains in the extreme fibre of a concrete beam at failure diminish from  $\epsilon_u$  at the load bearing plate quite rapidly to a distance approximately 8" from the load bearing plate (1) (3). The compressive strains outside this region are similar to those predicted by the elastic theory.

If the value  $k_2$  is assumed constant in the cracked section of the beam and the position of the inclined crack is known or assumed, a prediction of the ultimate moment of a beam failing in shear compression



may be computed as follows:

- (1) Assume a value of  $k_u d$  at the maximum moment section.
- (2) Assume a value for  $f_{cu}$  and calculate the corresponding steel stress  $f_{su}$ .
- (3) From the stress-strain relationship of the steel determine  $\epsilon_{su}$ .
- (4) Deduct the effective steel pre-strain  $\epsilon_{se}$  to obtain  $\epsilon_{sa}$ .
- (5) Determine the assumed ultimate moment.
- (6) From equations (8) or (9), depending on the type of beam, compute the variation in neutral axis over the length of the inclined crack.
- (7) By substituting the concrete strain distribution previously described, and the distances to the neutral axis in equation (10), compute the corresponding increase in steel strain.
- (8) If the value  $\epsilon_{sa}$  computed in step 7 does not agree with that computed in step 4, assume a new value for  $k_u d$  and repeat the procedure.

Step 8 in the procedure could involve a very lengthy graphical or algebraic computation. Hawkins (1) suggests that curvature distributions, as shown in FIGURE 2.3(b) and (c), may be used with little sacrifice in accuracy.

It should be pointed out that the preceding analysis was developed for the ultimate moment with a shear compression type of failure and that many other types of failure (outside the scope of this investigation) are possible.





## 2.4 CURVATURES AND DEFLECTIONS

A relationship between the increase in steel strains and the increase in concrete strains at points of maximum moment had been established for sections in flexure (12) and sections containing inclined cracks (1). This relationship is demonstrated in FIGURE 2.4. Hence the curvature before inclined cracking may be computed as

$$\frac{\epsilon_{sa}}{d - kd} \quad \text{or} \quad \frac{F \epsilon_{ca}}{kd}$$

The curvature is assumed to be distributed as shown in FIGURE 2.3(b). After inclined cracking, the curvature and curvature distribution may be obtained in a manner similar to that discussed in section 2.3.

The deflections of the beams may be determined from the moment curvature relationship and the curvature distribution and using ordinary geometric methods.

In the test program, the following characteristics of the performances of the pretensioned and post-tensioned beams were compared to each other and to calculated values.

- (1) Load-carrying capacity
- (2) Flexural cracking loads
- (3) Load-deflection relationships
- (4) Reactions
- (5) Load-curvature relationships



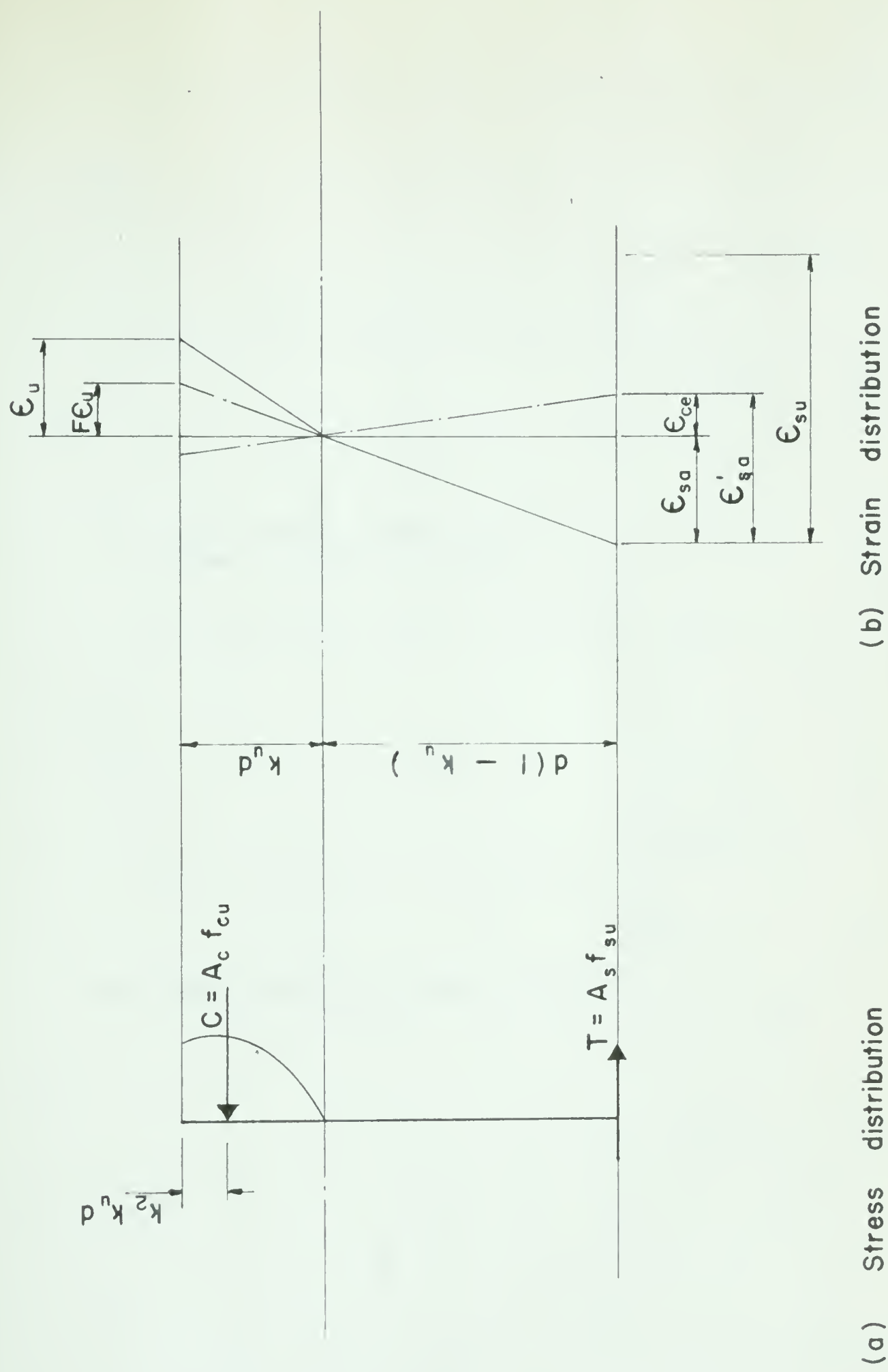
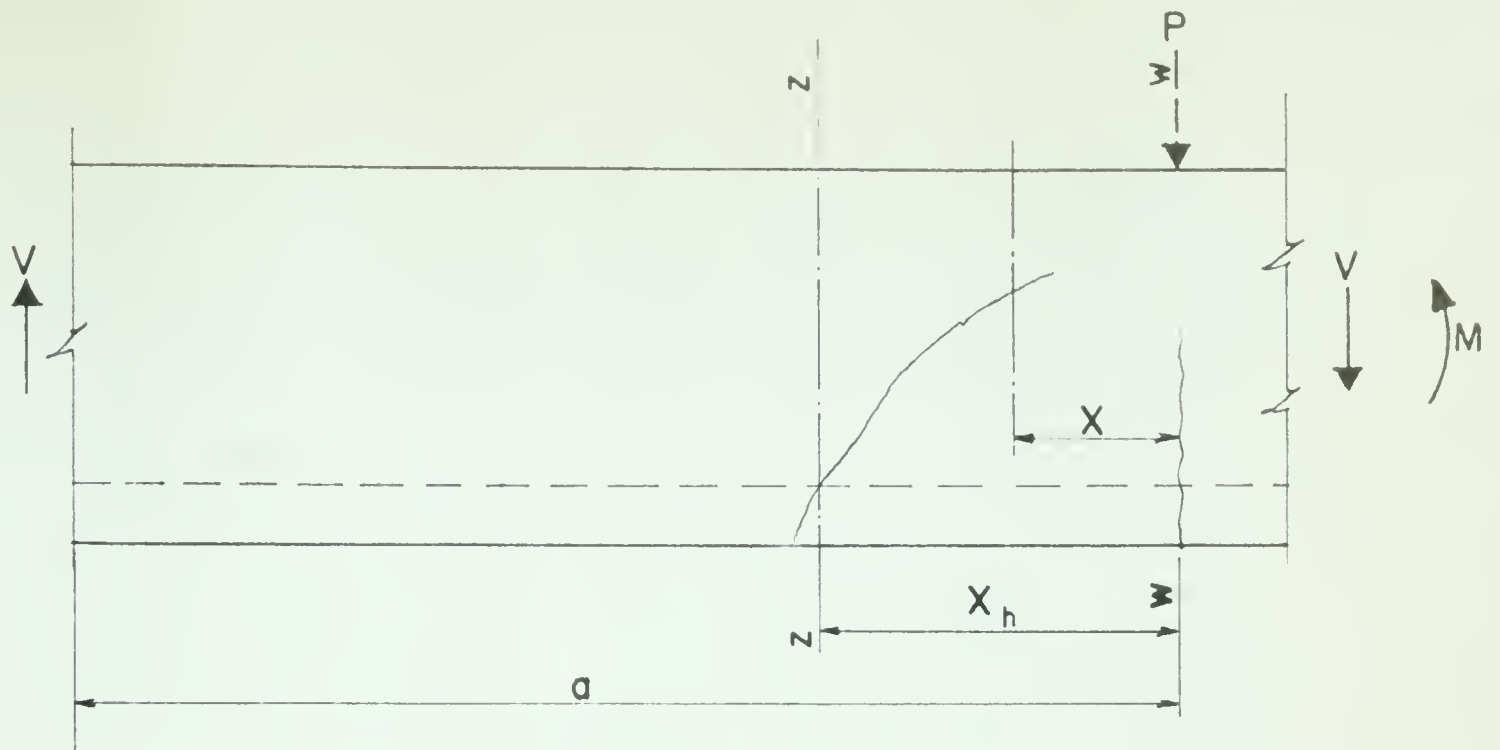
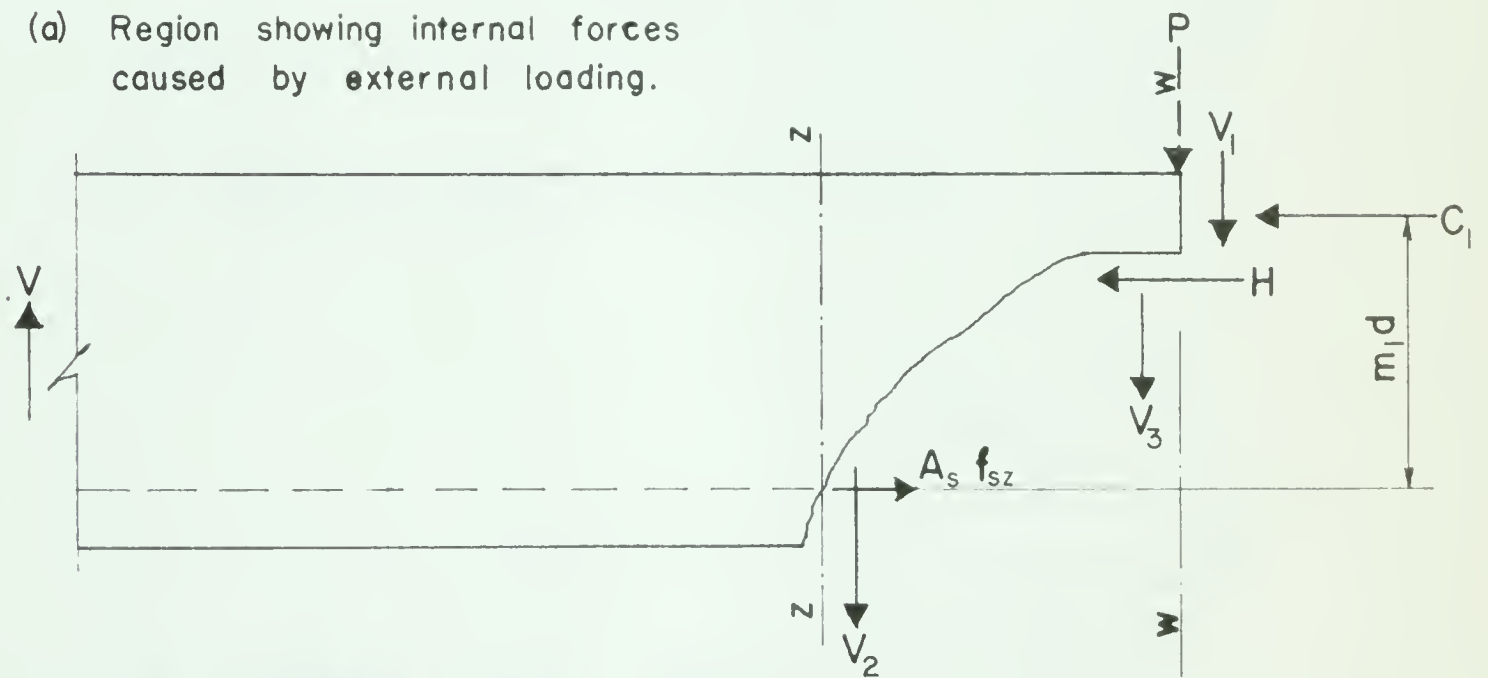


FIG. 2.1 STRESS AND STRAIN DISTRIBUTION ON A BEAM SECTION AT ULTIMATE FLEXURAL MOMENT

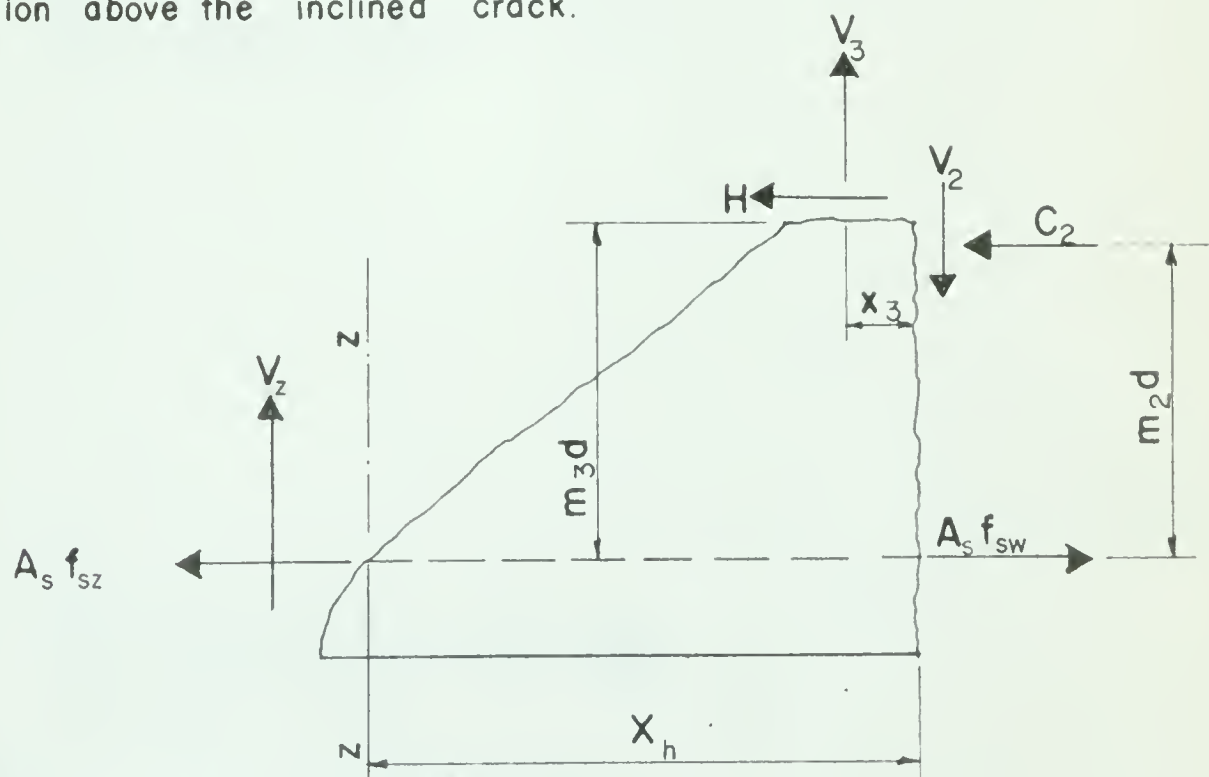




(a) Region showing internal forces caused by external loading.



(b) Section above the inclined crack.



(c) Section below the inclined crack.

Fig. 2.2 Free Body Diagrams for a Section with an Inclined Crack





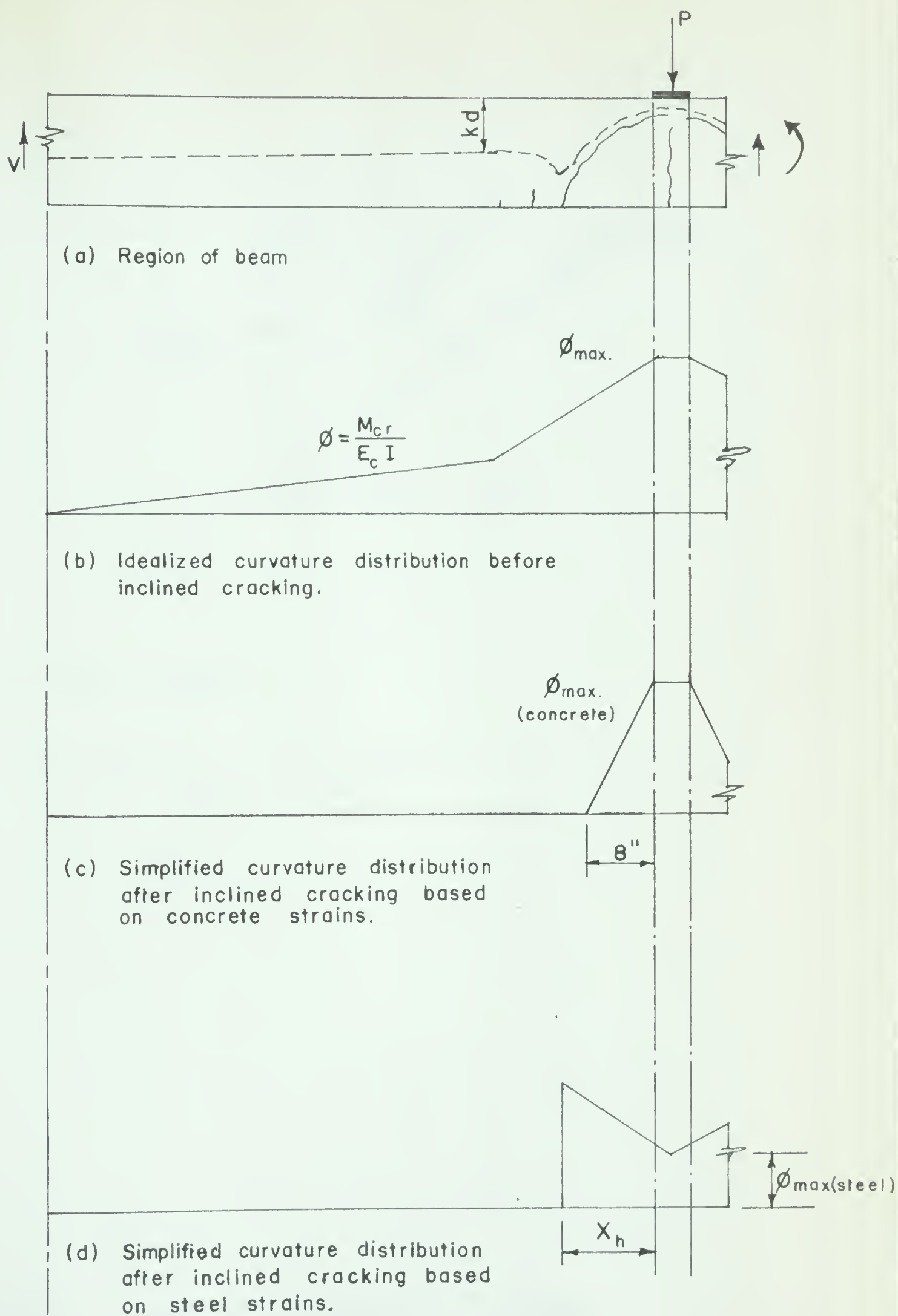


Fig. 2.3 CURVATURE DISTRIBUTIONS



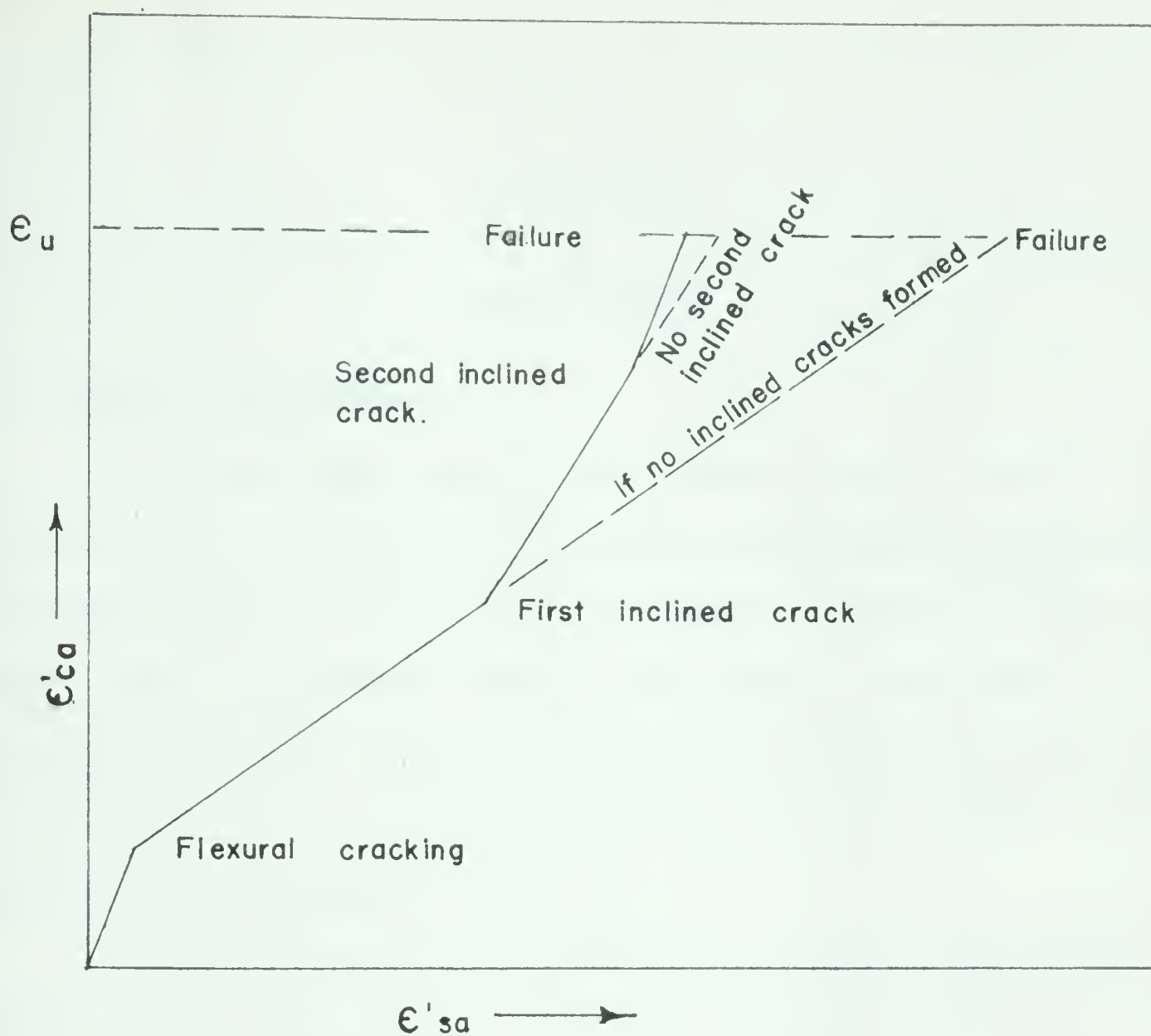


Fig. 2.4 IDEALIZED INCREASE IN STRAIN RELATIONSHIP



## CHAPTER III

### TEST SPECIMENS

#### 3.1 GENERAL DESCRIPTION

The four beams cast for this investigation were identical as to section, area and type of reinforcement, and magnitude of prestress. They were designed to span continuously over two 10'0" spans, and to support equal concentrated loads at each midspan. Reinforcement was provided by ten 0.162" diameter prestressed wires which were deflected up or down to suit the design requirements. The only variable introduced was the method of achieving prestress.

Beams PE-1 and PE-2 were prestressed using a pretensioning system. The ten high tensile wires were tensioned and anchored to the end plates of the form before the beams were cast. After the forms were stripped, the anchorages were released and the prestress was transferred to the concrete section by bond and end anchorage. Details of these beams are shown in FIGURE 3.1.

Beams PO-1 and PO-2 employed a post-tensioning system. They were cast with two 7/8" diameter cable ducts draped to design requirements. After the end forms were removed, five high tensile wires were inserted in each duct, tensioned, anchored to the end plates, and then grouted. It should be noted that the profile of the ducts matched very closely the profile of the steel in the prestressed beams, PE-1 and PE-2. Details of the post-tensioned beams are shown in FIGURES 3.2(a) and (b).





The remaining details were identical for both beam types. L-stirrups were placed at 1'0" on centre along the beams as nominal shear reinforcement and two welded box stirrups were placed at both ends of each beam to provide reinforcement against anchorage stresses. Appendices A and B describe further details concerning the casting and the construction of the beams.

### 3.2 PRESTRESSING STEEL STRESSES

The final prestress  $f_{se}$  was assumed to be the same in all beams and equal to 125 k.s.i. which was 60% of the ultimate strength of the steel. The force produced by this stress was assumed to act at the centroid of the steel area (FIGURE 3.3) and, by its eccentricity, to produce the initial moments as shown in FIGURE 3.4. It should be noted that the beams were allowed to deflect during the prestressing operation. The supports were raised to bear on their respective rocker plates after the deflections, due to prestressing, had taken place.

The initial prestress was measured and the final prestress estimated by subtracting the assumed losses. TABLE III-1 shows a summary of the estimated losses determined in the detailed calculations shown in Appendix F.

### 3.3 PRESTRESSING CONCRETE STRESSES

The initial flexural stresses in the beam were determined by using the properties, as shown in TABLE III-2, and by the initial and dead load moments, as shown in FIGURE 3.4. Maximum fibre stresses were calculated by the equation

$$f_c = \frac{T_{se}}{A} \pm \frac{M_{se}}{S} \pm \frac{M_d}{S}$$



where  $T_{se}$ , the initial prestressing force, was equal to  $f_{se} A_s = 125 \text{ k.s.i.} \times 0.206 \text{ square inches} = 25.8 \text{ kips}$  at all sections of the beam. Stresses due to prestressing were computed for extreme fibres in the sections at the midspans and at the centre support as follows:

(a) at midspan

$$f_c = 1030 \text{ p.s.i. compression in bottom fibre}$$

$$f_c = 50 \text{ p.s.i. tension in top fibre}$$

(b) at centre support

$$f_c = 1058 \text{ p.s.i. compression in top fibre}$$

$$f_c = 78 \text{ p.s.i. tension in bottom fibre}$$



TABLE III-1

## ESTIMATED STEEL STRESSES

## (a) Pretensioned beam

Desired final prestress	$f_{se} = 125.0 \text{ k.s.i.}$
Estimated loss due to:	
(1) anchorage slip	12.0 k.s.i.
(2) elastic strain of concrete	5.9 k.s.i.
(3) creep of concrete	3.0 k.s.i.
(4) shrinkage of concrete	2.0 k.s.i.
(5) steel relaxation	3.7 k.s.i.
(6) friction	0
Initial prestress required	151.6 k.s.i.

Jacking force required =  $151.6 \text{ k.s.i.} \times 0.206$   
square inches = 31.6 kips

$$\text{Percentage loss} = \frac{151.6 - 125}{151.6} \times 100\% = 17.5\%$$

## (b) Post-tensioned beam

Desired final prestress	$f_{se} = 125.0 \text{ k.s.i.}$
Estimated loss due to:	
(1) anchorage slip	12.0 k.s.i.
(2) elastic strain of concrete	1.5 k.s.i.
(3) creep of concrete	3.0 k.s.i.
(4) shrinkage of concrete	1.0 k.s.i.
(5) steel relaxation	3.7 k.s.i.
(6) friction	15.4 k.s.i.
Initial prestress required	161.6 k.s.i.

Jacking force required =  $161.6 \text{ k.s.i.} \times 0.206$   
square inches = 33.6 kips

$$\text{Percentage loss} = \frac{161.6 - 125}{161.6} \times 100\% = 22.6\%$$





TABLE III-2

## SECTIONAL AND MATERIAL PROPERTIES

## (a) Section Properties

Moment of inertia	765.0 inches <sup>4</sup>
Area of concrete	52.6 inches <sup>2</sup>
Area of steel	0.206 inches <sup>2</sup>

## (b) Material Properties

28-day cylinder strength of concrete	5000 p.s.i.
Modulus of elasticity of concrete	$3.3 \times 10^6$ p.s.i.
Ultimate strength of steel	208,000 p.s.i.
Modulus of elasticity of steel	$30.0 \times 10^6$ p.s.i.
Shrinkage of concrete	0.06% at test
Coefficient of creep of concrete	0.5 at test
Relaxation of steel	3%
Wobble coefficient (K)	0.001 per foot
Curvature coefficient ( $\mu$ )	0.3





2



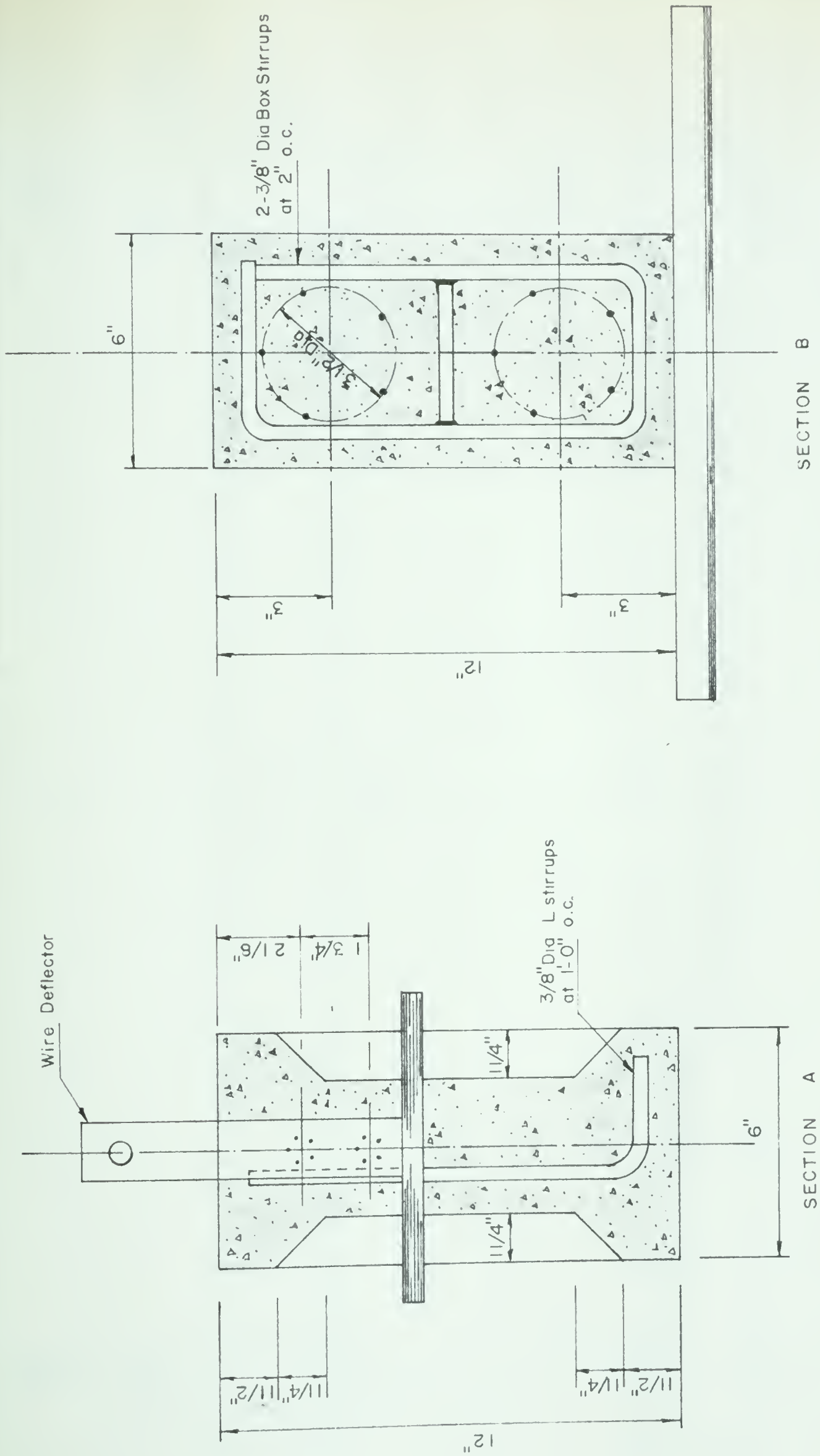


Fig. 3.1 (b) DETAILS OF THE PRETENSIONED BEAMS





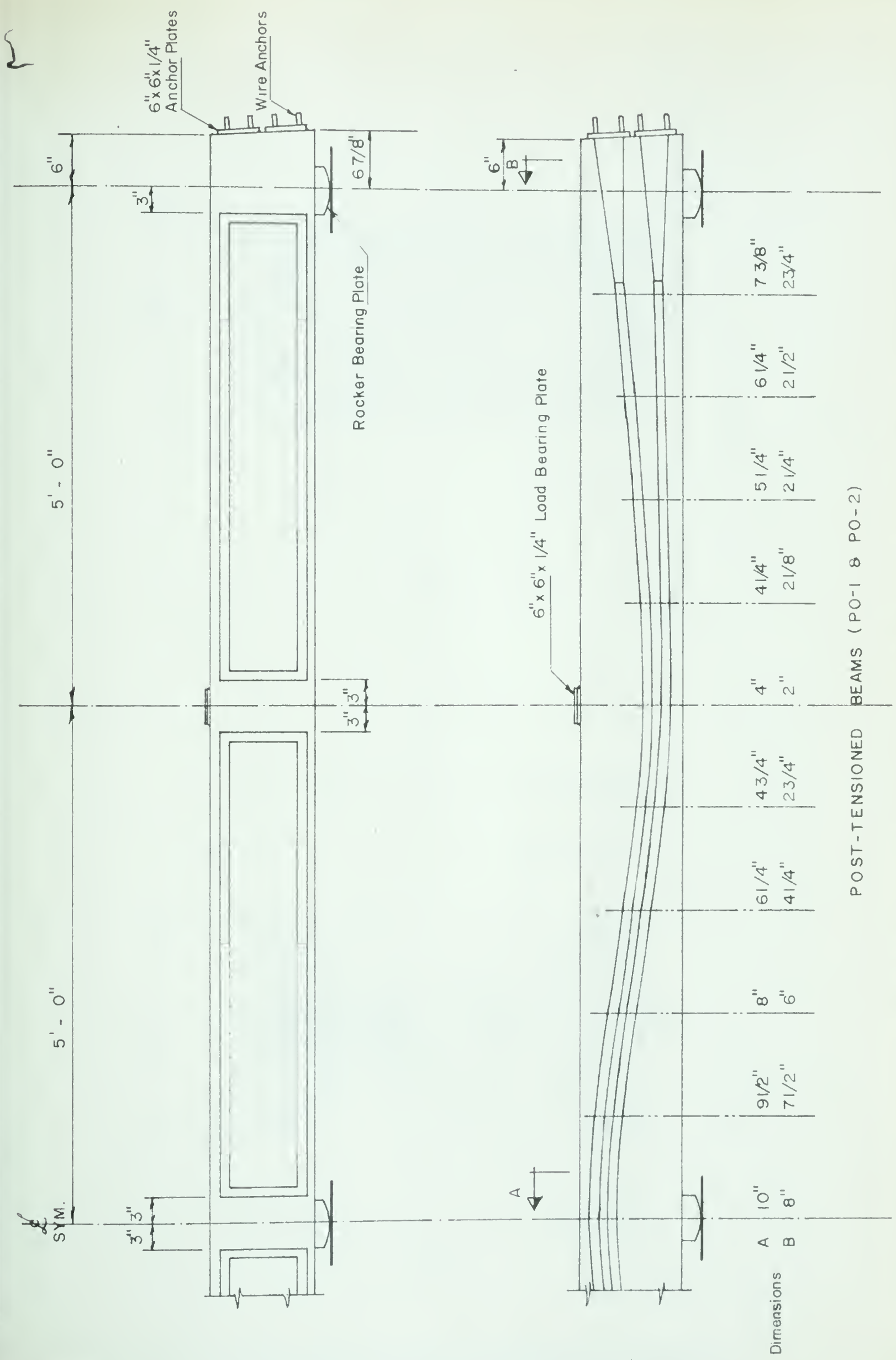


Fig. 3-2 (a) DETAILS OF POST-TENSIONED BEAMS



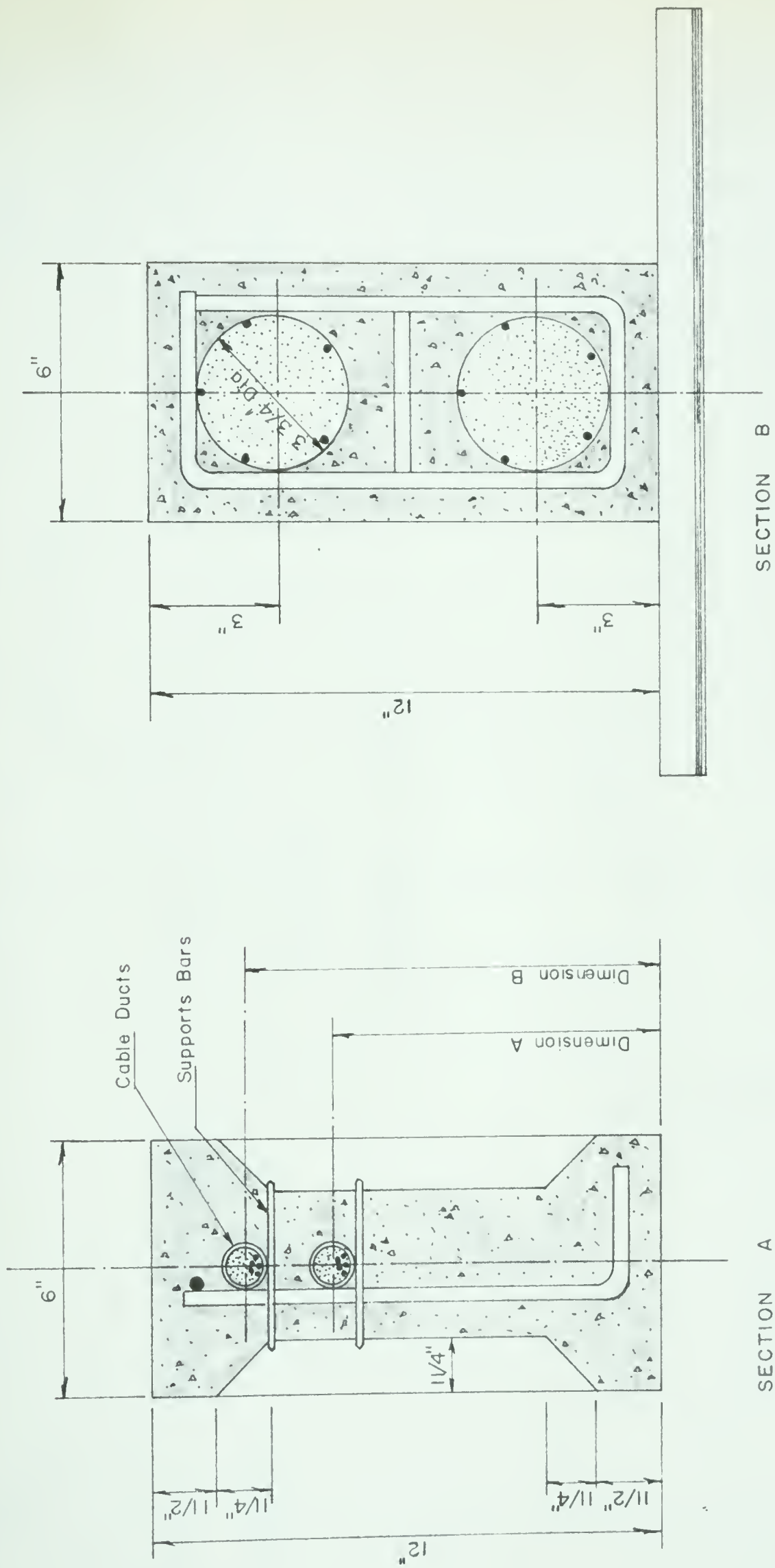


Fig. 3. (b) DETAILS OF POST-TENSIONED BEAMS



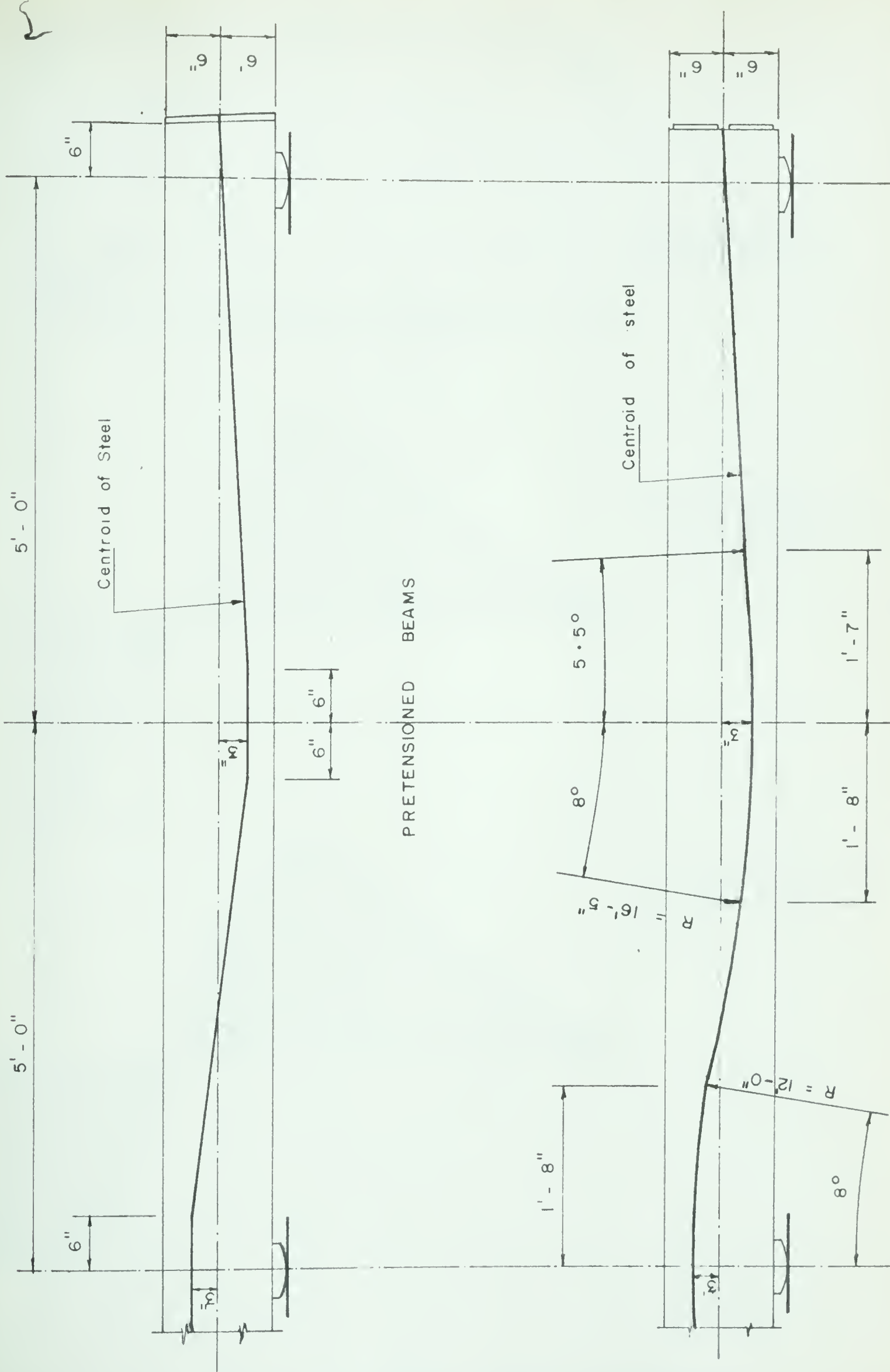


Fig. 3.3 DESIGN DIAGRAMS OF BEAMS





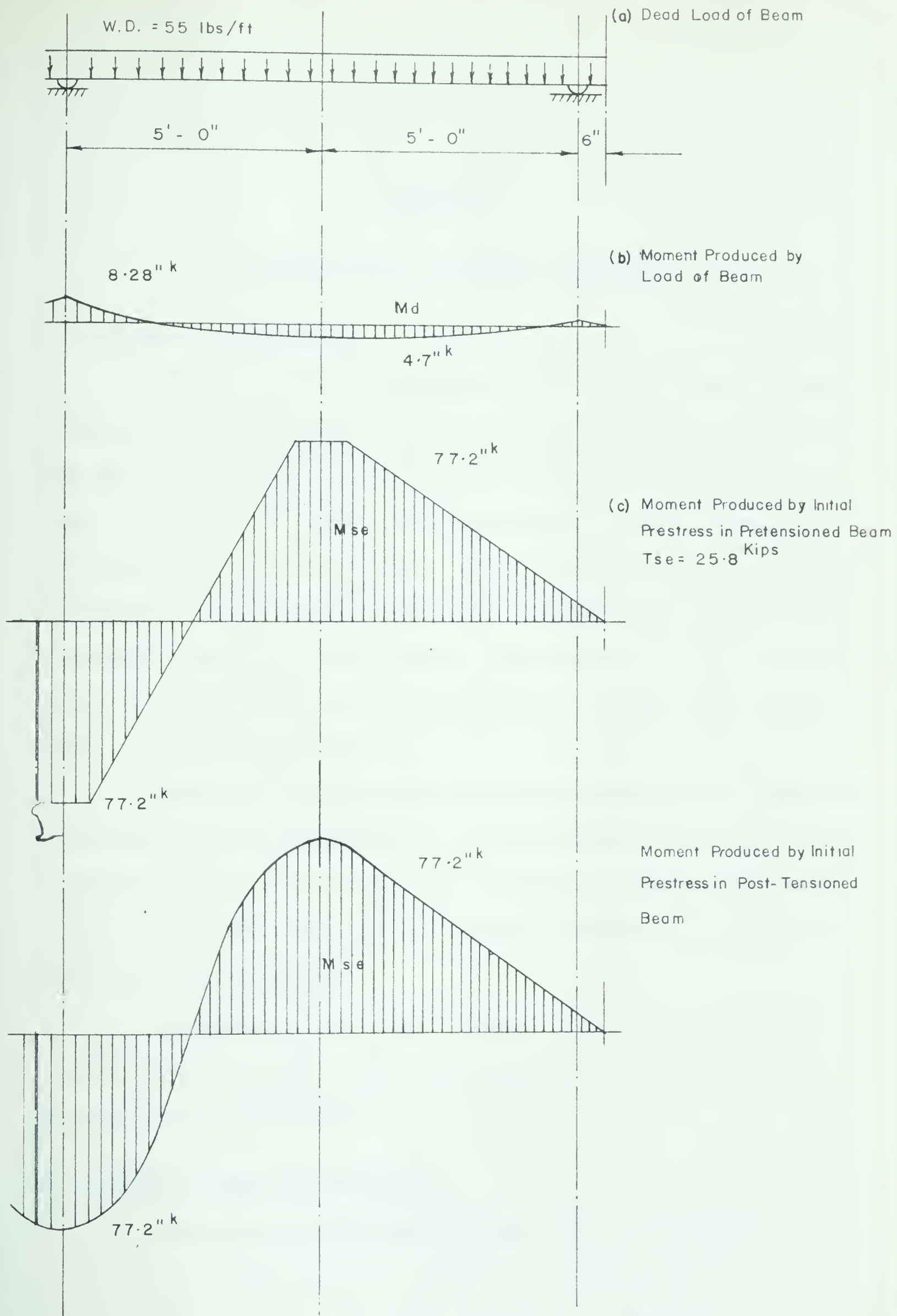


Fig. 3.4 INITIAL BENDING MOMENTS



## CHAPTER IV

### INSTRUMENTATION AND LOADING EQUIPMENT

#### 4.1 DEFLECTION MEASUREMENTS

Vertical deflection measurements were taken at both midspans. Each measurement was obtained from a deflection dial mounted under the beam with its probe bearing on the centre of the bottom surface of the beam. The dials were mounted on a light angle instrument frame, which was supported directly on the floor. Steel scales, affixed to one side of the beam, at each midspan, were used to obtain vertical deflection measurements beyond the range that the deflection dials could provide. These scales were read as they moved relative to a stationary reference point on the instrument frame.

Horizontal movement of the reactions was measured at both ends of the beam. These measurements were taken by means of deflection dials which were mounted on the loading beam with their probes bearing on the housing of the roller reactions. A schematic diagram of the instrumentation is shown in FIGURE 4.1.

The deflection dials had a travel of one inch and readings were taken to the nearest 0.001". The twelve inch steel scales were graduated in 0.02" increments.

#### 4.2 CONCRETE STRAIN MEASUREMENTS

Flexural strain measurements were taken at both midspans,



and at the centre support by means of a Demec gage. Mild steel Demec gage plugs were attached to the side of the beam, by means of sealing wax, as described in Reference 13. The Demec gage, when applied to these plugs, accurately measured the change in distance between the plugs. The readings obtained were analyzed as follows:

$$\text{Strain} = (R_o - R_n) \times 0.098$$

where  $R_o$  = initial gage reading at zero load

$R_n$  = gage reading at a load increment

0.098 = gage factor

At each strain station the gage plugs were placed in patterns on both sides of the beam as shown in FIGURE 4.2. A Berry gage with a two-inch gage length, was used for measuring the strains in beams PO-1 and PE-1. Unfortunately, the gage used was found to be defective, and the strain measurements from these two beams were discarded. As the only other gage available was a Demec gage with an eight-inch gage length, a different plug pattern was used in measuring the strains on beams PO-2 and PE-2. These readings were acceptable and were analyzed. The accuracy of the eight-inch Demec gage used was  $\pm 5 \times 10^{-6}$  inches per inch.

#### 4.3 REACTION MEASUREMENTS

The three support reactions were measured by means of load cells. Each load cell consisted of a six-inch length of four-inch steel pipe, to which SR-4 strain gages were attached. Strains, resulting from the reaction loads, were read on a Baldwin strain indicator





and referred to a calibration curve previously obtained for the load cell. Each reaction was determined from its corresponding strain on the curve. Load cell calibration curves and a more detailed description of the load cells are presented in Appendix C.

#### 4.4 LOADING SYSTEM

The concentrated loads, located at both midspans, were applied by ten ton capacity Blackhawk hydraulic jacks with a twelve-inch extension. Both jacks were connected to a common pump and pressure gage. As the jacks were identical, it was assumed that the loads applied to each span were equal. The load applied to one span of a test beam was defined as the load on the beam (P) for this investigation.

The loading jacks were calibrated and the readings obtained are given in Appendix D.



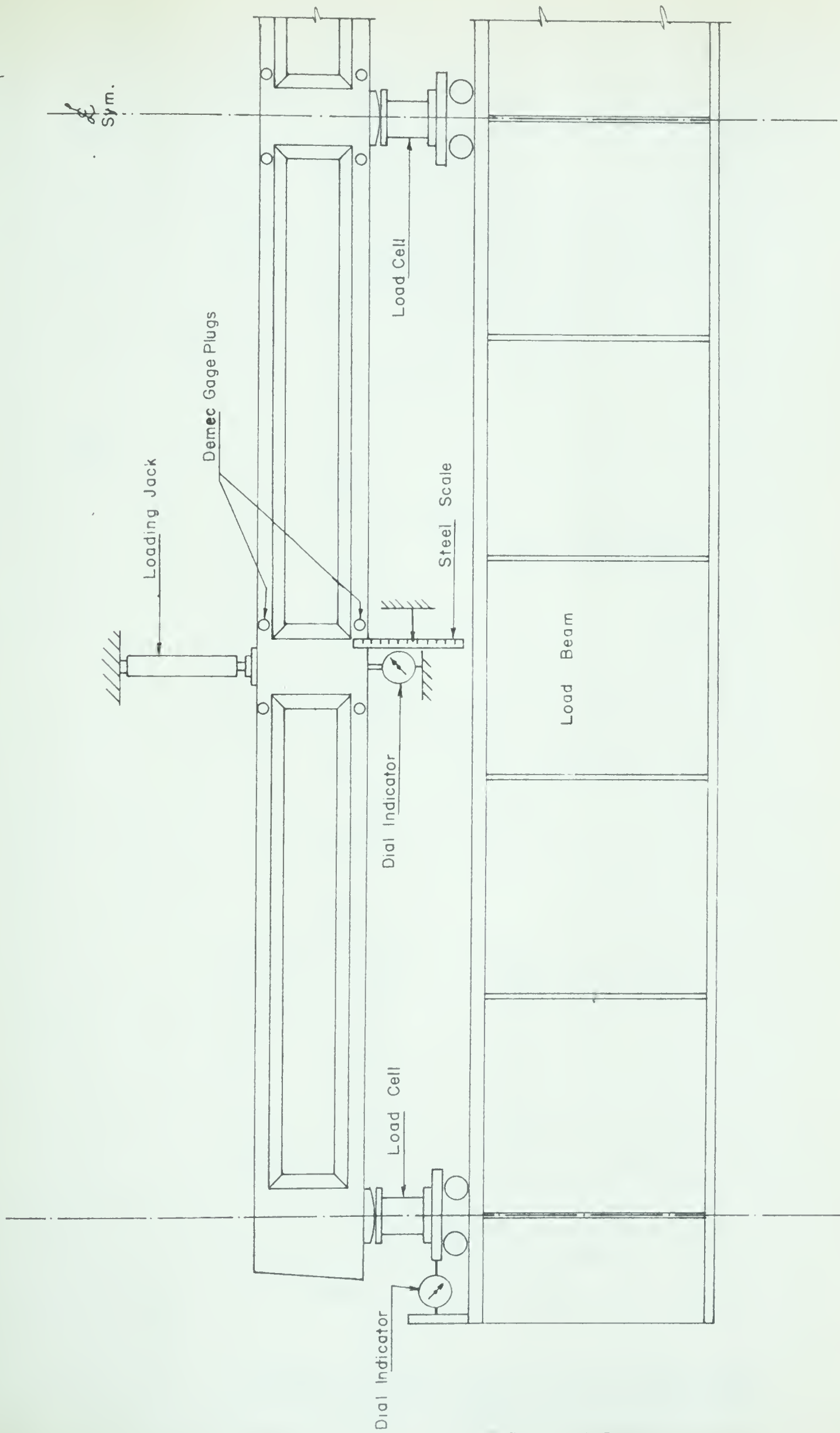


Fig. 4.1 INSTRUMENTATION



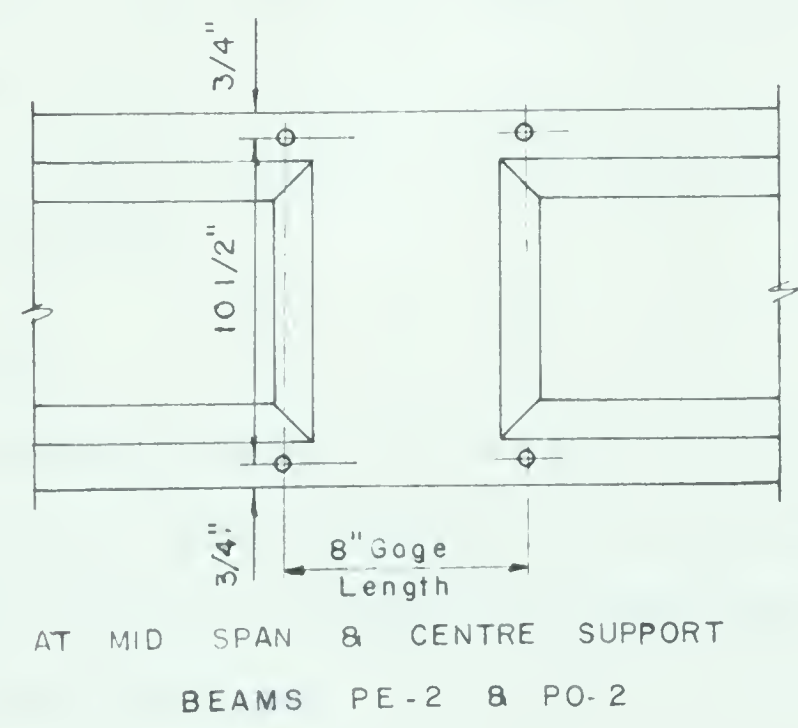
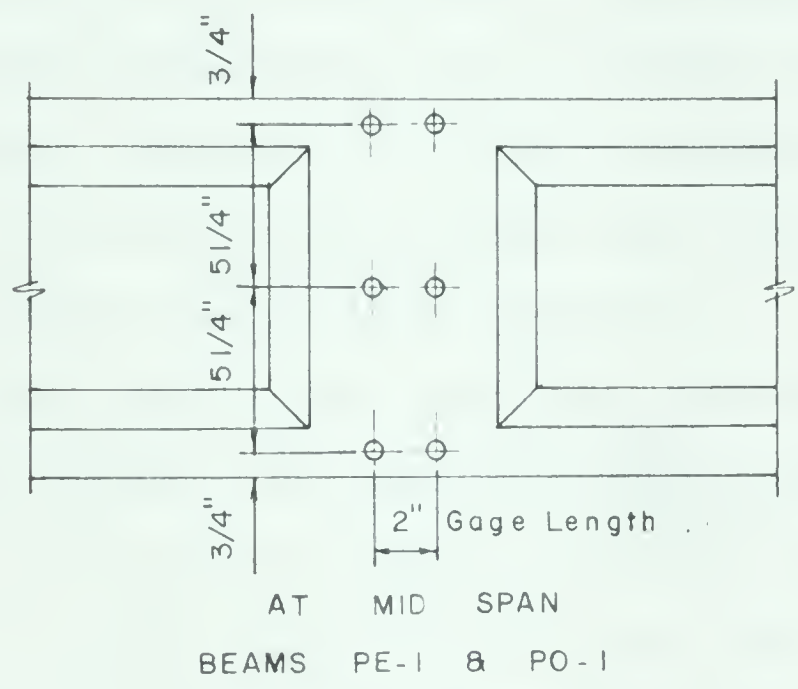
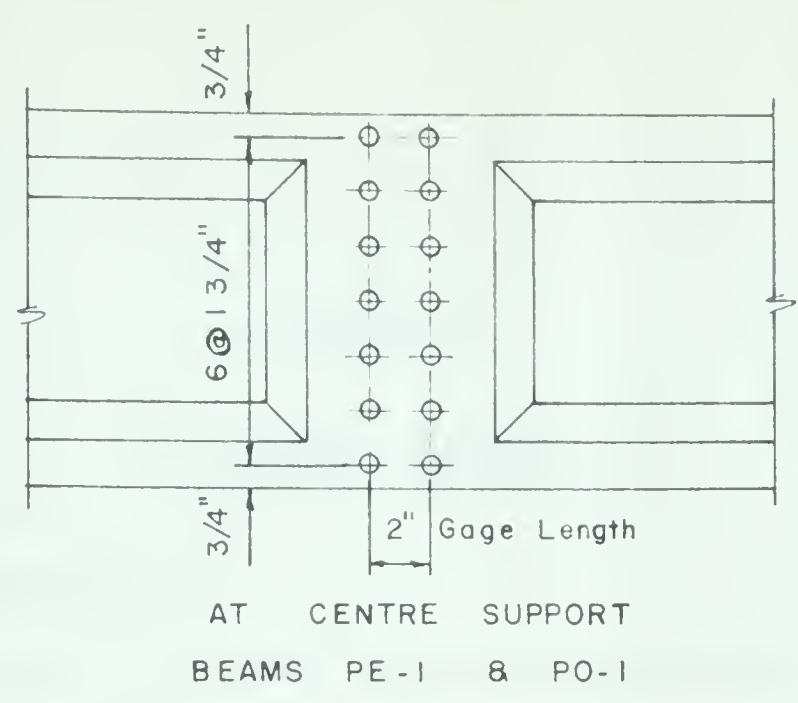


Fig. 4.2 GAGE PLUG LOCATIONS



## CHAPTER V

### EXPERIMENTAL PROCEDURE

#### 5.1 PRE-TEST PREPARATION

Each beam, in its form, was positioned with the three rocker plates located on their reaction load cells. After stripping the beam forms, the side rods, loading heads, and the instrument frame were assembled in position. One (or both) of the end supports was then raised to bear on its rocker plate by placing shims under the load cell. The beam was then centred on the loading beam.

Demec gage plugs and steel scales were then attached to the beam, as described in Chapter IV. Load cells and dummy gages were connected to the strain indicator located at the north end of the beam. The deflection dials, located under the beam, were attached to the instrument frame. The dials used to measure the horizontal movement at each end of the beam were positioned. Load point bearing plates were set on beds of grout and the loading jacks were positioned and extended to seat the bearing plates.

#### 5.2 TEST PROCEDURE

Three men were employed in a load test. One man recorded all readings and read the strain indicator. The second man operated the hydraulic hand pump which activated the loading jacks. All instruments were read by the third man.





To obtain the data for a specific load the following procedure was followed. Pressure was increased on the jacks until the pressure gage indicated the required load. The Demec gage readings were taken, followed by the reading of the deflection instruments. Reaction measurements were then taken from the strain indicator and the time was noted. The load was increased by the next load increment, and the above procedure was repeated. As the test proceeded, some readings had to be discontinued because tensile cracks which developed in the concrete dislodged many Demec gage plugs.

The sequence of loading was varied slightly for different beams. Beam PE-1, the first beam tested, was loaded in two kip increments up to 8.5 kips, unloaded in the same increments, and then reloaded to failure. However, as the first loading cycle did not give readings significantly different from the failure cycle this procedure was modified for the other beams. The remaining three beams were loaded to an initial load of seven kips, unloaded, then loaded in two kip increments up to a load of 18 kips, and then by one kip increments to failure.



## CHAPTER VI

### MATERIAL PROPERTIES

#### 6.1 CONCRETE AND GROUT

The concrete was obtained from a local transit mix supplier and was delivered to the laboratory in a rotating mixer. Each batch of concrete consisted of:

- 800 pounds of Portland cement
- 1500 pounds of 1/2 inch aggregate
- 1390 pounds of fine aggregate
- 270 pounds of water

This mix, as designed by the supplier, was intended to produce a 5000 p.s.i., 28-day cylinder strength and to have a two inch slump.

Six standard 6" x 12" test cylinders were cast from the concrete used in each beam. Two of these cylinders were cured in a moist room at 100% relative humidity, while the remaining four cylinders were placed beside the beam and cured under job conditions. A standard slump test was performed for each batch of concrete.

Seven days after casting, one moist cured and one job cured cylinder were tested. The remaining cylinders were tested on the day of the beam test (approximately 28 days after casting). Stress-strain curves were obtained from the tests conducted on the 28-day job cured cylinders. Strain measurements were taken using a device developed



by Taylor (14). A summary of the cylinder strengths and slump test is shown in TABLE VI-1. Stress-strain curves are shown in FIGURE 6.1 (a, b, c and d).

The grout mixture used to fill the cable ducts of the post-tensioned beams, consisted of Portland cement possolith and water. As the grout was to be pumped into the cable ducts, a thin grout was required. The cement and water were therefore proportioned so that the mixture had a consistency similar to that of thick paint. Two 3" x 6" test cylinders were cast from the grout of each beam and cured in the moist room. One of these cylinders was tested at the time of the beam test. The other cylinder was tested 28 days after grouting. Compressive strengths of the grout cylinders are shown in TABLE VI-1.

## 6.2 STEEL REINFORCEMENT

The prestressing tendons consisted of plain, high tensile wires, 0.162 inches in diameter. This wire was supplied by British Wire Ltd. in 26" diameter rolls.

Tensile strength tests were run on two samples of the wire, cut at random from the rolls. A constant rate of stress was applied by a Baldwin testing machine while strains were measured over an 8" gage length using a Baldwin wire extensometer. The stress-strain curves obtained for the wire samples are shown in FIGURE 6.2.





TABLE VI-1

## CONCRETE AND GROUT STRENGTHS

Strength in p.s.i.				
Beam	PE-1*	PE-2	PO-1	PO-2
Concrete cylinders (in p.s.i.)				
7-day moist room	5530	5020	4930	5140
28-day moist room	6420	7000	5600	5570
7-day job cured	4820	4870	--	5150
28-day job cured	6950 7060 6940	6110 6250 6600	5160 5120 5390	5400 5300 5000
Grout cylinders (in p.s.i.)				
at test of beam			1885 (16 day)	--
28-day			4970	4370
Slump (in inches)	4	6	1	4

\* The concrete cylinders cast with beam PE-1 were compacted using an electric vibrator.



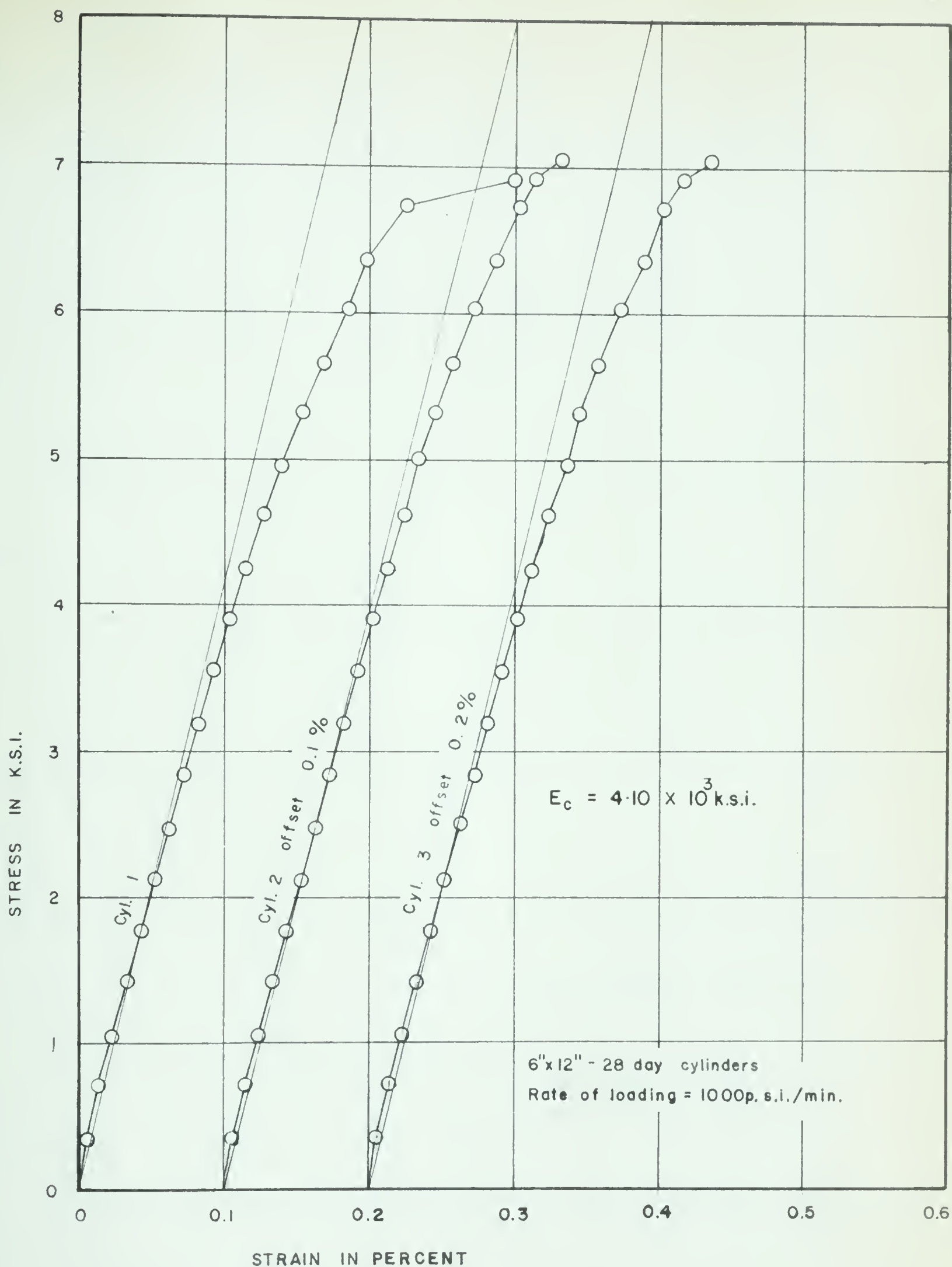


Fig. 6.1 (a) STRESS vs STRAIN GRAPHS FOR CONCRETE  
CYLINDERS FROM BEAM PE-I



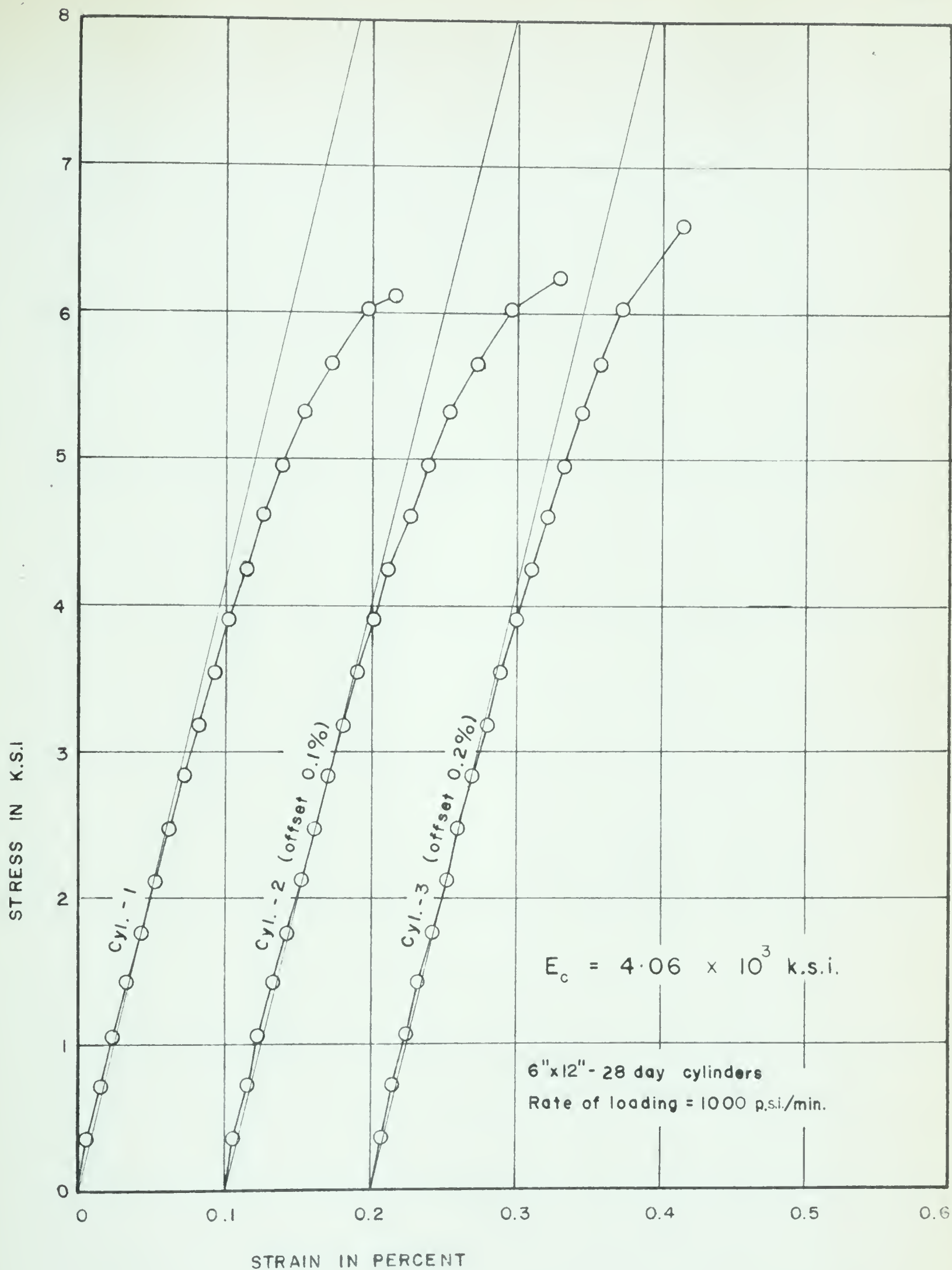


Fig. 6.1 (b) STRESS vs STRAIN GRAPHS FOR CONCRETE  
CYLINDERS FROM BEAM PE-2



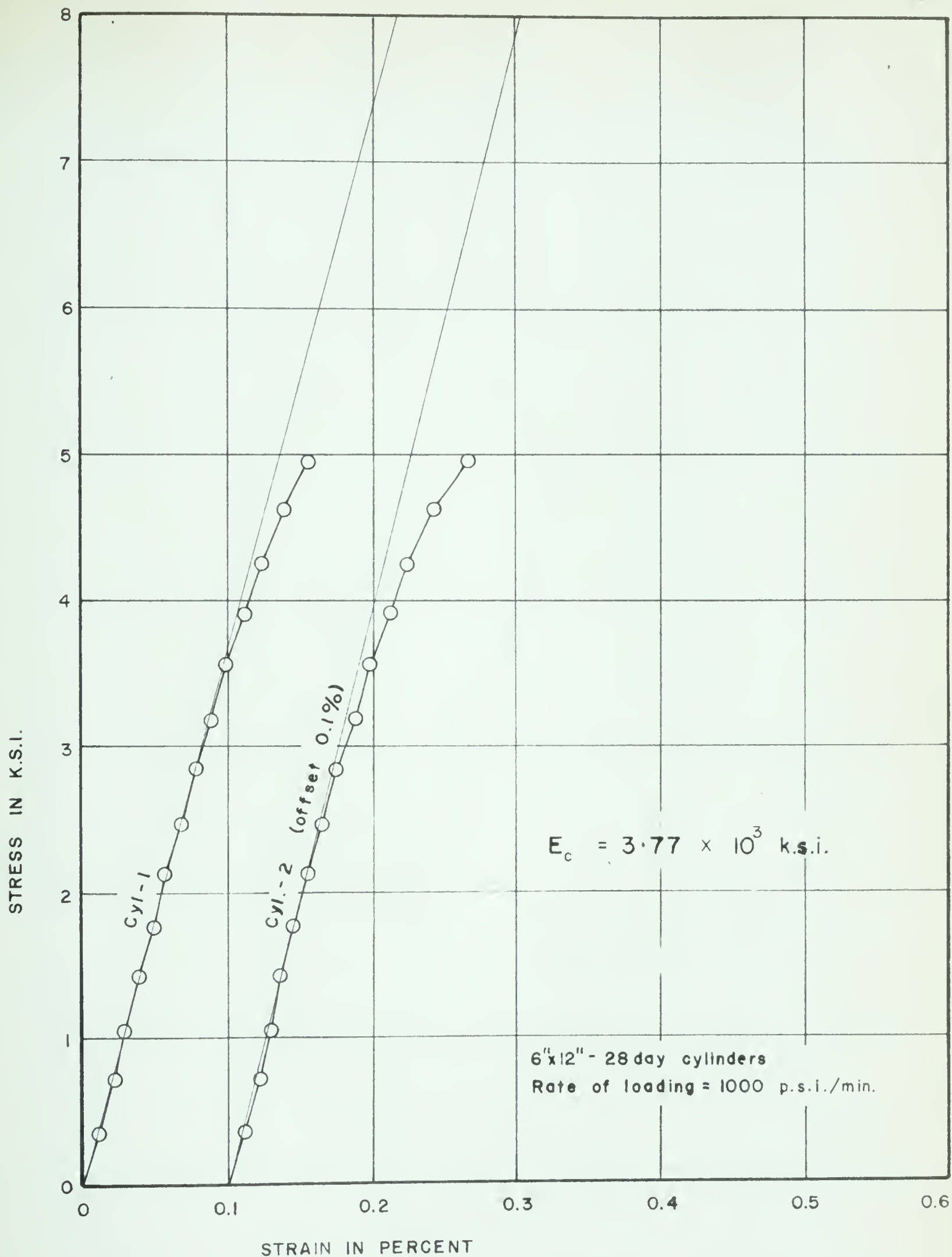


Fig. 6.1 (c) STRESS vs STRAIN GRAPHS FOR CONCRETE  
CYLINDERS FROM BEAM PO-1





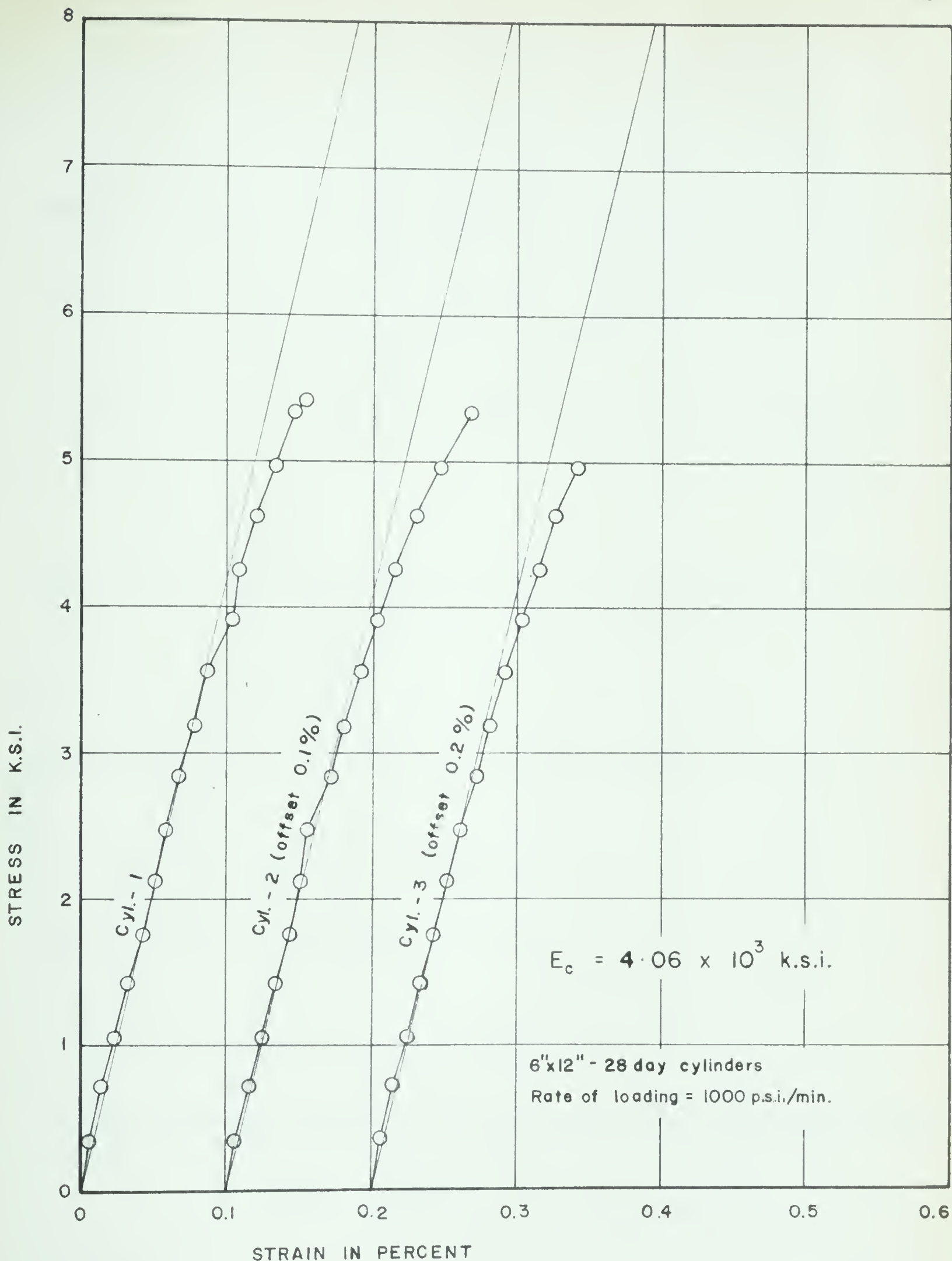


Fig. 6.1 (d) STRESS vs STRAIN GRAPHS FOR CONCRETE CYLINDERS FROM BEAM PO-2



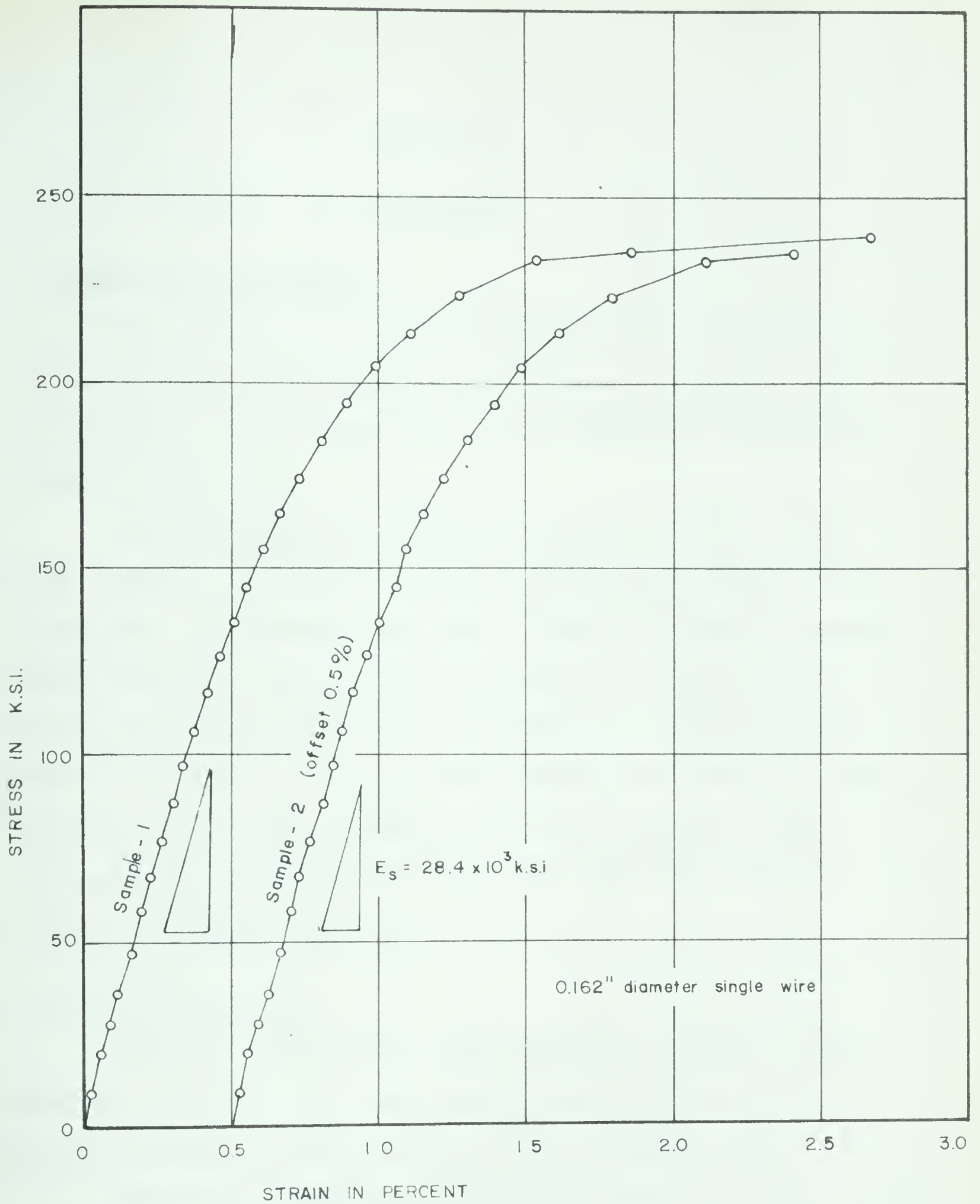


Fig. 6.2 STRESS vs STRAIN FOR PRESTRESSING WIRE



## CHAPTER VII

### TEST RESULTS

#### 7.1 DEFLECTIONS AND MOVEMENTS

Test results are presented in graphical form. The load versus vertical deflection graph for each midspan is shown in FIGURES 7.1 (a), (b), (c), and (d). The average curves for all beams are plotted on common axes in FIGURE 7.2.

The horizontal movement of the end supports is shown in two graphs. FIGURE 7.3 is a plot of the average horizontal movement of the end reactions. This movement represents the numerical average (assuming movement toward the centre support to be positive) of the horizontal deflection dial readings from each end of the beam. The second graph (FIGURE 7.4) is a plot of the load versus one-half the difference in the horizontal deflection dial readings at each end of the beam. Graphs of this type were obtained for all beams except beam PE-1 on which no horizontal measurements were taken.

#### 7.2 REACTION MEASUREMENTS

The load versus reaction graphs are shown in FIGURES 7.5 (a) and (b) and 7.6 (a) and (b). Also plotted on these figures are the theoretical elastic reactions calculated from the applied loads.

FIGURE 7.7 is plotted to illustrate the accuracy of the loading and reaction measurements. The ratio of the total of the three reactions to the total of the two concentrated loads is plotted against the applied load.





### 7.3 STRAIN MEASUREMENTS

Concrete strain measurements from Beams PE-2 and PO-2 are illustrated in FIGURES 7.8 to 7.12. The first group of curves (FIGURES 7.8 and 7.9) show the applied load plotted against the average compressive or tensile strain at the level of the Demec gage plugs for each midspan and centre support. The load versus curvature relationships shown in FIGURES 7.10, 7.11 and 7.12 were also plotted using the strain data.

During the analysis of data it was discovered that the strain measurements taken at the same location on the two sides of the beam were not equal. As this would indicate a lateral movement and/or twisting of the beam, differences in strain readings are plotted against the applied load in FIGURE 7.12. The difference is plotted in the direction of the lateral movement indicated. That is, a larger tensile strain on the east side of the beam indicates a lateral movement to the east, whereas, a larger compressive strain on the east side indicates a movement to the west.

### 7.4 PHOTOGRAPHS

FIGURES 7.14 and 7.15 are photographs of the beams after failure.



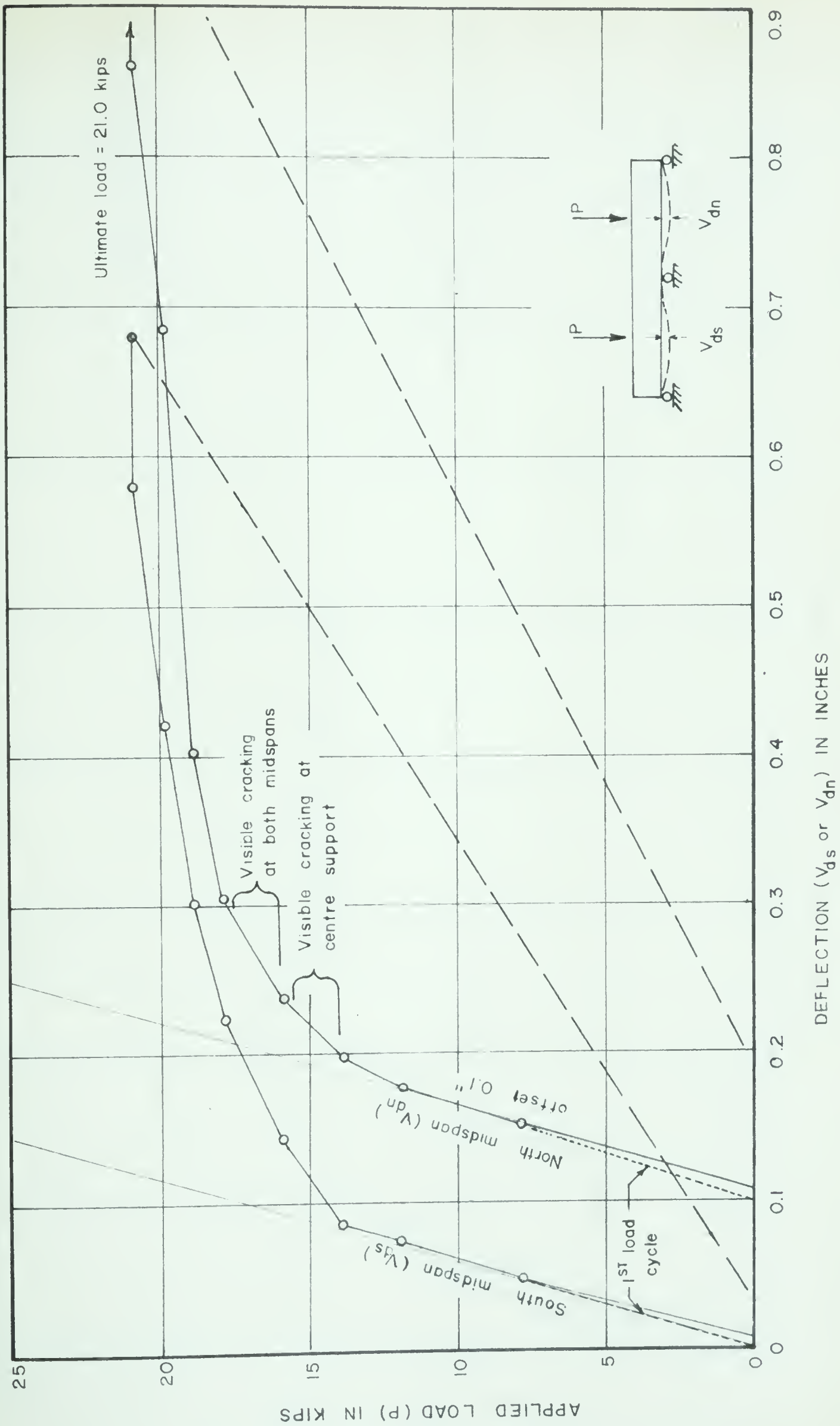


Fig. 7.1(a) APPLIED LOAD vs VERTICAL DEFLECTION AT MIDSPANS BEAM PE-I



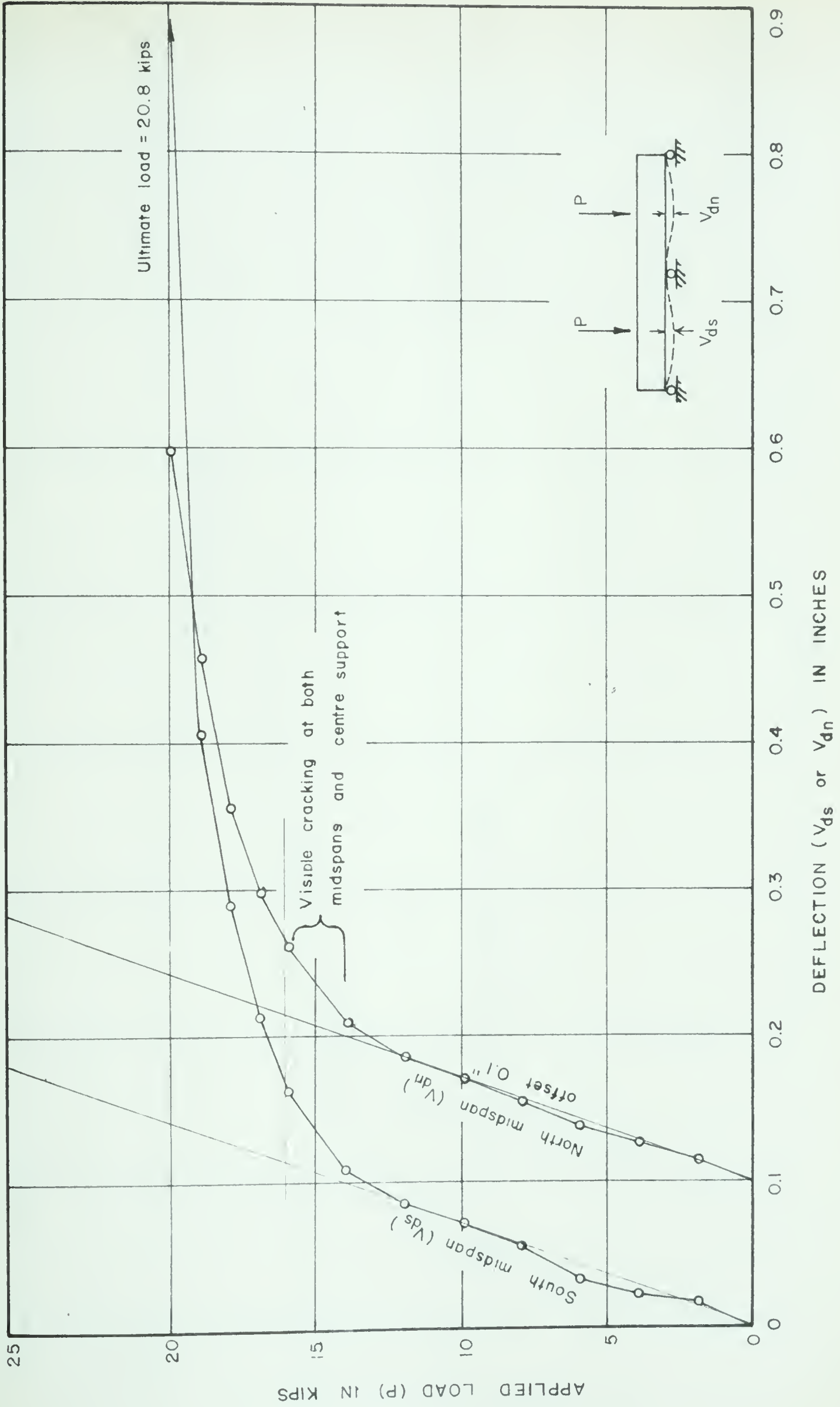


Fig. 7.1 (b) APPLIED LOAD vs VERTICAL DEFLECTION AT MIDSPANS BEAM PE-2



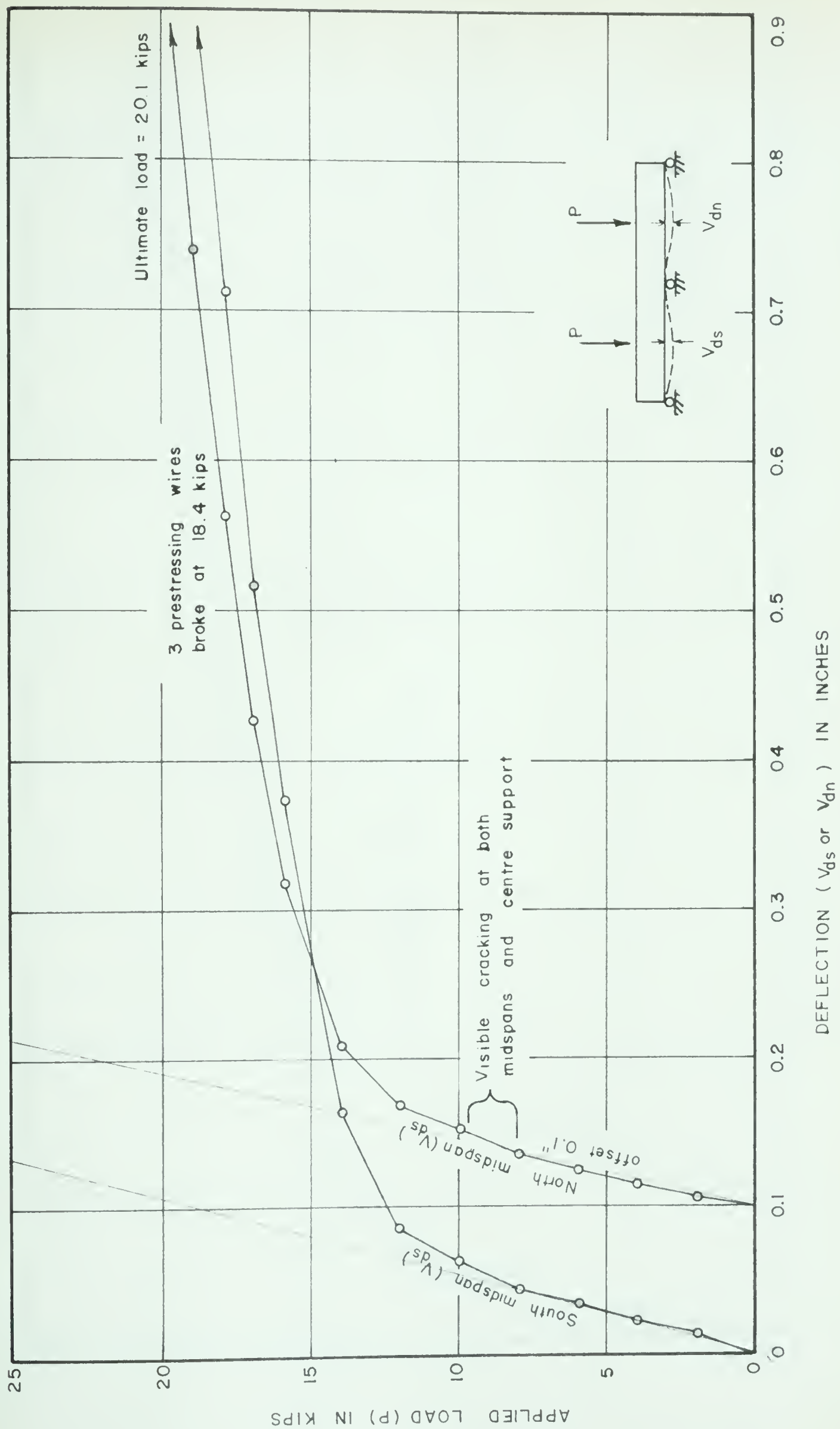


Fig. 7.1 (c) APPLIED LOAD vs VERTICAL DEFLECTION AT MIDSPANS BEAM PO-I





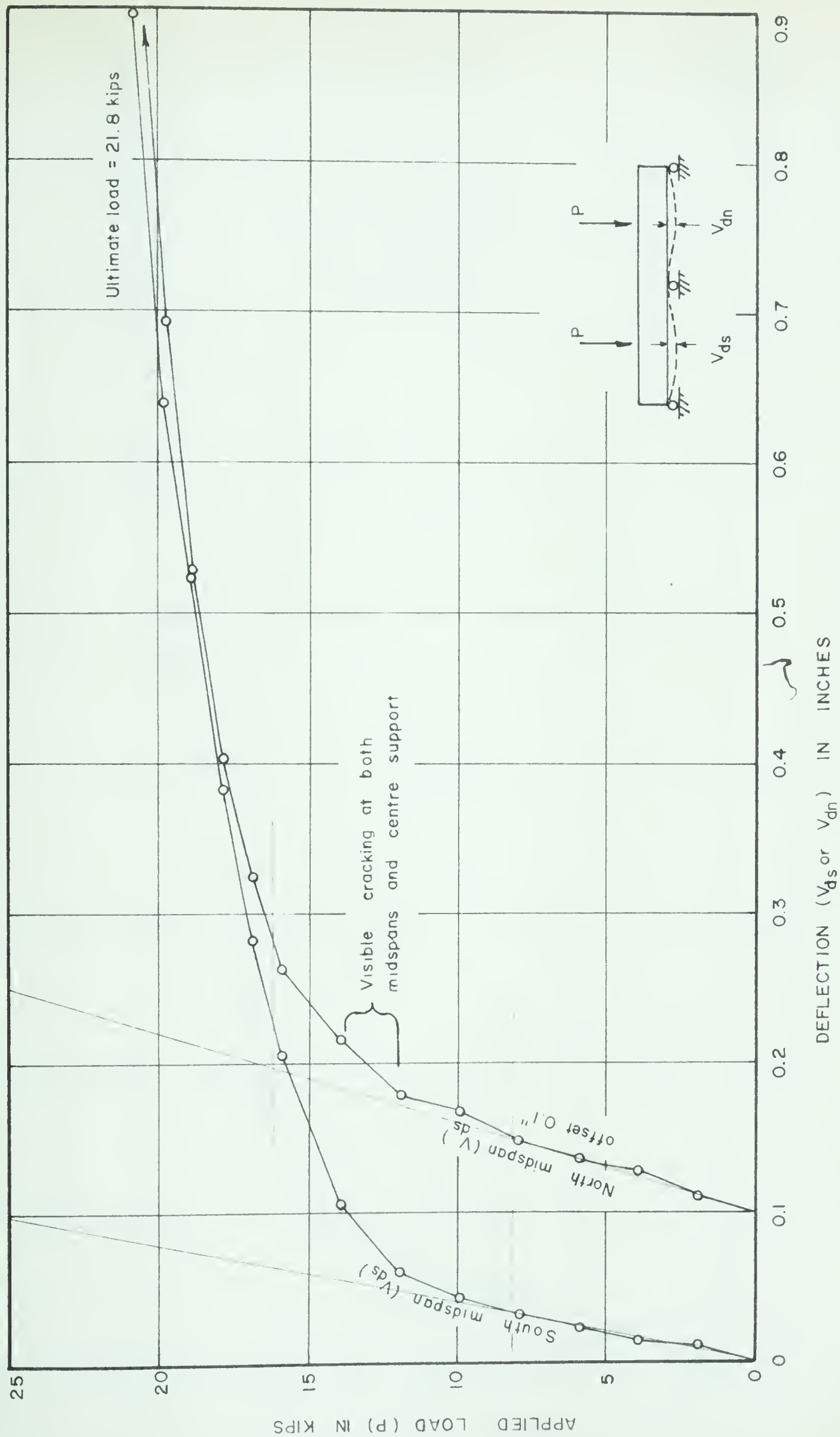


Fig. 7.1 (d) APPLIED LOAD vs VERTICAL DEFLECTION AT MIDSPANS BEAM PO-2



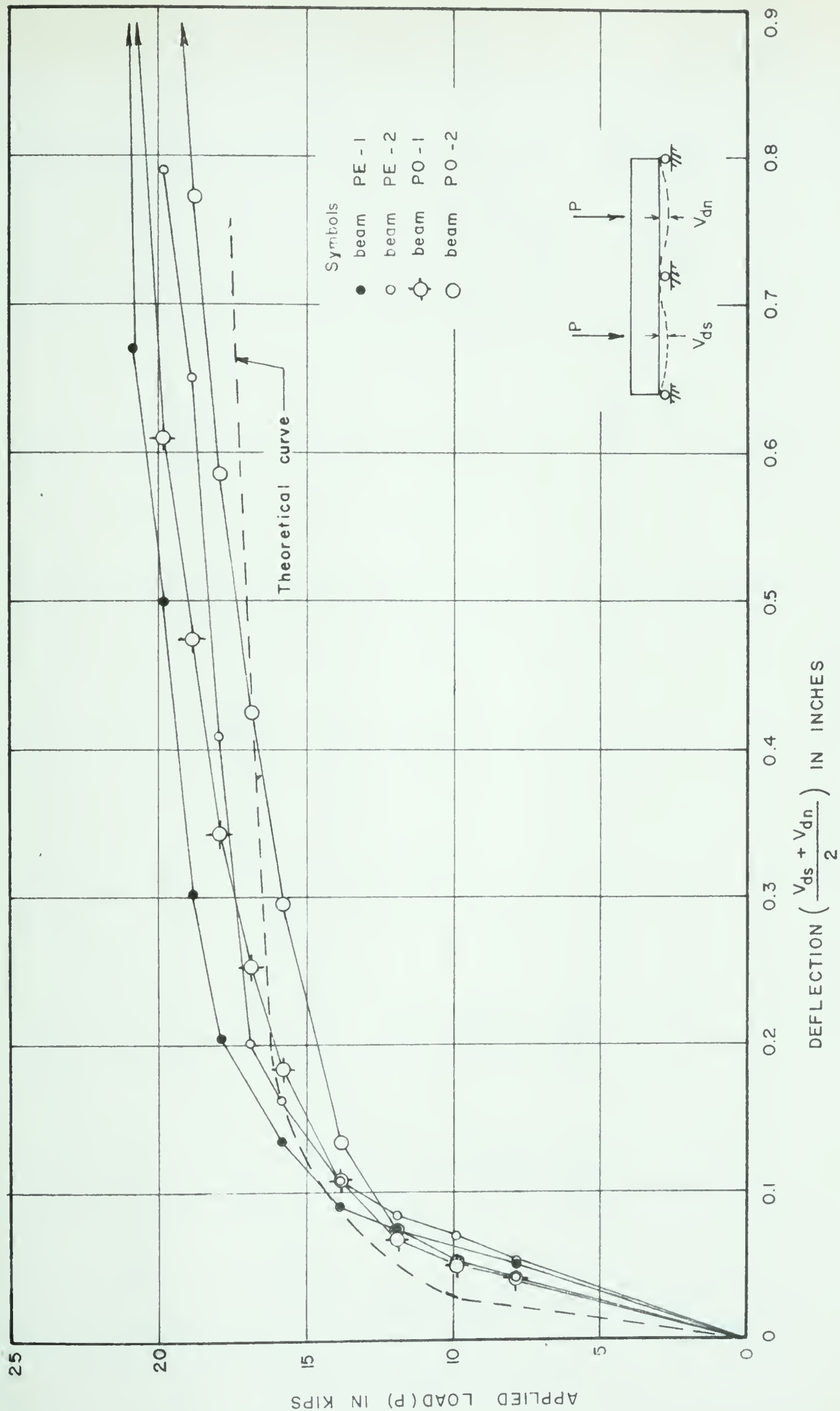


Fig. 7.2 APPLIED LOAD vs AVERAGE VERTICAL DEFLECTION AT MIDSPAN



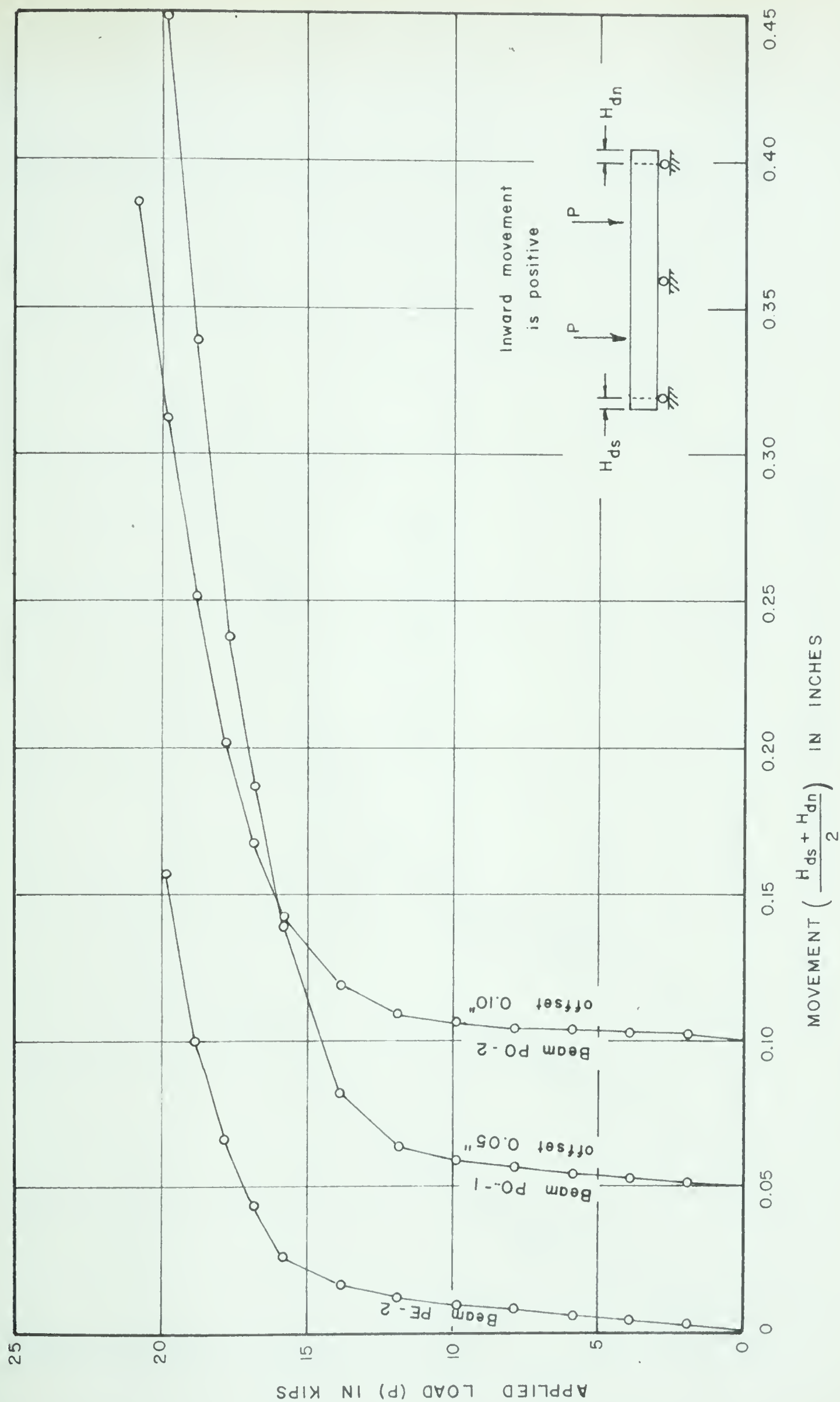


Fig. 2.3 APPLIED LOAD vs AVERAGE SUPPORT MOVEMENT BEAMS PE-2, PO-1 and PO-2









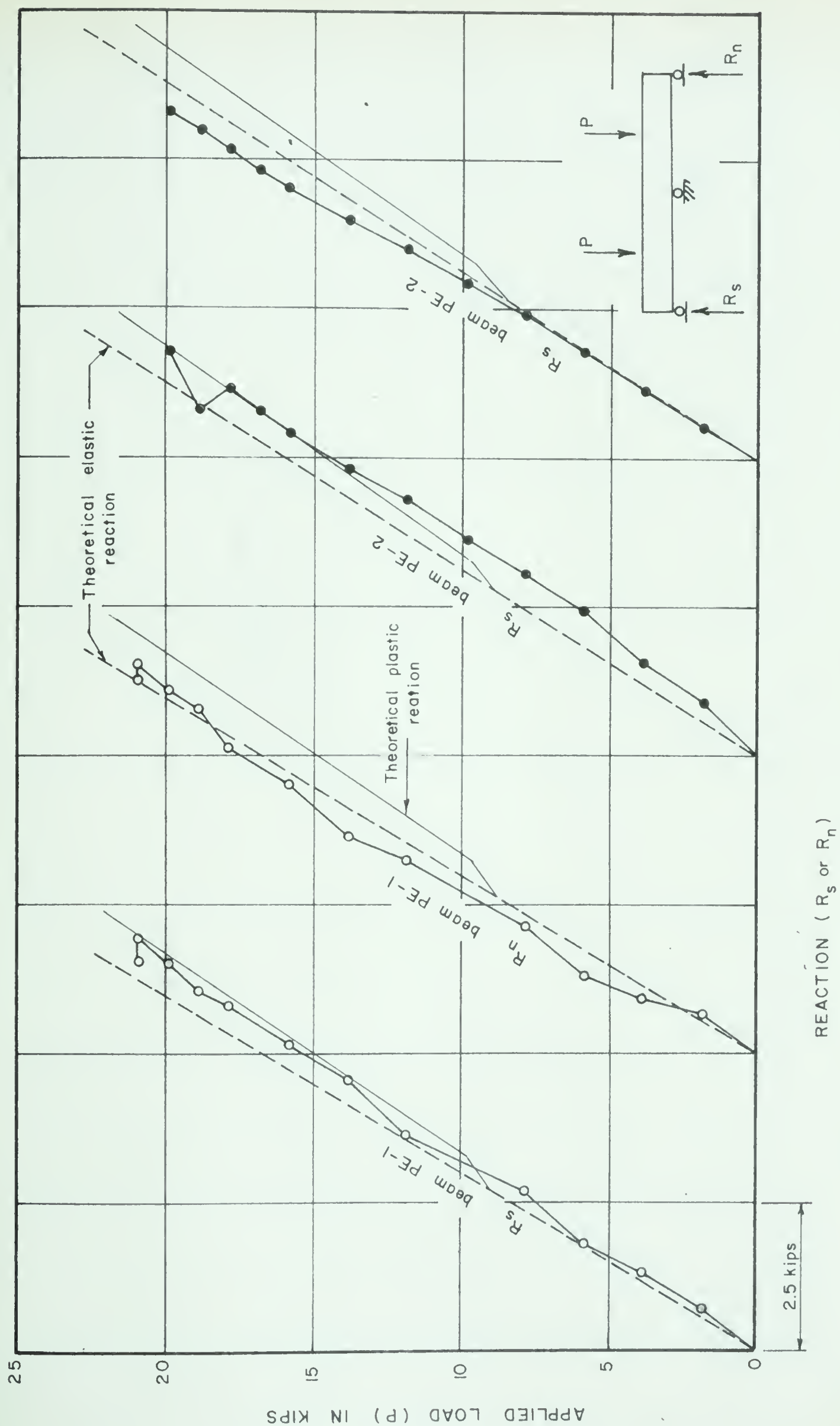


Fig. 7.5 (a) APPLIED LOAD vs END SUPPORT REACTIONS BEAMS PE-1 AND PE-2



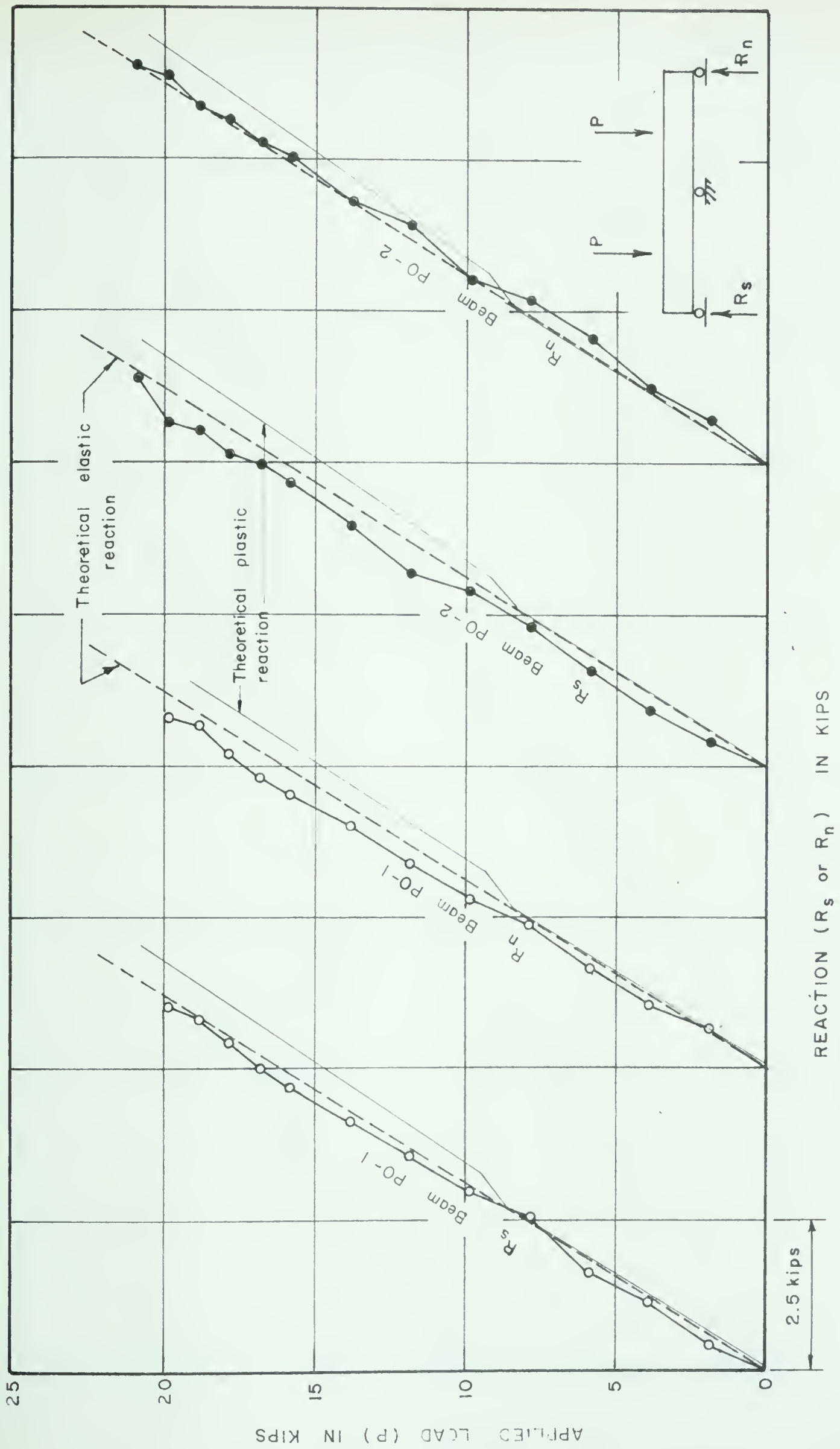


Fig. 7.5 (b) APPLIED LOAD vs END SUPPORT REACTIONS BEAMS PO-1 AND PO-2



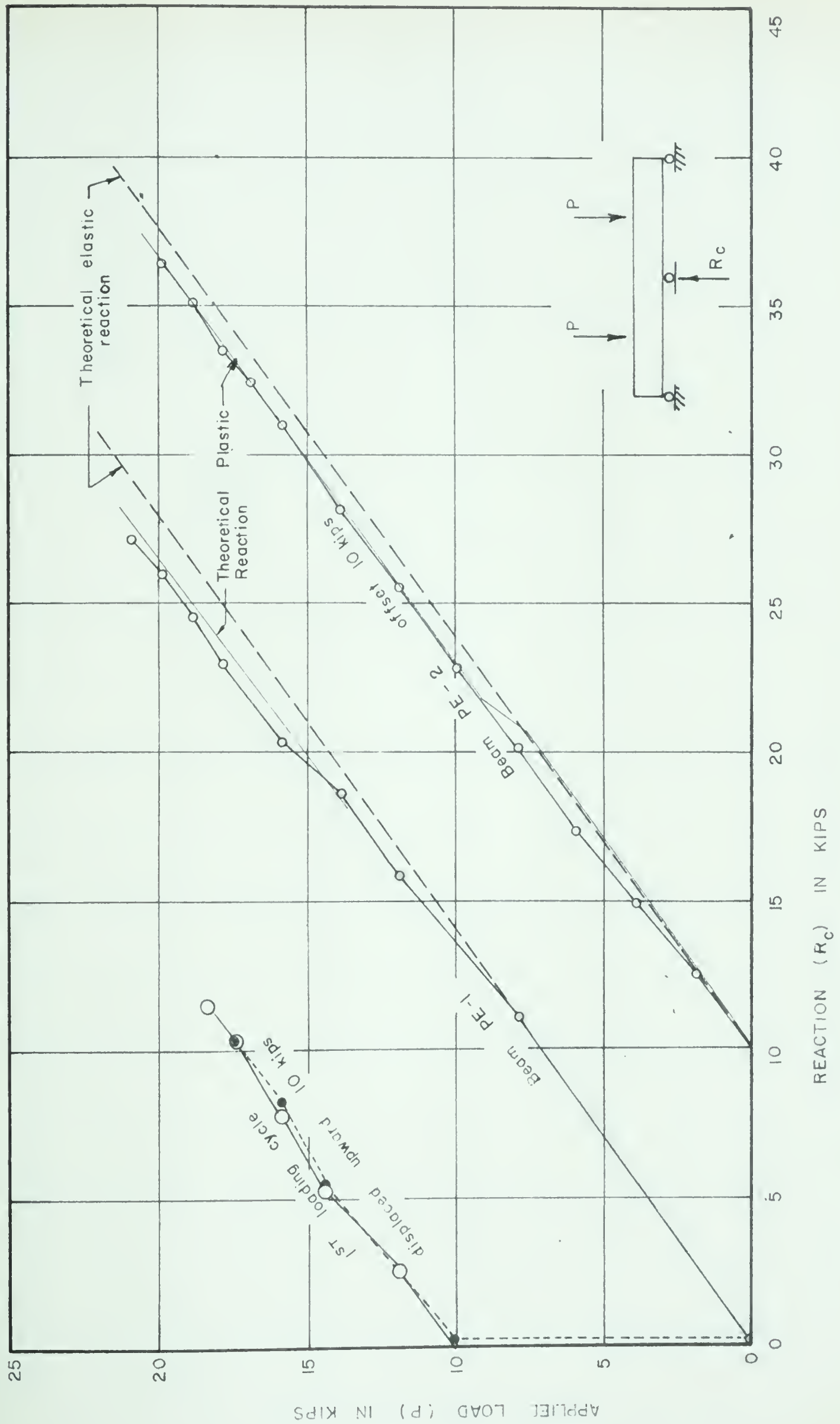


Fig. 7.6 (a) APPLIED LOAD vs CENTRE SUPPORT REACTION BEAMS PE-1 AND PE-2





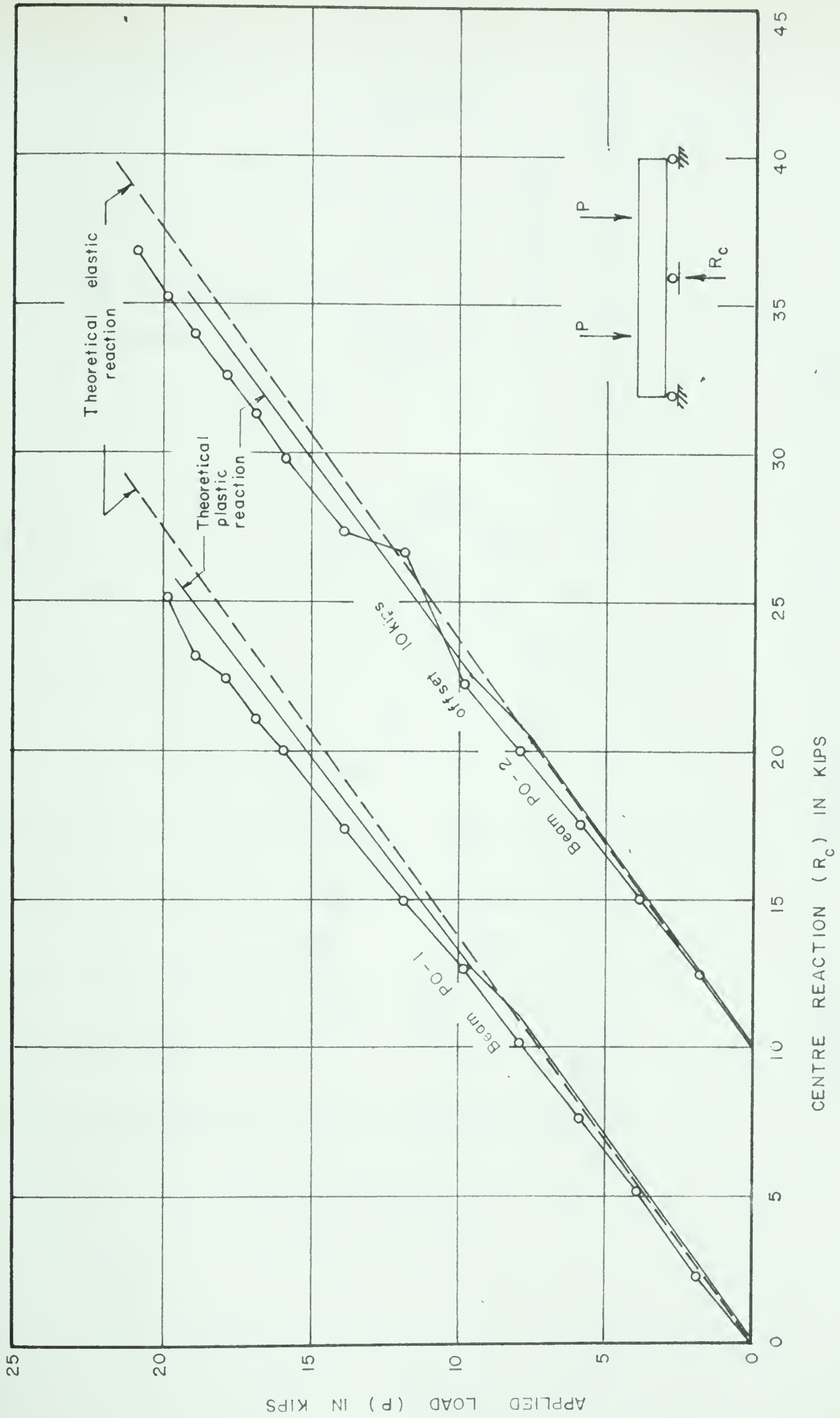


Fig. 7.5 (L) APPLIED LOAD vs CENTRE SUPPORT REACTION BEAMS PO-1 AND PO-2



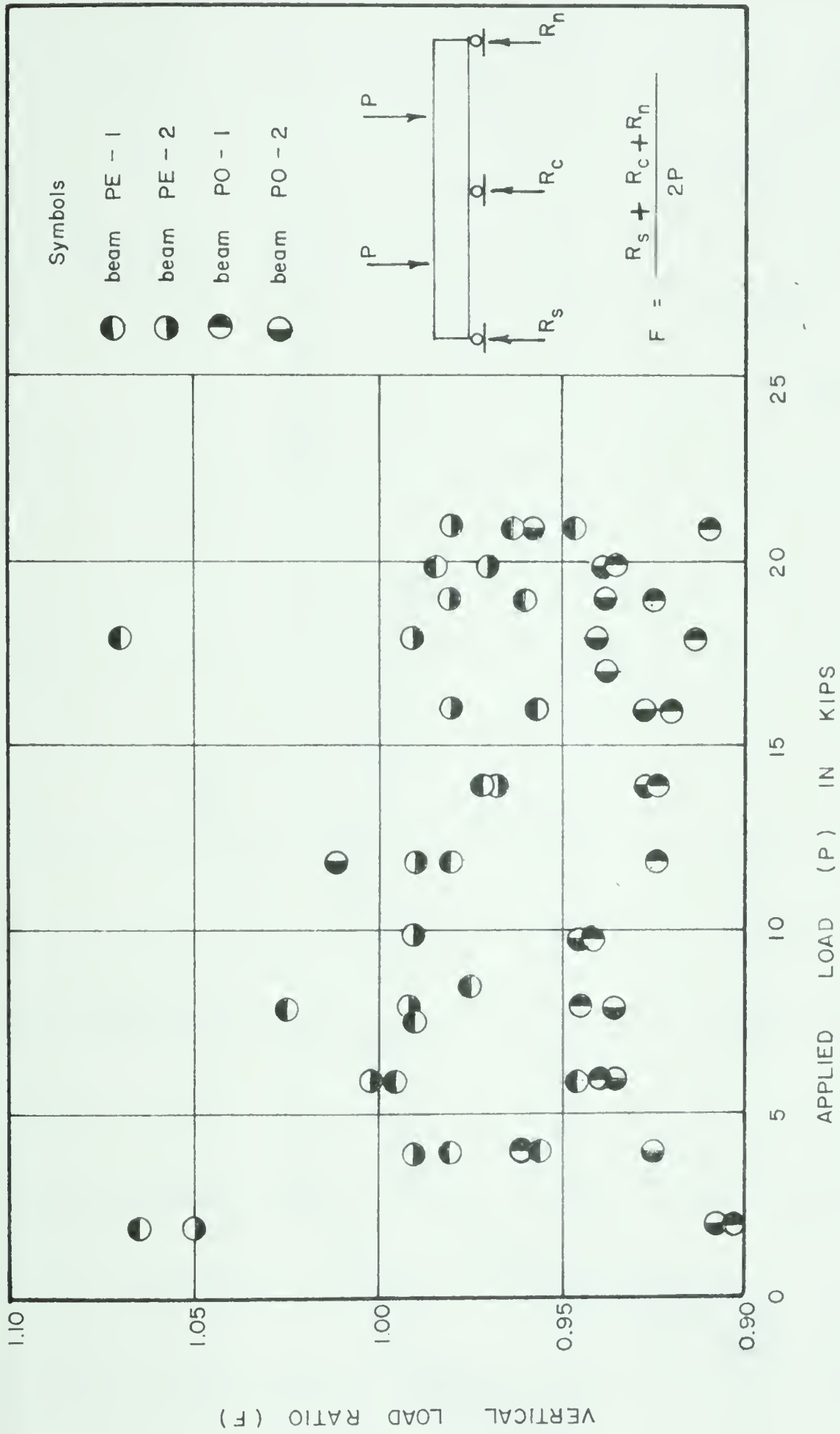


Fig. 3.3 APPLIED LOAD vs VERTICAL FORCE RATIO  
ALL BEAMS



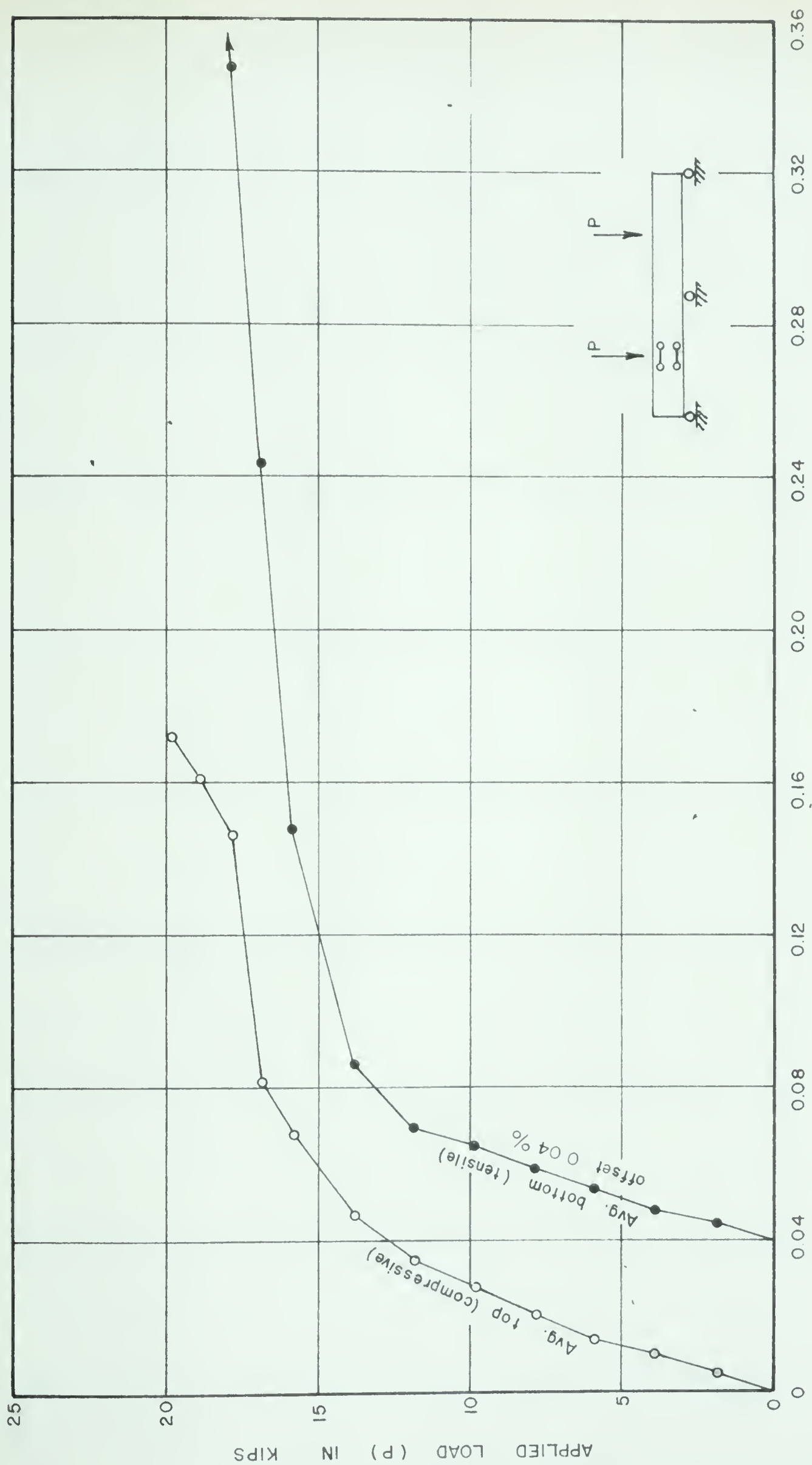


Fig. 7.8 (a) **STRAIN IN PERCENT** **APPLIED LOAD** **VS** **CONCRETE STRAINS** **SOUTH MIDSPAN** **PE-2**





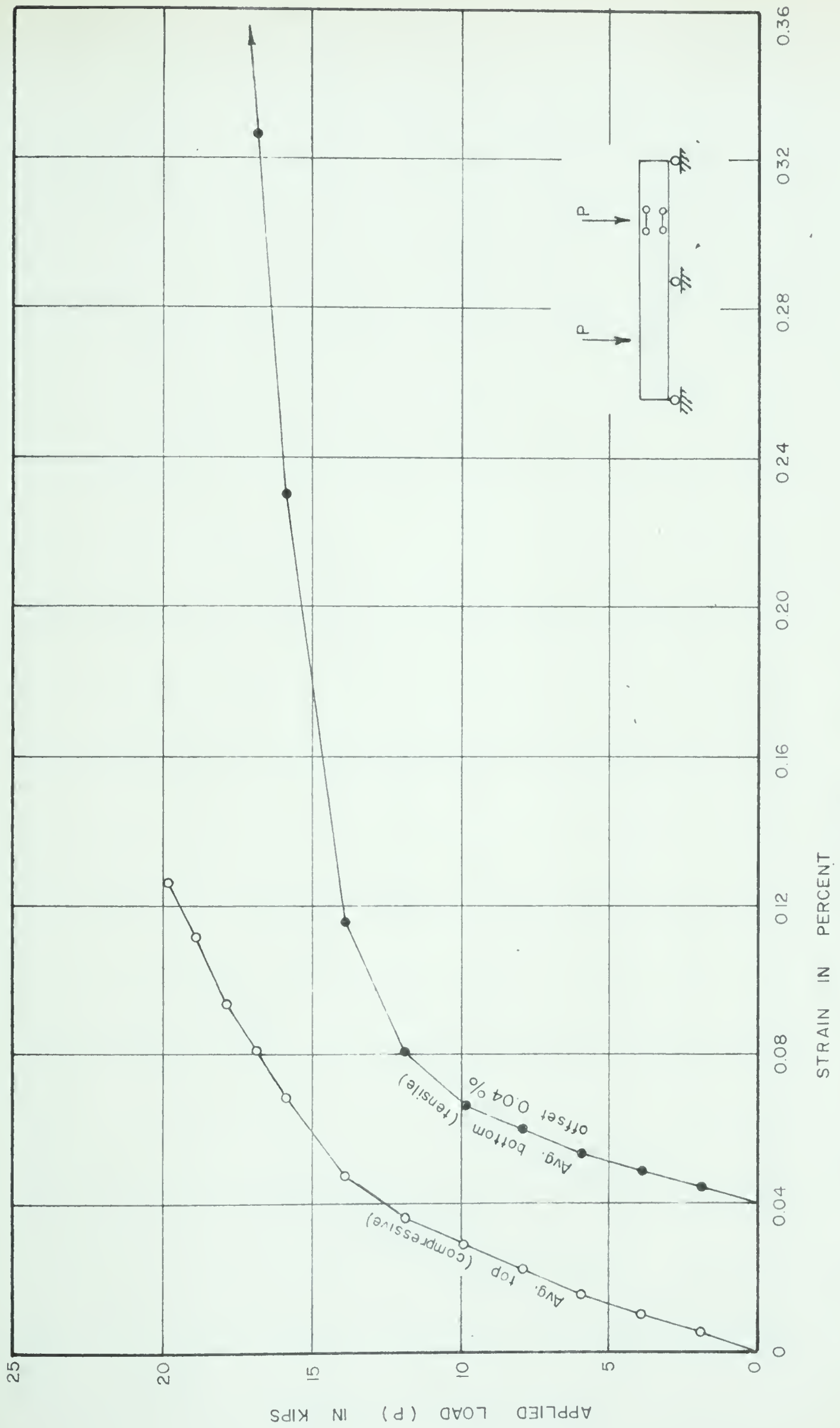


Fig. 7.8 (b) APPLIED LOAD vs CONCRETE STRAINS  
NORTH MIDSPAN BEAM PE-2



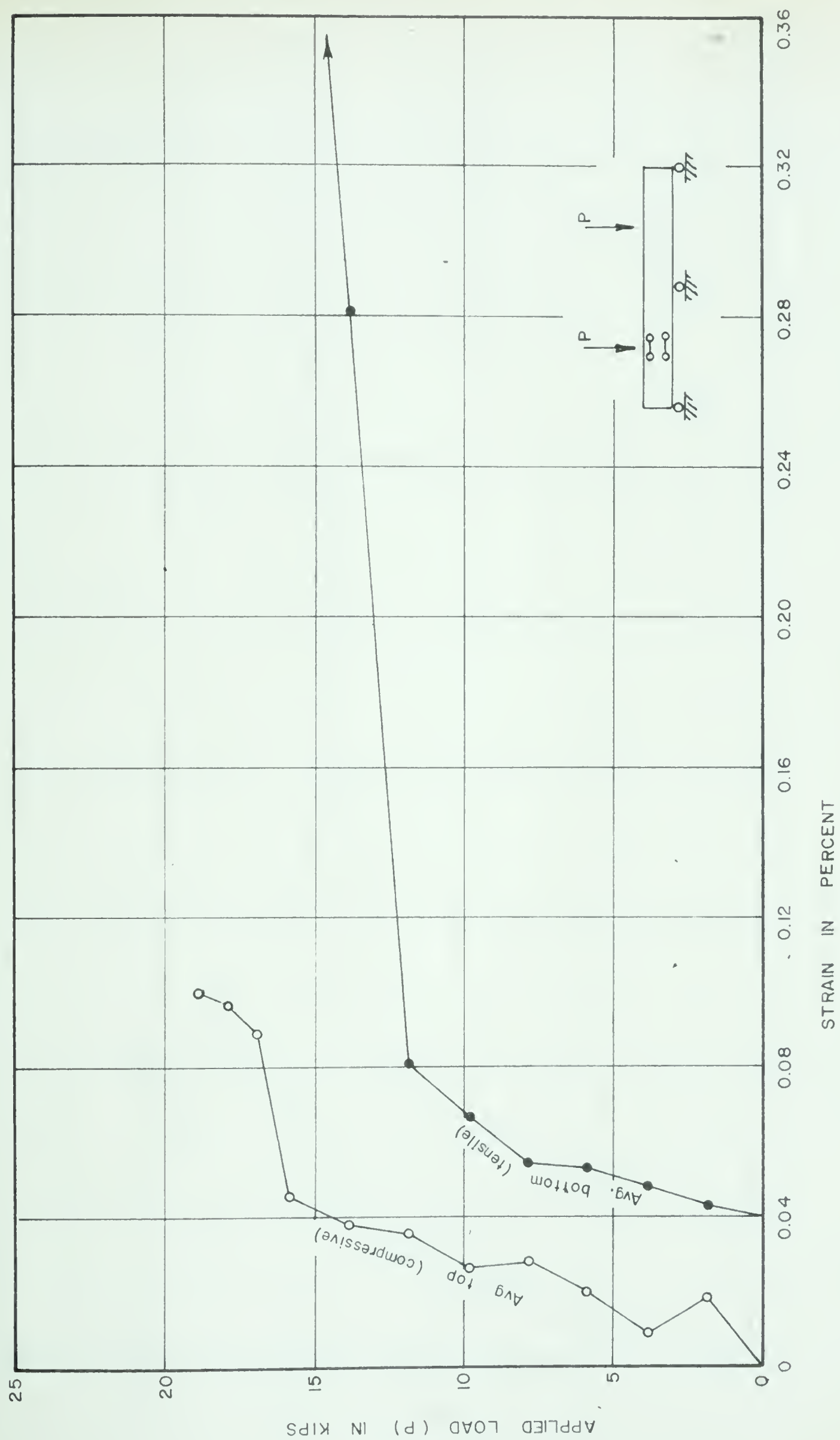


Fig. 7.3 (c) APPLIED LOAD vs CONCRETE STRAINS SOUTH MIDSPAN  
BEAM PO-2



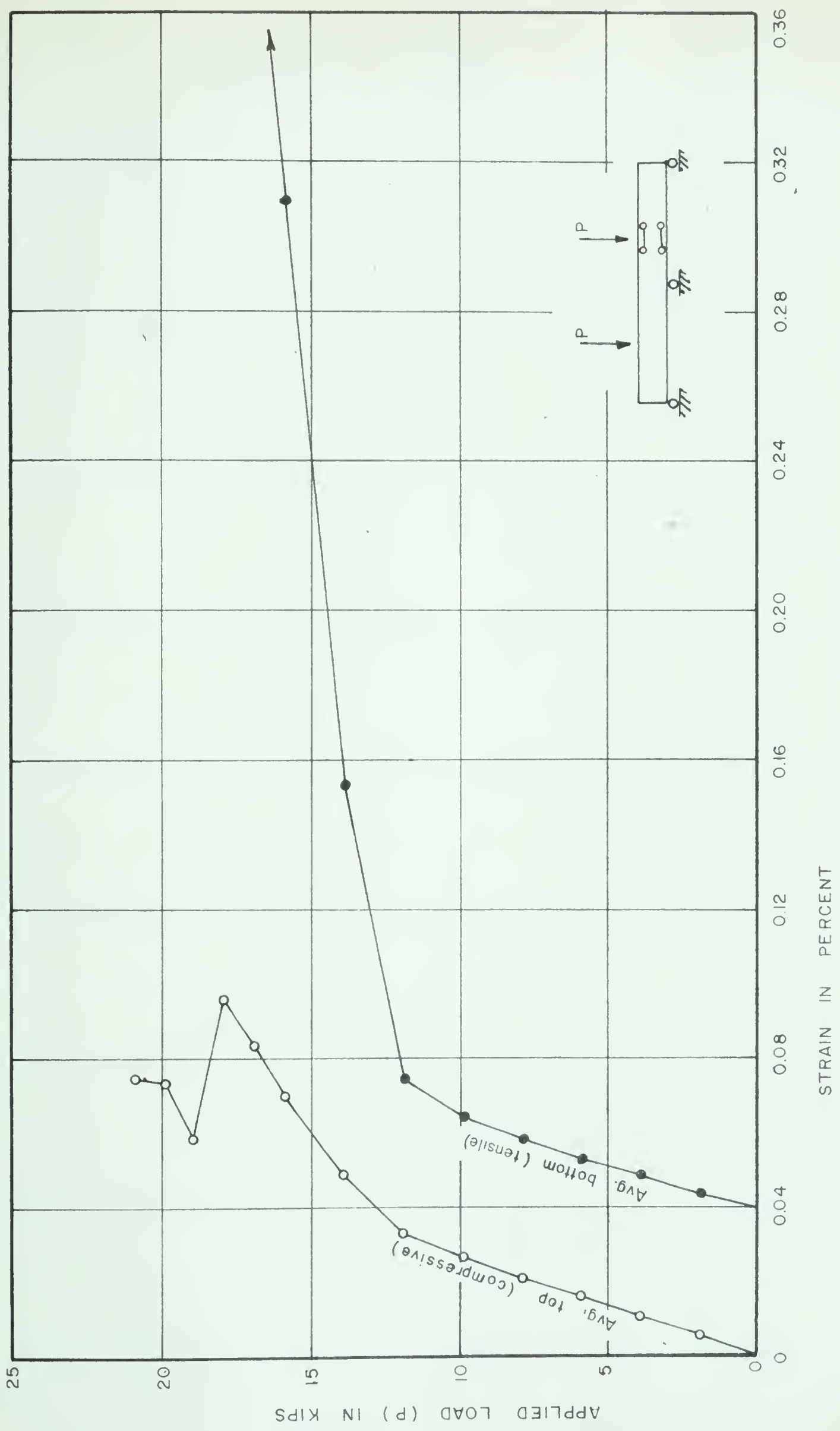


Fig. 7.8 (d) APPLIED LOAD vs CONCRETE STRAIN NORTH MIDSPAN BEAM PO-2



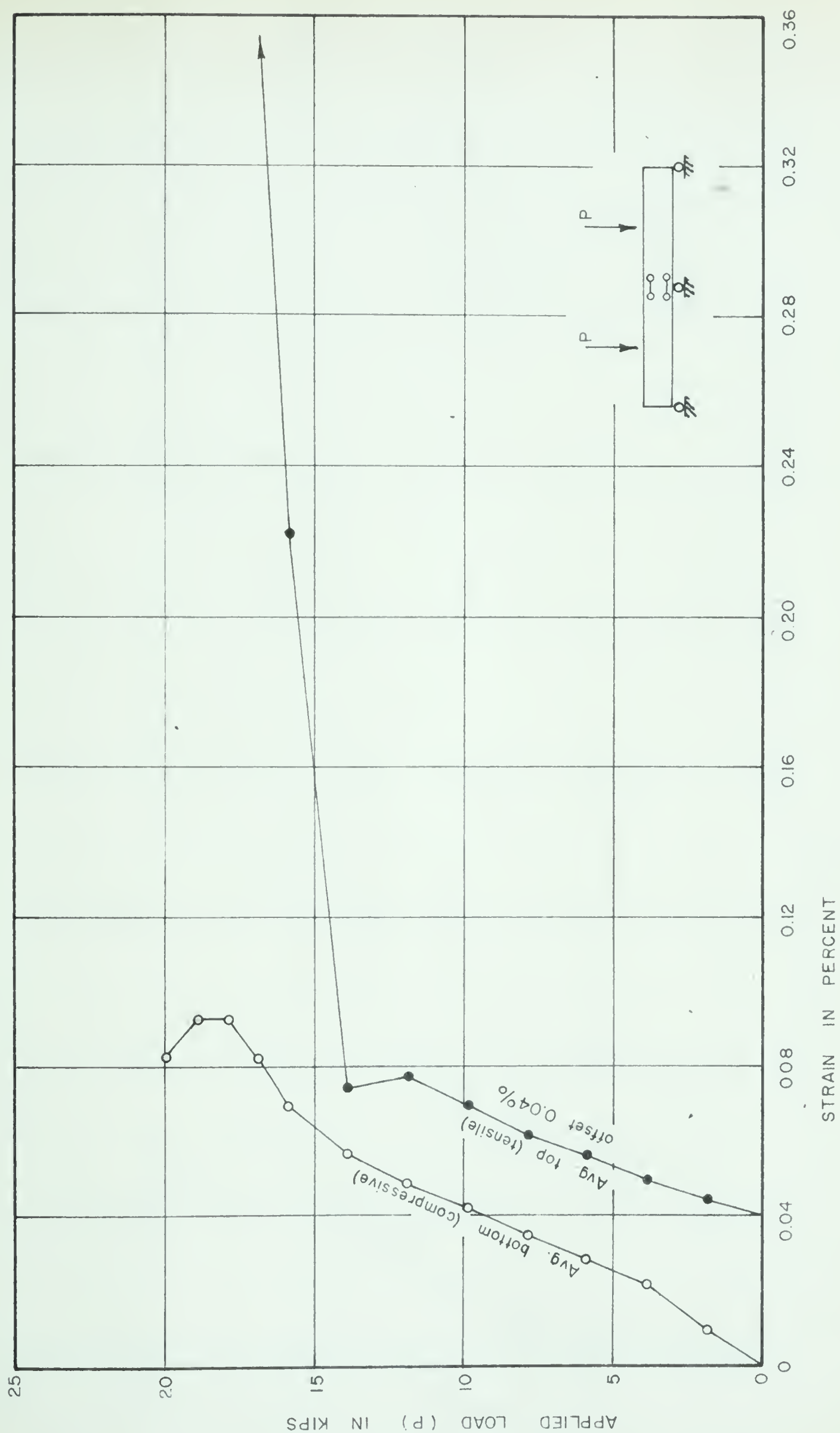


Fig. 7.9 (a) APPLIED LOAD vs CONCRETE STRAINS CENTRE SUPPORT BEAM PE-2





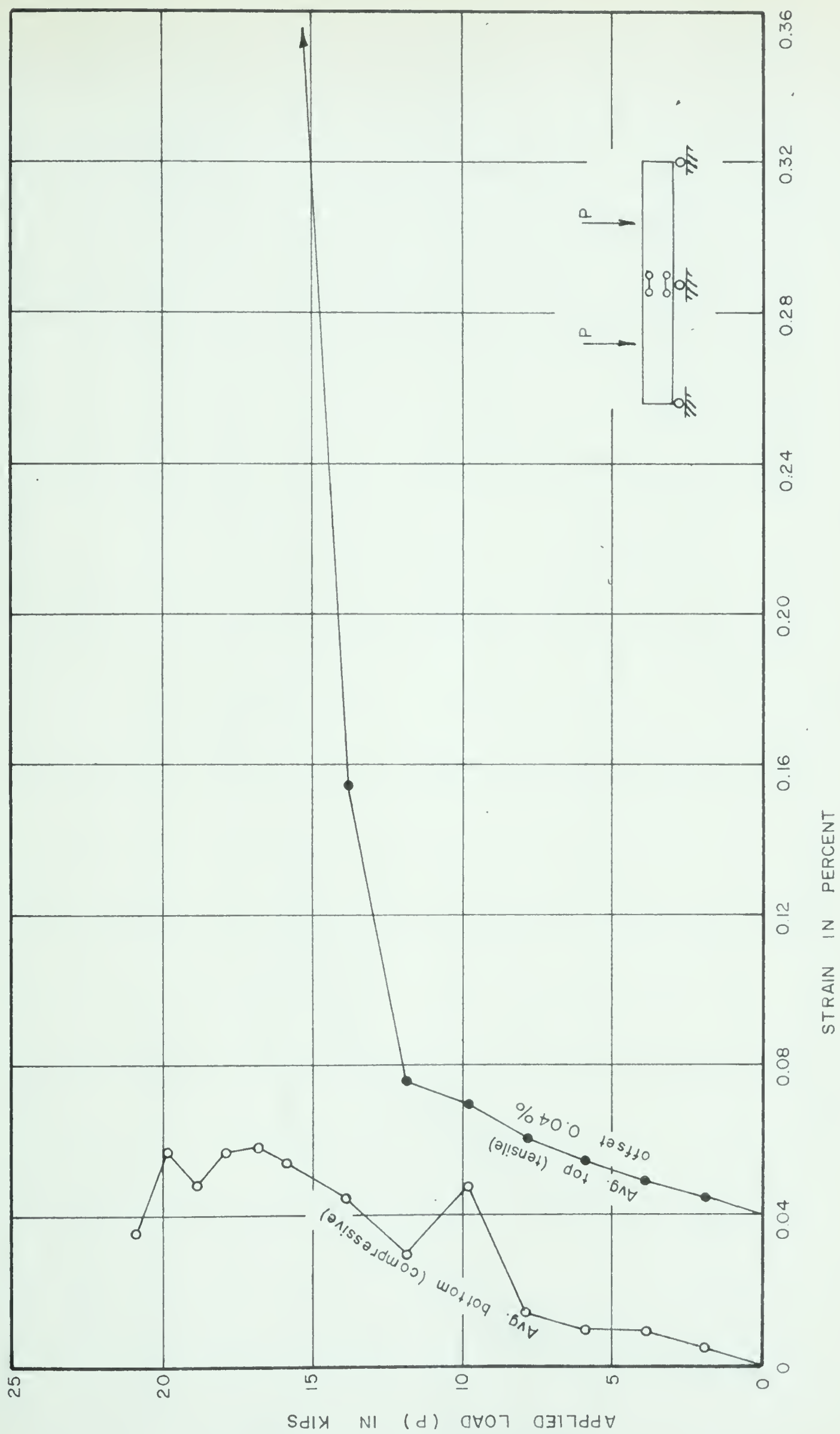


Fig. 7.9 (b) APPLIED LOAD vs CONCRETE STRAINS OVER CENTRE SUPPORT BEAM PO-2



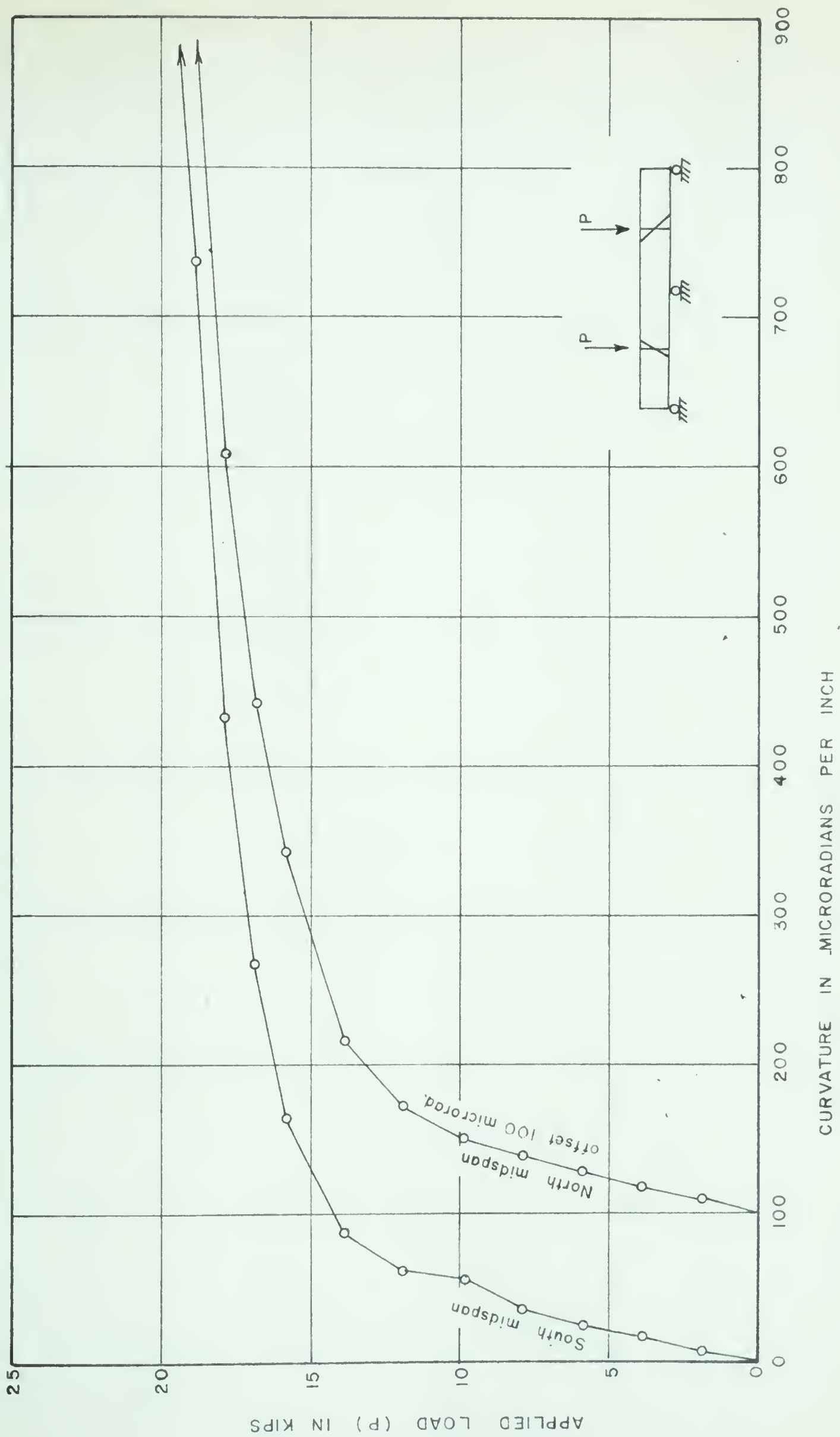


Fig. 7.10 (a) APPLIED LOAD vs CURVATURE AT MIDSPANS BEAM PE-2



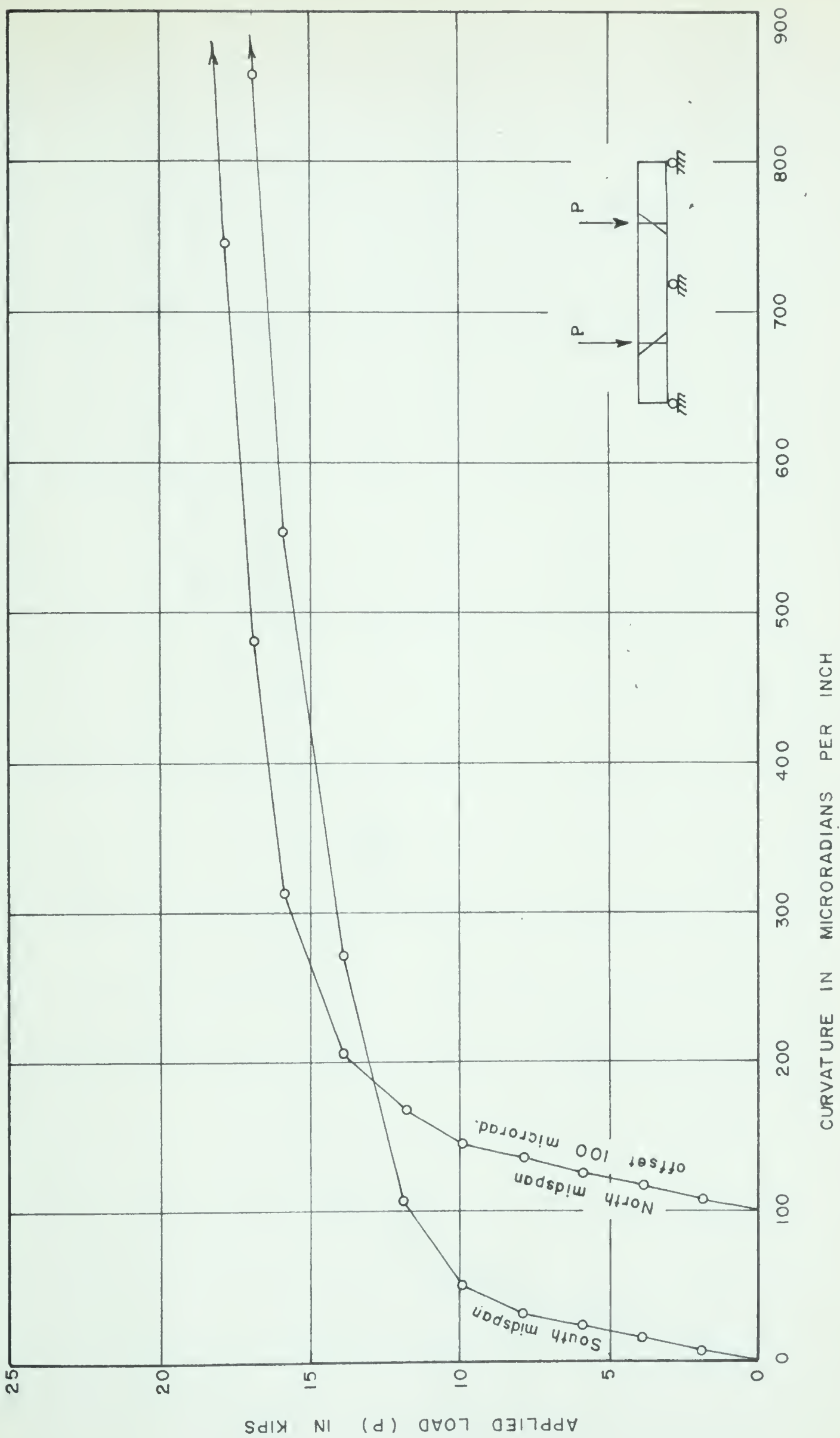


Fig. 7, 10 (b) APPLIED LOAD vs CURVATURE AT MIDSPANS PO-2





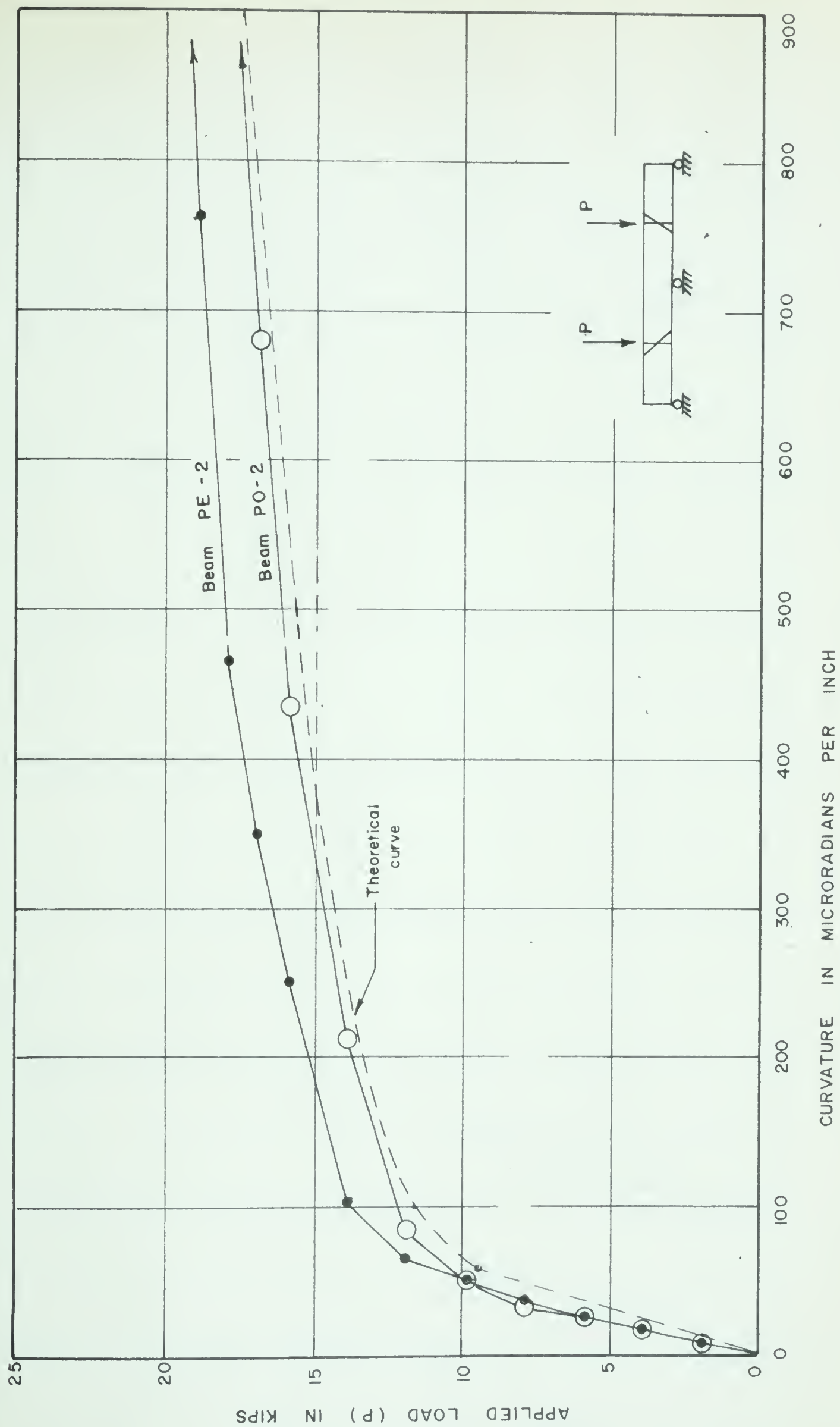


Fig. 7.11 APPLIED LOAD vs AVERAGE CURVATURE AT MIDSPANS BEAMS PE-2 PO-2



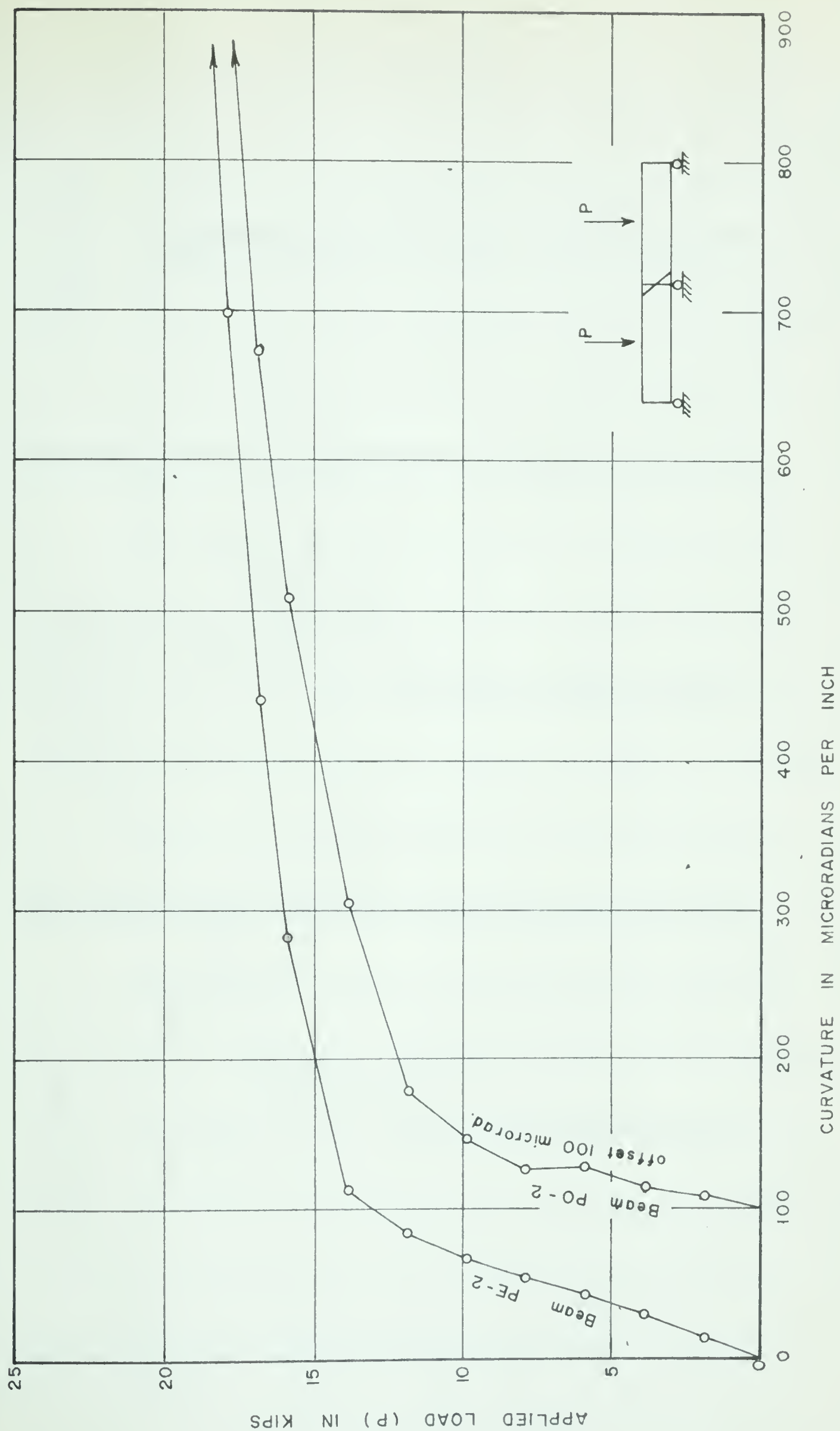


Fig. 7.12 APPLIED LOAD vs CURVATURE AT CENTRE SUPPORT BEAMS PE-2 and PO-2



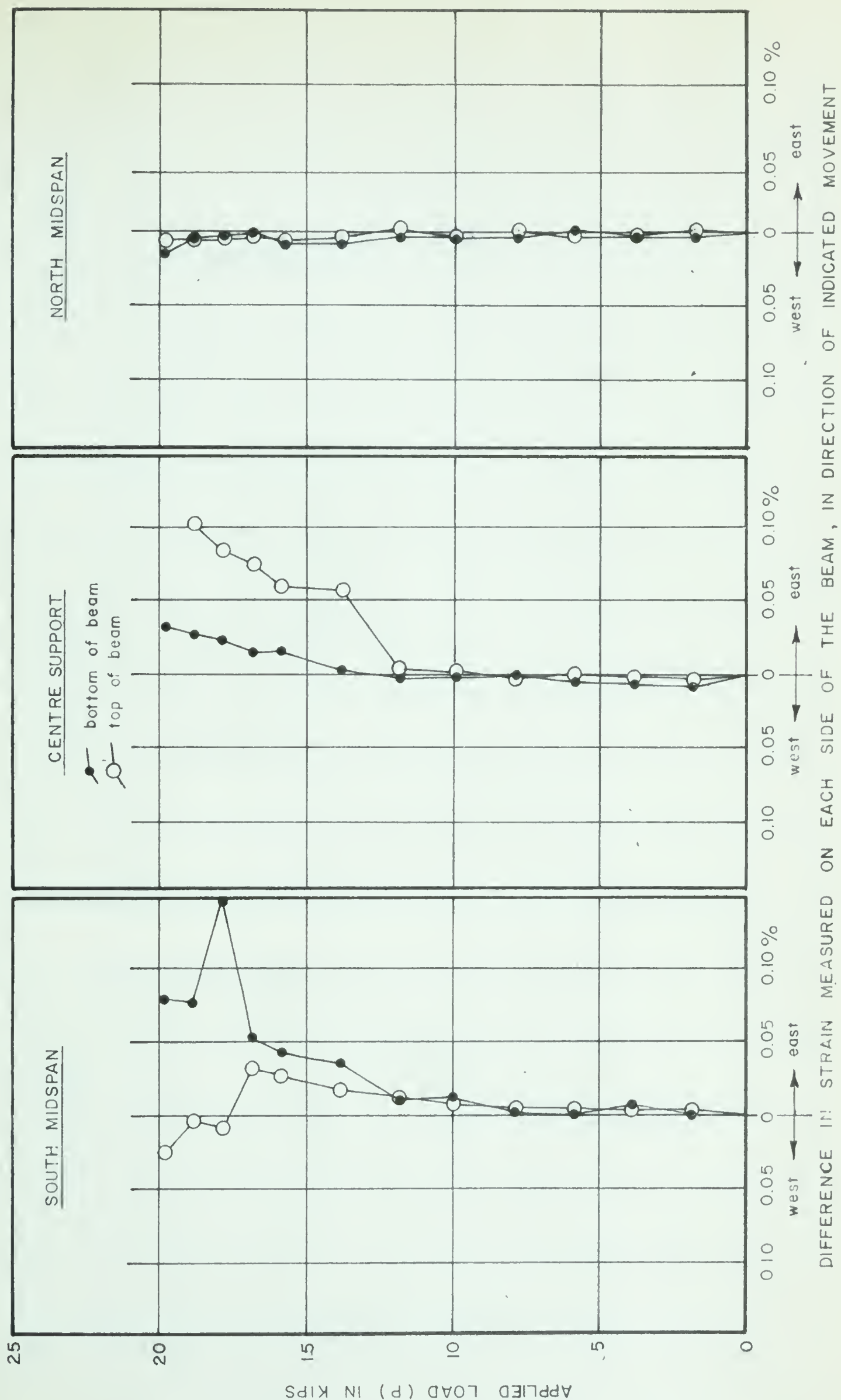


Fig. 7.13 (a) APPLIED LOAD vs DIFFERENCE IN STRAINS BEAM PE-2



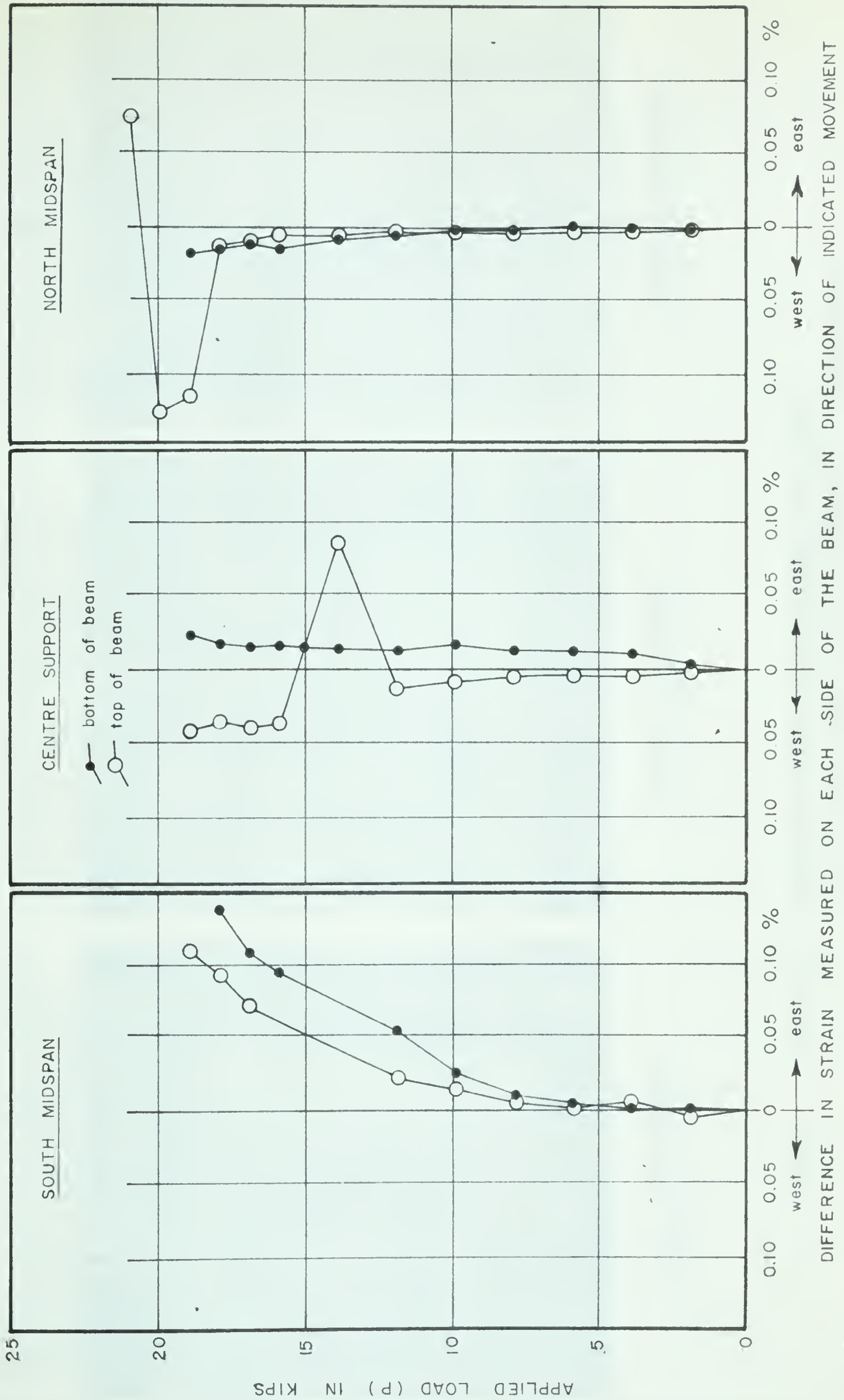
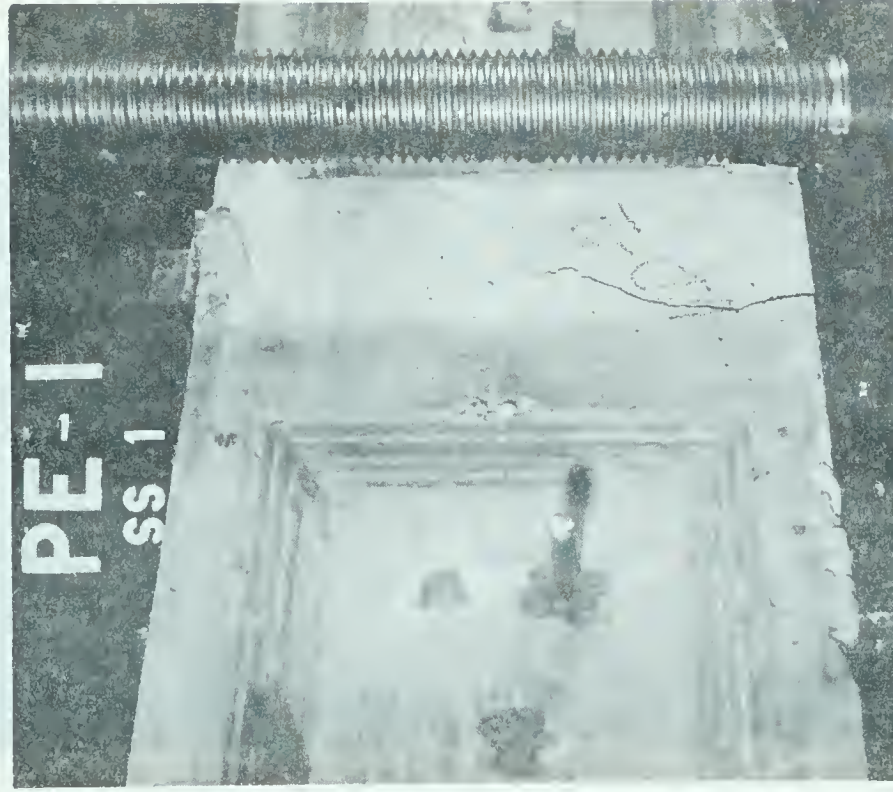


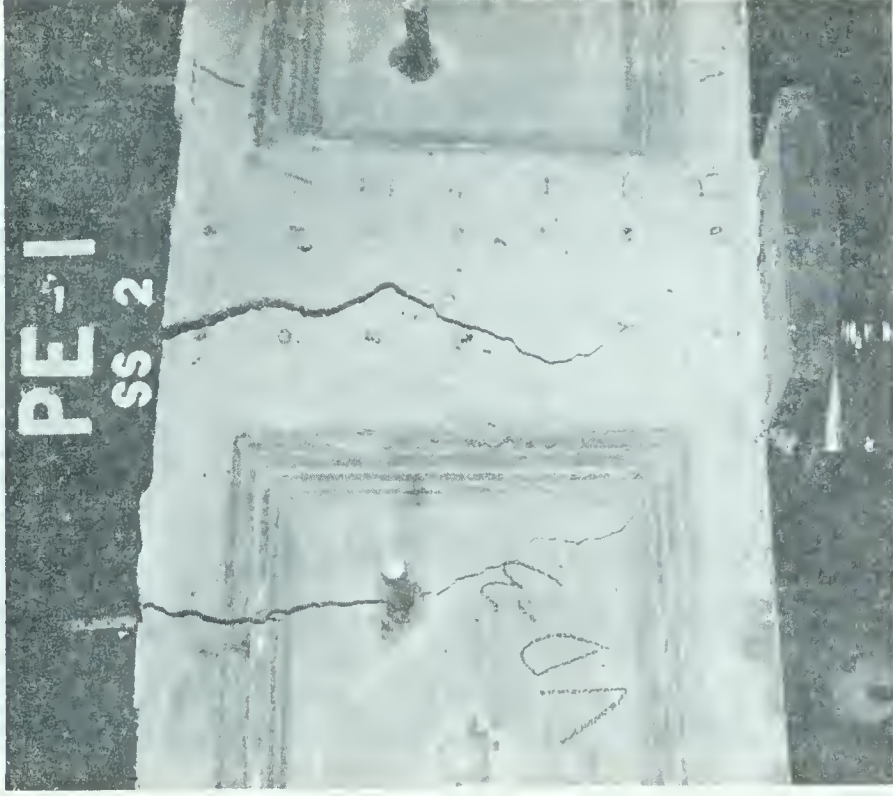
Fig. 7.13 (b) APPLIED LOAD vs DIFFERENCE IN STRAINS BEAM PO-2



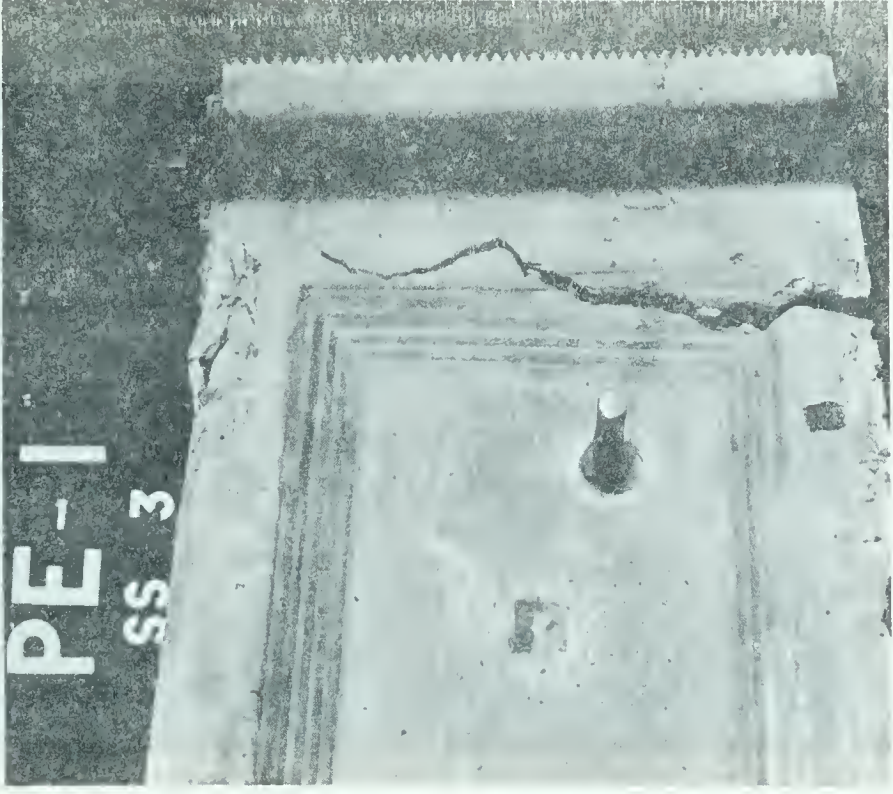




SOUTH MIDSPAN



CENTRE SUPPORT

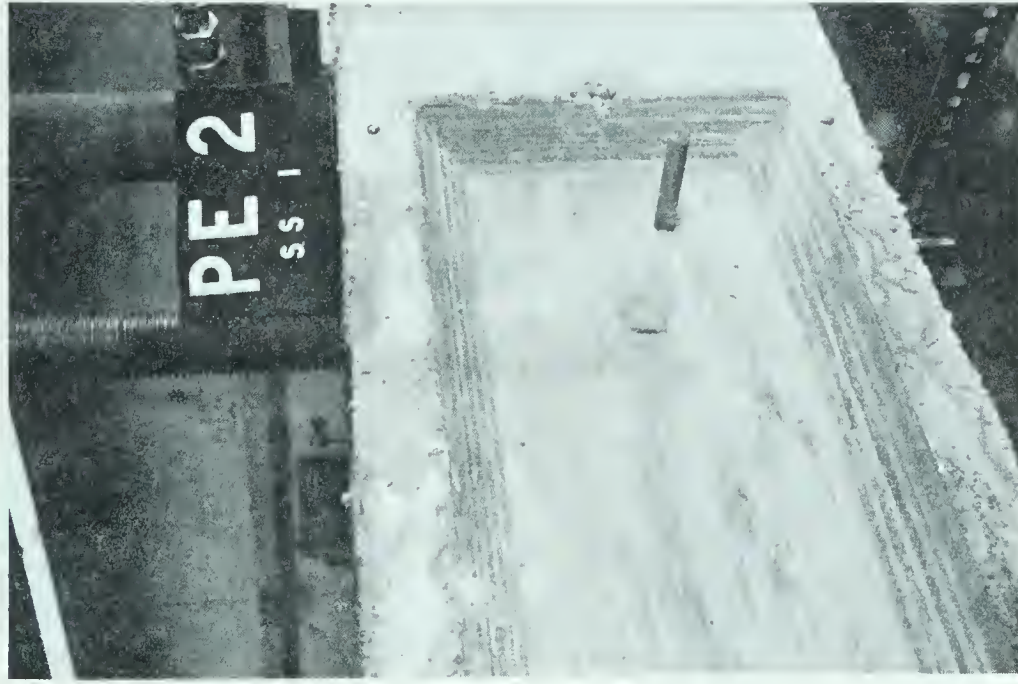


NORTH MIDSPAN

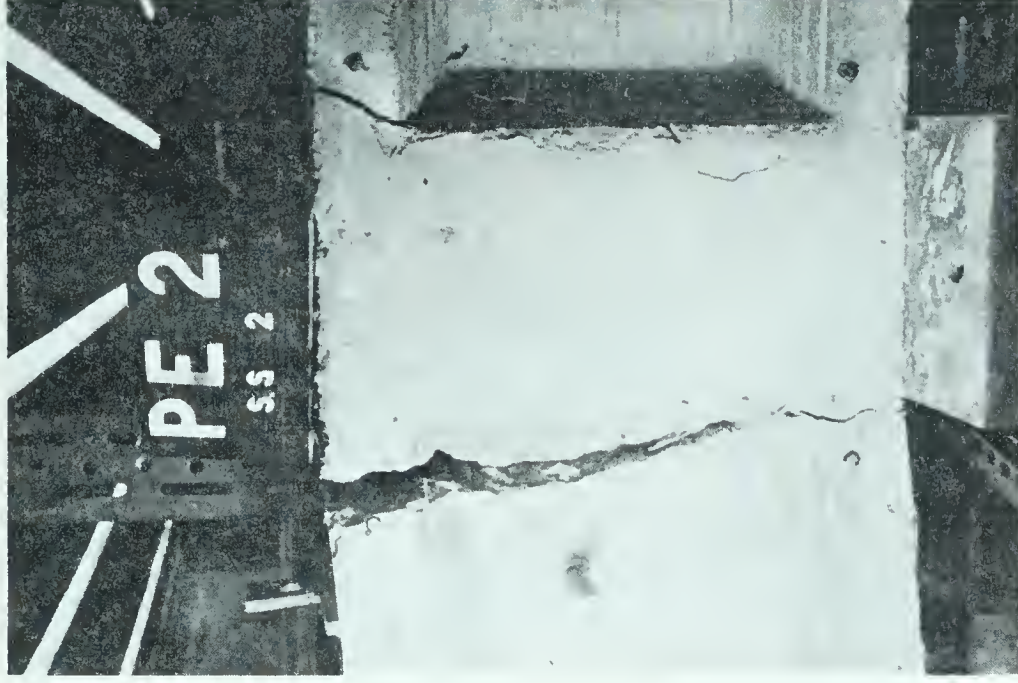
FIG. 7.14 (a) PHOTOGRAPHS OF BEAM AFTER FAILURE  
AT MIDSPAN AND CENTRE SUPPORT - BEAM PE-I







SOUTH MIDSPAN



CENTRE SUPPORT

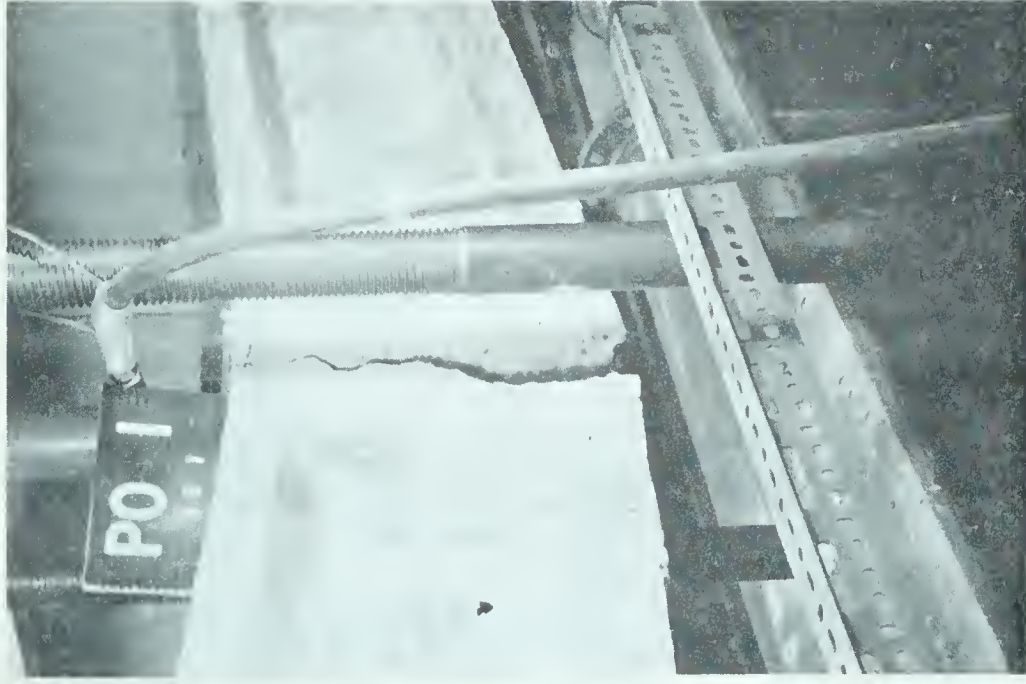


NORTH MIDSPAN

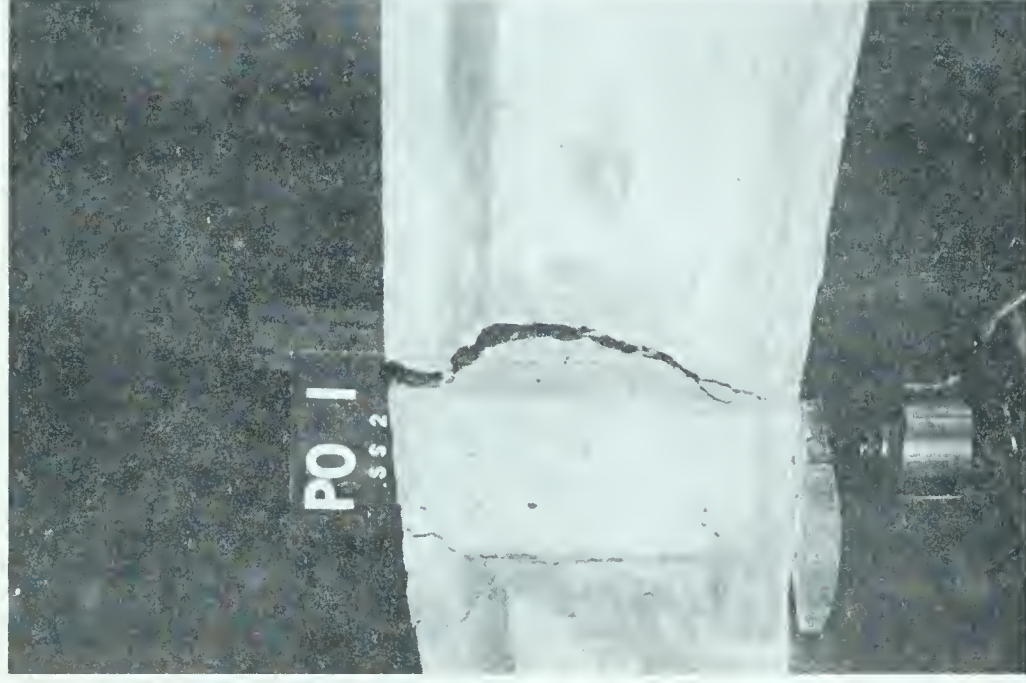
FIG. 7.14 (b) PHOTOGRAPHS OF BEAMS AFTER FAILURE  
AT MIDSPAN AND CENTRE SUPPORT - BEAM PE-2



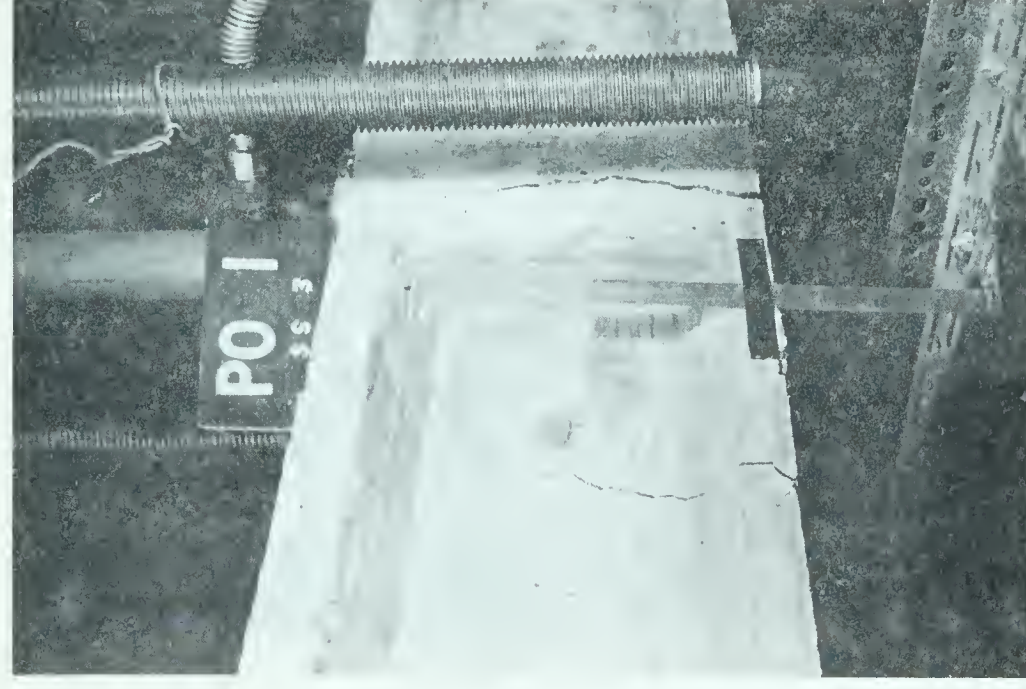




SOUTH MIDSPAN



CENTRE SUPPORT

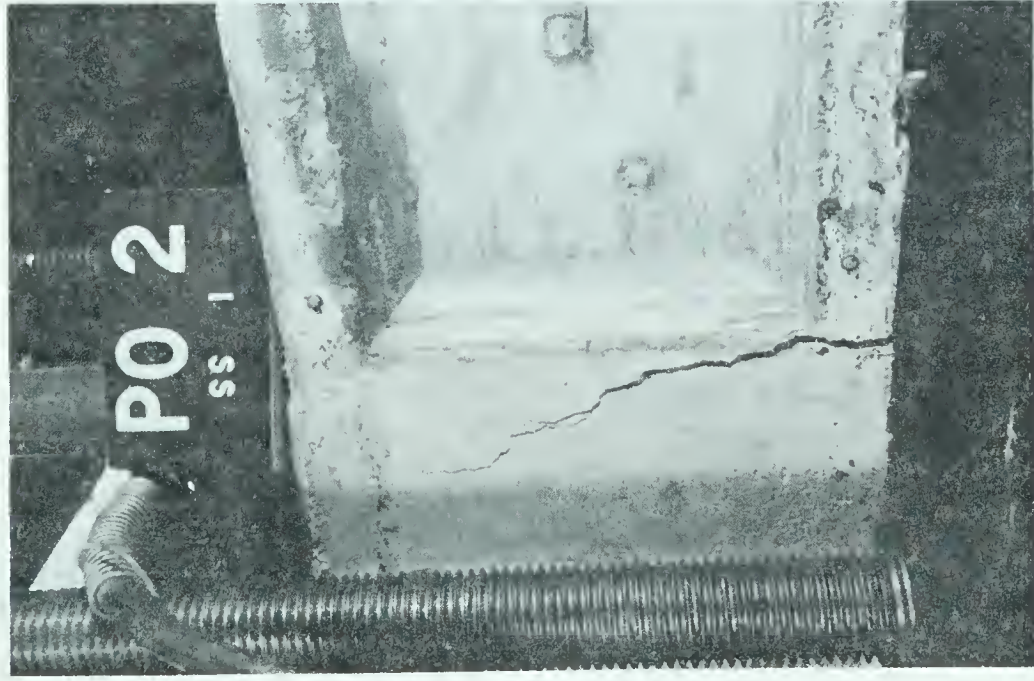


NORTH MIDSPAN

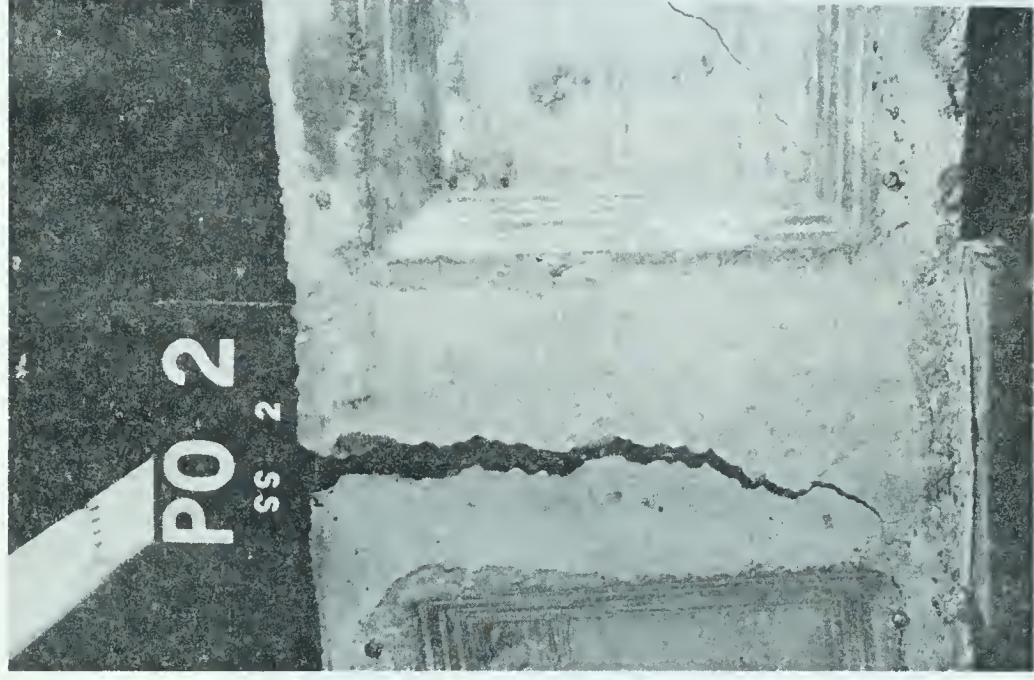
FIG. 7.14 (c) PHOTOGRAPHS OF BEAMS AFTER FAILURE  
AT MIDSPAN AND CENTRE SUPPORT - BEAM PO-1



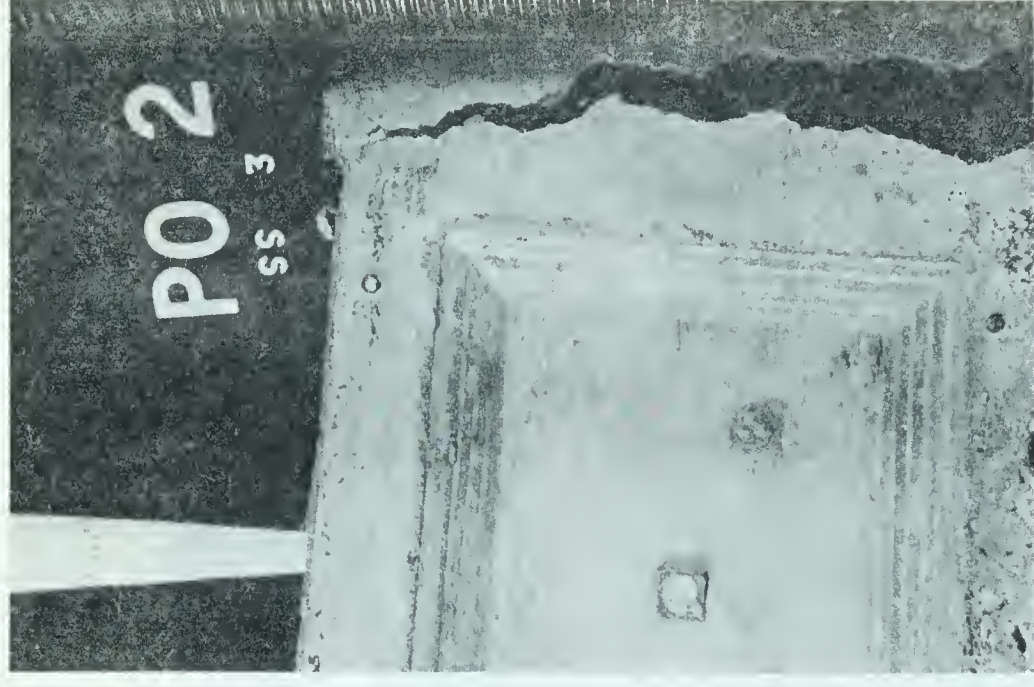




SOUTH MIDSPAN



CENTRE SUPPORT

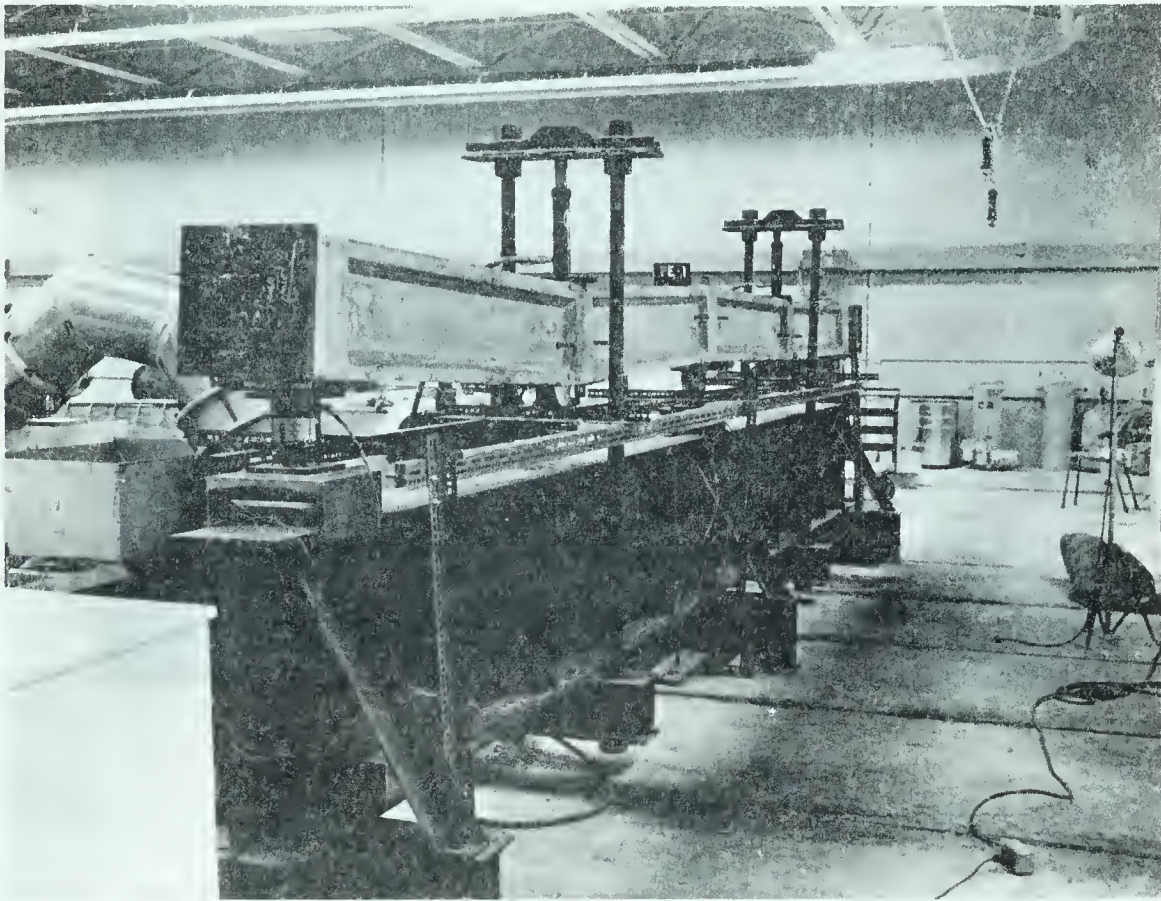


NORTH MIDSPAN

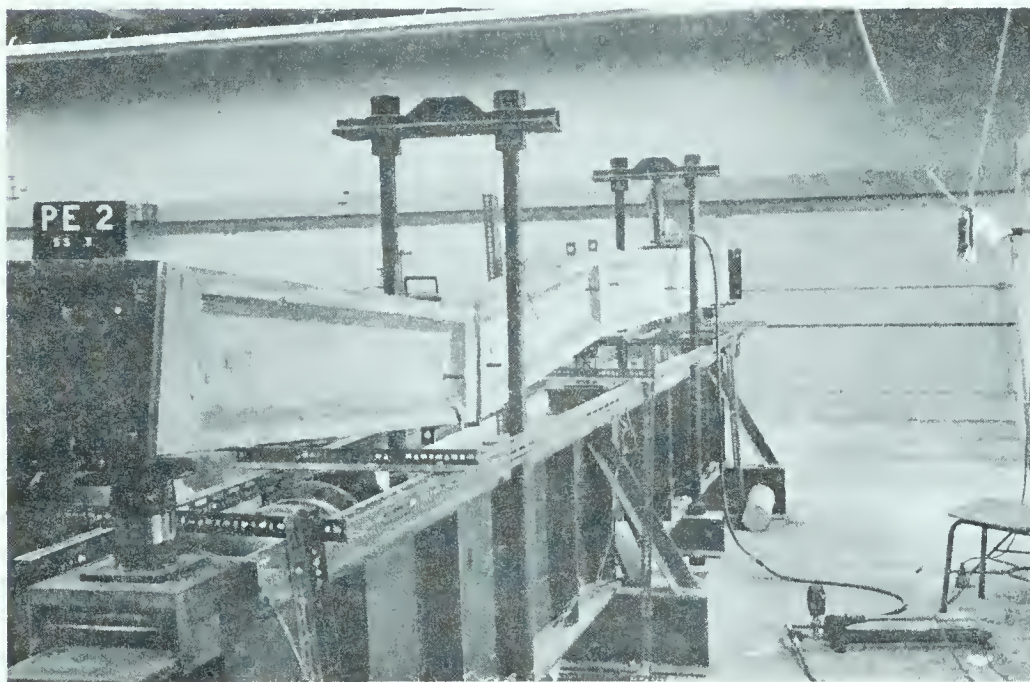
FIG. 7. 14 (d) PHOTOGRAPHS OF BEAMS AFTER FAILURE  
AT MIDSPAN AND CENTRE SUPPORT - BEAM PO-2







BEAM PE-1



BEAM PE-2

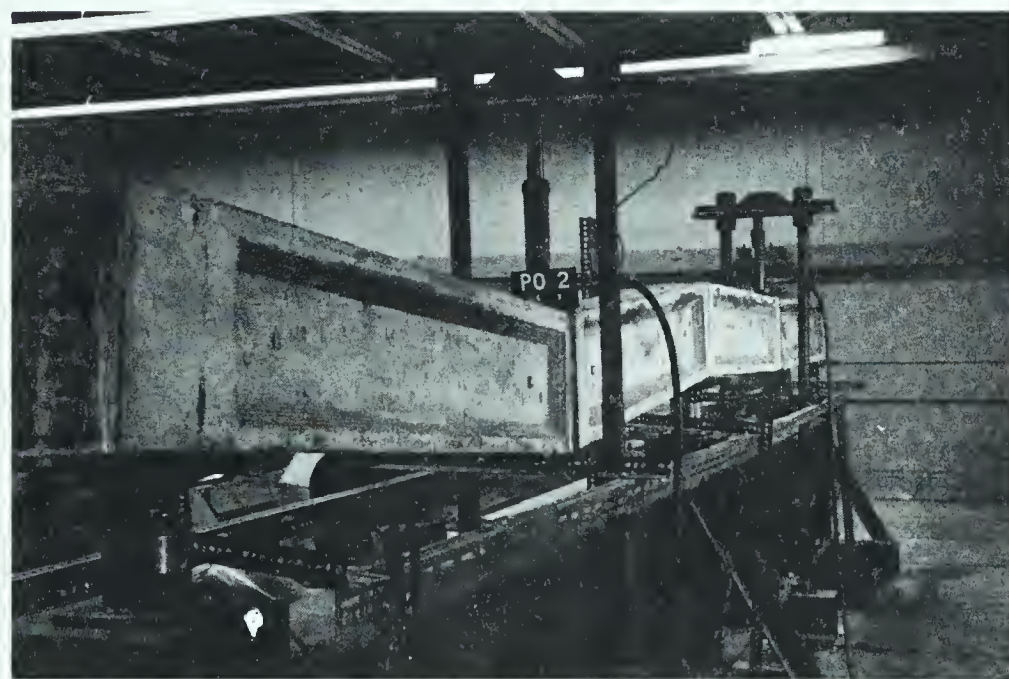
FIG. 7.15 (a) PHOTOGRAPHS OF BEAMS AFTER FAILURE







BEAM PO-1



BEAM PO-2

FIG. 7.15 (b) PHOTOGRAPHS OF BEAMS AFTER FAILURE



## CHAPTER VIII

### DISCUSSION

#### 8.1 MATERIAL PROPERTIES

##### (a) Steel

The stress-strain relationship for the two cylinders shown in FIGURE 6.2 are very similar. However for sample No. 1, larger stains were obtained in the yield zone. This is not necessarily an indication of variations in the properties of the steel but rather reflects the skill in "catching" the large strain readings just before fracture of the sample. The elastic modulus of  $28.4 \times 10^3$  k.s.i. agrees favorably with values obtained in previous tests on similar wire.

No tests were performed on the 3/8" diameter deformed mild steel web reinforcement as it was anticipated that the web reinforcement would have a minor effect on the performance of the test beams.

##### (b) Concrete and Grout

The modulus of elasticity of the concrete was measured by determining the slope of a line drawn through the origin, and the strain at a stress of 2.0 k.s.i., on the stress-strain relationship for the 28-day job cured concrete cylinder (FIGURES 6.1 (a) (b) (c) (d)). The value of  $E_c$  indicated on the graph is the average value for the curves plotted on that graph. The average value of  $E_c$  for the eleven cylinders tested was  $4.0 \times 10^3$  k.s.i.





The cylinder strengths of the concrete cylinders are presented in TABLE VI-1. The strengths of cylinders cured in the moist room were, in general, slightly higher than those of the job cured cylinders. This indicated that the concrete in the beams was cured under good conditions. The average cylinder strength of all the 28-day job cured cylinders was 5900 p.s.i. This average value was reduced to 5600 p.s.i. when the cylinder strength of cylinders cast with Beam PE-1 were ignored.

Various empirical formulae relating the elastic modulus to cylinder strengths have been devised by many investigators. Two such formulae are as follows:

- (1) The Building Code of the American Concrete Institute (15)

$$E_c = w^{1.5} 33 \sqrt{f'_c}$$

where  $w$  is the density of the concrete in pounds per cubic foot.

Hence

$$E_c = 145^{1.5} \times 33 \times 5900 = 3.82 \times 10^3 \text{ k.s.i.}$$

- (2) Hawkins (1)

$$E_c = \frac{30,000}{6 + \frac{10,000}{f'_c}} = \frac{30,000}{6 + \frac{10,000}{5900}} = 3.9 \times 10^3 \text{ k.s.i.}$$

The values obtained in this investigation were in reasonable agreement with the preceding empirical values. No relationship between  $E_c$  and  $f'_c$  was established from values obtained in this investigation due to the small number of cylinders tested and a limited range of  $f'_c$ .



The cylinder strengths of the grout (TABLE VI-1) indicated that the strength of the grout was considerably less than the strength of the concrete at the time of the test. It was difficult to evaluate the effect that this had on the performance of the post-tensioned beam. However it should be noted that, when these beams were demolished after testing, the grout was observed to be well packed in the cable duct and around the prestressed reinforcement.

## 8.2 PREDICTED BEHAVIOR OF THE TEST BEAMS

The theory, summarized in Chapter II, was utilized for comparison, of the actual and theoretical behaviour of the test beams. Load-deflection and load-curvature relationships were established for a hypothetical beam. This beam had the same dimensions and tendon profile as the pretensioned beams, and was constructed of concrete having a cylinder strength of  $f'_c = 5600$  p.s.i. and a modulus of elasticity,  $E_c = 4.0 \times 10^3$  k.s.i. However, as the flexural cracking loads were very dependent on the modulus of rupture of the concrete, these loads were calculated for each individual beam. No tensile tests were performed, and the relationship  $f_r = 6 \sqrt{f'_c}$  (11) was adopted for the modulus of rupture of the concrete.

The adaptation of the theory in predicting the performance of the test beams was complicated because the beams were rectangular for a length of six inches in the regions of maximum bending moment, and the tendon profile, though draped, was not linear between regions of maximum bending moment. Where the stresses and strains on a single vertical section were calculated, the properties of the shape and the position of the steel at that section were utilized. Prediction of the ultimate





moment required that the value  $k_d$  be computed for the length of beam along the inclined crack. This length included both the rectangular and I section. At the top of the inclined crack a rectangular section existed and the value  $k_u d$  was computed on this basis. One of the necessary simplifications in the development of the expressions for calculating the variations in  $k_d$  at sections away from the top of the inclined crack, (equation 7), was that the value  $k_2$  be considered a constant. The largest possible variation in  $k_2$  on a rectangular section is from  $1/3$  to close to  $1/2$ . Hawkins (1) suggests the value of 0.40. On an I section the value of  $k_2$  can vary from a value greater than  $1/3$  to close to  $1/2$ . Hence, for the beams in this investigation, the value  $k_2 = 0.42$  was assumed to exist along the inclined crack.

Another simplification necessary in the development of equation (7), was that the line of action of the tensile force, at the inclined crack, must intersect the line of action of the tensile force at the flexural crack. That is, the tendon profile must be straight for the length of the inclined crack. This was not true for the beams tested in this investigation. Therefore the angle  $\beta$  in equation (7) was taken as the angle made by a line intersecting the steel centroid at the edge of the bearing plate, and at the predicted inclined crack. This had the effect of neglecting a force equal to  $A_s f_s$  multiplied by the tangent of the angle of drape at inclined crack minus assumed angle of drape which acts in the same direction as the doweling force.

The web reinforcement did not cross the first inclined crack and so had no effect on the calculation of the ultimate moment. However Hawkins (1) points out the possibility of a second inclined crack forming





a distance  $d/2$  outside the first inclined crack. The occurrence of a possible second inclined crack was ignored in the calculation because (a) the first inclined crack was predicted to occur at a relatively high load (78% of the ultimate load), (b) a stirrup intersected the possible second inclined crack, and (c) no such cracks were observed on the test beams.

When the moment curvature relationship and curvature distributions were established, it was possible to accurately compute the load-deflection relationship. This would have been a tedious process as the shape of the bending moment diagram and the curvature distribution vary with the applied load. The calculations were simplified greatly by assuming that the bending moment at the centre support remained constant from the start of flexural cracking at the centre support until moment redistribution had taken place. The error introduced by this assumption was slight because (a) the required amount of moment redistribution was small (20% increase at midspan), and (b) the rate of curvature increased greatly after flexural cracking (a moment 10% higher than the flexural cracking moment produced nearly twice the curvature at flexural cracking).

Detailed calculations predicting the behavior of the test beams are given in Appendix G.

### 8.3 EVALUATION OF TEST RESULTS

The initial portions of the load-deflection relationships (FIGURES 7.8, 7.9, 7.10) were essentially straight up to and following the predicted first flexural cracking load. A straight line was drawn



through this portion of these curves. The deflection indicated by this line at the predicted flexural cracking load of 8.3 kips was obtained and is listed in TABLE VIII-1. The average of these deflections observed in all the beams was 17% higher than predicted. It is impractical to discuss all the possible sources of error in the method of obtaining the observed deflections and in the assumptions made when calculating the predicted behavior of the beams. However it should be noted that the calculated deflections were determined on the basis of a value  $E_c$  obtained from cylinders that had been loaded to destruction in a few minutes. The beams however were loaded to destruction in approximately six hours. It is well established that the apparent modulus of elasticity decreases with a decrease in rate of loading. Furthermore the stress distribution in the concrete of a beam is not linear as assumed in calculations. This would especially effect the tensile stresses at moment approaching the flexural cracking moment. Both these factors would give deflections larger than those predicted. The elastic deflection listed in TABLE VIII-1 also indicate that these deflections were 32% larger for the pretensioned beams than for the post-tensioned beams. The author has no explanation for this phenomenon other than the possibility that premature cracks existed, or occurred prematurely at the wire deflectors of the pre-tensioned beams. The presence of such cracks would not have had a noticeable effect on the strain measurements, as they would have occurred outside the strain gage length.

The observed flexural cracking loads are presented in TABLE VIII-1. A noticeable feature of these observations is the wide range of





values obtained, with respect to the method of observation. The values, listed on line 5 of TABLE VIII-1, are the loads at which cracks were easily visible to the naked eye. As cracks may have been well developed before becoming visible, these values may be well above the actual cracking loads. The value, listed in lines 7 and 8 of TABLE VIII-1, are the loads at which the load deflection and load-average support movement curves deviated noticeably from their initial straight line relationship. Theoretically this deviation would occur with the formation of the first flexural cracks at the centre support. However, this change in slope would be so slight that it would not be noticeable on these curves. Therefore, the load at which the load-deflection and load-average support movement curve deviated from their initial straight portion was taken as the load that caused flexural cracking at the mid-spans. The most accurate observation of the actual cracking load was most likely given by the load-tensile strain relationship (FIGURE 7.8 and 7.9). The cracking loads, indicated by a rapid increase in the rate of measured tensile strains, were in reasonable agreement with calculated values. However these observed values were only accurate to within one load increment of two kips. In summary, no accurate comparison of the actual and computed cracking loads was possible.

A comparison of the values, listed in TABLE VIII-1 indicates that the cracking load of the pretensioned beams was higher than that of the post-tensioned beams. The compressive stress induced by prestress in the extreme fibre of the test beams was calculated to be more than twice the estimated modulus of rupture of the concrete. The amount of prestress was calculated by estimating the loss in prestress and deducting





this from the initial prestressing force. A summary of these losses is presented in TABLE IV-1. The largest, and most susceptible to variation, was the estimated loss due to friction between the cable duct and prestressing tendon. No specific tests were conducted to determine this loss. The frictional and wobble coefficients were estimated from information in the A.C.I. Building Code (15). It is reasonable to conclude that the existing prestress force was lower and varied more along the post-tensioned beams than the pretensioned beams.

An indication of the plastic behavior of the beam is given in lines 9 and 10 of TABLE VIII-1. Here the observed and computed deflections at the predicted inclined cracking load are compared. Unfortunately the load at which the inclined cracks formed was not noted in the test as the importance of the cracks was not appreciated at the time of testing. However the presence of these cracks is evident in many of the photographs taken after failure of the beam (FIGURE 7-14). As the formation of inclined cracks and yielding of the reinforcement occurred at similar loads, and because both phenomena have the effect of reducing the stiffness of the beam, the occurrence of inclined cracks was not evident in the load-deflection relationships. Hence no comparison of the observed and predicted inclined cracking load was made. The observed deflections at this load were considerably lower than the predicted deflections. However as the stresses in both the steel and the concrete were approaching ultimate values, the deflection of the beam was much less sensitive to increases in the applied load. Therefore, a large variation in the observed deflections was expected at this stage of loadings. One effect not considered in the calculations was a restraint



to the development of strains in the concrete due to the load bearing, and support bearing plates. Compressive strain measurements taken  $3/4$ " inside the extreme fibre of the beam, (FIGURE 7.8 and 7.9) show a decrease in strain near ultimate loads. This effect was more noticeable in the strain measurements taken at the wider, heavier, support bearing plate as compared to the load bearing plate, which was set on a bed of grout.

The observed deflections at the predicted inclined crack are noticeably larger and varied more between the post-tensioned than the pretensioned beams. At this load the estimated prestrain of 0.0045 comprised a considerable portion of the calculated steel strain of 0.0079. Variations in the prestress, therefore, still had a significant effect on the deflection of the beam. Also significant is the effect of the amount of bond slip on the deflections after cracking. As previously noted the grout used to bond the tendons of the post-tensioned beams was considerably weaker than the concrete in the beams. It is very difficult to separate or evaluate these effects and no such attempt was made.

The ultimate loads are indicated on line 11 and 12 of TABLE VIII-1. For beams having a low percentage of steel, as in this investigation, an accurate prediction of the ultimate moment was expected because:

(a) The effects of shear were slight.

(b) The location of the compressive force is known quite accurately because the depth of concrete in compression was small.





(c) The steel stress is known accurately because this stress was in the yield zone of the stress-strain relationship of the steel and was therefore very insensitive to changes in strain. In calculations of the ultimate load, it was assumed that full moment redistribution had occurred. The good agreement between the ultimate load and the predicted ultimate load indicated that nearly full moment redistribution had occurred at failure.

A better indication of the distribution of moment should have been evident from measurements taken of the reactions. (FIGURES 7.5 to 7.6) However these measurements would need to be fairly accurate as the amount of possible moment redistribution was small. Unfortunately measurements of the reactions were not sufficiently accurate. FIGURE 7.7 indicates that the total of the three reactions was approximately 5% less than the total applied load. The error in measurements of the individual loads or reactions might be higher than 5%. It was not determined if the major portion of the error originated in measurements of the loads or of the reactions. However, it should be noted that, when the load cells were calibrated, the load was applied through the plane surfaces of the loading head of the testing machine, whereas in the beam test, the beam reactions were applied through the rocker plates.

The load-curvature relationships are presented in FIGURES 7.10 and 7.11. It is difficult to assess these relationships, because the observed curvature is the average curvature measured over an eight inch length of beam, whereas the actual curvature varied over this length. The predicted load-curvature relationships in FIGURE 7.11 were plotted from calculations of the maximum curvature. As was expected, the





observed curvatures were considerably lower than those predicted.

It was discovered during the analysis of the data, that strains measured at the same section on the two sides of the beam were quite different. This is illustrated by FIGURE 7.13. In some cases the strains measured on one side of the beam were nearly twice those measured on the other side. Any discussion concerning the effects of torsion or lateral deflection is beyond the scope of this investigation. However these differences in strains are an indication of a major fault in the load application. The beam supports were in direct contact with the rolled surface of the top flange of the 27 inch steel loading beam. Hence any warp or twist in the top flange of this steel beam produced torsion and lateral movement at the supports of the test beams.

Ideally, the horizontal movement, of the supports, measured at each end of the beam, should be equal. This was not expected because variations in the behavior of the test beams between the two spans. However, it was expected that the horizontal movement of the individual end supports would have a direct relationship to the midspan deflections. This was far from true, as one end support of the beam was observed to move away from the centre support when the first load was applied. The longitudinal movement, at the centre support, of the ideal beam may be calculated as one-half the difference in the horizontal movement of the end supports. These values were calculated for beams of this investigation and are presented in FIGURE 7.4.

#### 8.4 SUGGESTIONS FOR FUTURE INVESTIGATIONS

A lengthy discussion suggesting improvements in the methods of constructing and testing the beams in this investigation is pointless



because the laboratory facilities at this University have recently been greatly expanded and improved. However the following suggestions are offered:

(1) The devices used to measure the reactions did not function with sufficient accuracy. Commercially produced load cells now available should prove satisfactory.

(2) The methods of estimating the prestress loss were too inaccurate. While most of these methods could be refined by specific tests, it is unlikely that the friction loss in the post-tensioned beams can be evaluated with consistent accuracy. The only constructive suggestion that the author can offer is to measure the concrete strains in the beam at the level of the reinforcement and thus deduce the amount of prestress.

(3) A great deal of care should be directed at the design and placement of the load bearing and support bearing plates. These plates should be as small as possible with a friction reducing agent applied between the plate and the beam.

(4) More precise methods of detecting and locating cracks, such as electric strain gages and magnifying glasses, should be utilized.



TABLE VIII-1

## SIGNIFICANT OBSERVED LOADS AND DEFLECTIONS

	Avg. all beams	Avg. PE-1 PE-2	Avg. PO-1 PO-2	PE-1			PE-2			PO-1			PO-2		
				S	N	C	S	N	C	S	N	C	S	N	C
1	Observed deflection at P = -8.3 kips	0.50	0.57	0.42	0.52	0.555	0.60	0.60		0.43	0.40		0.31	0.52	
2	Computed deflection at P = 8.3 kips	0.42	0.43	0.42	0.43	0.43	0.43	0.43		0.41	0.41		0.43	0.43	
3	Observed/computed	1.17	1.32	1.00	1.21	1.26	1.40	1.40		1.05	0.97		0.72	1.21	
4	Computed cracking load				9.8	9.8	8.3	9.6	8.5	9.3	9.3	8.2	9.3	9.3	8.2
5	Cracking load indicated by:														
5	(a) Visible cracking				16	16	14	14	14	8	8	8	12	12	12
6	(b) Strain measurement							12	10				10	10	8
7	(c) A change in slope of the load-deflection curve				14	12		12		8	8		10	10	
8	(d) A change in slope of the load-support movement curve							12		10	10		10	10	
9	Observed deflection at P = 16.2 kips	0.21	0.16	0.26	0.16	0.14		0.17		0.25	0.40		0.22	0.18	
10	Observed/computed	0.57	0.43	0.71	0.42	0.38		0.46		0.67	1.08		0.60	0.48	
11	Ultimate load	20.9	20.9	20.9		21.0			20.8		20.1			21.8	
12	Observed/computed	1.01	1.01	1.01		1.01			1.00		0.97			1.05	

All loads are in kips and deflections are in inches







## CHAPTER IX

### CONCLUSIONS

Conclusions based on the results of this investigation are summarized as follows:

- (1) The methods of constructing, loading and instrumenting the test beams were generally satisfactory.
- (2) The post-tensioned and pretensioned beams behaved in a similar fashion under load.
- (3) The measured ultimate loads compared favorably with those predicted by calculation.
- (4) Full moment redistribution had occurred at, or before, the ultimate load.
- (5) The measured deflections did not compare favorably with those predicted by calculations.
- (6) Values of the modulus of elasticity as determined from cylinder tests, compared favorably with standard design values based on concrete strength.



## LIST OF REFERENCES

1. Hawkins, H.M.,  
Sozen, M.A.,  
Siess, C.P.      "Strength and Behavior of Two-span Continuous Prestressed Concrete Beams", Civil Engineering Studies, Structural Research Series No. 225, University of Illinois, September 1961.
2. Guyon, Y.      "Etude Expérimentale de Poutres Continues en Béton Précontraint", Travaux, April, May, June and July, 1953, V. 37.
3. Guyon, U.      "Prestressed Concrete Volume II", Wiley, 1960.
4. Magnel, G.      "Prestressed Concrete", New York, McGraw-Hill, 1954.
5. Lin, T.Y.      "Strength of Continuous Prestressed Concrete Beams Under Static and Repeated Loads", Journal of the American Concrete Institute, Proc. V 51, June 1955.
6. Morice, P.B.,  
Lewis, H.S.      "The Ultimate Strength of Two-span Continuous Prestressed Concrete Beams as Affected by Tendon Transformation and Untensioned Steel", Second Congress of the Fédération Internationale de la Précontrainte, Amsterdam, 1955, published by the Cement and Concrete Association, London, 1958.
7. Macchi, G.      "Etude Experimentale de Poutres Continues Précontraintes dans la Domain Plastique et à la Rupture", Second Congress of the Fédération



Internationale de la Précontrainte, Amsterdam, 1955, published by the Cement and Concrete Association, London, 1958.

8. Morice, P.B. "Research in Great Britain on Moment Redistribution in Prestressed Concrete Continuous Beams", Second Congress of the Fédération Internationale de la Précontrainte, Amsterdam, 1955, published by the Cement and Concrete Association, London, 1955.
9. Zekeria, I. "Shear Failure of Two-span Continuous Concrete Beams Without Web Reinforcement", Journal of the Prestressed Concrete Institute, June, 1958.
10. Mattock, A.H.,  
Kaar, P.H. "Precast-Prestressed Concrete Bridges, Part 4. Shear Tests of Continuous Girders", Journal of the P.C.A. Research and Development Laboratories, Vol. 3, No. 1, January, 1961.
11. MacGregor, J.G.,  
Sozen, M.A.,  
Siess, C.P. "Strength and Behavior of Prestressed Concrete Beams with Web Reinforcement", Civil Engineering Studies, Structural Research Series No. 201, University of Illinois, August 1960.
12. Warwaruk, J.,  
Sozen, M.A.,  
Siess, C.P. "Investigation of Prestressed Reinforced Concrete for Highway Bridges, Part II - Strength and Behavior of Flexure of Prestressed Concrete Beams", University of Illinois Bulletin, Vol. 60, No. 5, August, 1962.





13. Base, G.D.      "Further Notes on the Demec, A Demountable Mechanical Strain Gage for Concrete Structures", Magazine of Concrete Research, Vol. 7, No. 19, March, 1955. Reprinted by the Cement and Concrete Association, London.
14. Taylor, D.      "Stress-strain Relationships in Lightweight Concrete", M.Sc. thesis, University of Alberta, 1960.
15.                    "Building Code Requirements for Reinforced Concrete", American Concrete Institute Publication 318-63, June 1963.



## APPENDIX A

### PROCEDURE FOR CONSTRUCTION OF BEAMS



## APPENDIX A

### PROCEDURE FOR CONSTRUCTION OF BEAMS

#### (a) PRETENSIONED BEAMS

The form (Appendix B) was assembled with the end anchorage plates adjusted in position by means of their 1/2" set screws. Plywood pieces were cut and fitted to fill any gaps between the metal form parts and box stirrups were placed in each end of the form. Ten twenty-six foot lengths of high-tensile wire were cut and placed in the form. The five wires of each group were bundled together at two feet on centre. Hence the high tensile wires of each group were approximately the same length between end anchorage plates.

Each group of five wires was prestressed as follows. Anchors were placed and seated against one end anchorage plate. Anchors were also placed, though not seated, against the other end anchorage plate. The prestressing jack (Appendix E) was positioned so that its head was against this end anchorage plate and the five high tensile wires ran through the holes in the jack tail piece. Another set of anchors was placed and seated against the tail piece of the jack. The wires were then stressed to their initial prestress by applying pressure to the jack. The initial prestress was applied for approximately five minutes. Then the anchors, which previously had been placed against the end plate of the beam, were seated and the jack pressure was released. The wires were then trimmed off close to the anchors, and the prestressing





operation was repeated on the other group of five wires. Photographs and drawings of the form at this stage of construction are shown in FIGURES A-1 and A-2.

The L-stirrups were placed and tied to the prestressing wire and to the 1/4" diameter support bar. The concrete was transported directly from the delivery truck into the form by means of a chute. A small electric vibrator, applied both internally and externally, aided in compacting the concrete. Six test cylinders were also cast and a slump test performed at this time.

After the final set of the concrete had taken place, the beam and four test cylinders were covered with water-soaked burlap which, in turn, was covered by a sheet of polyethylene film.

Fourteen days after casting the prestress was transferred to the concrete by releasing the set screws on the end anchorage plates. A few days before the beam was to be tested it was placed on the load beam as described in Chapter V.

#### (b) POST-TENSIONED BEAMS

The same form that had been used to cast the pretensioned beams was re-used to cast the post-tensioned beams. However 1/4" end plates replaced the heavier end anchorage plates and duct support rods were placed in pairs approximately 1'-6" on centre along the beam. These rods were positioned under each of the cable ducts and were set into holes which had been drilled into the sides of the form. The cable ducts were then placed and tied on top of the support rods. Conical duct end forms, which had been greased and wrapped in wax paper, were fitted through the end plate and into the cable ducts. The stirrups were



placed and wires to the cable ducts, support rods, and the 1/4" diameter support bar. Photographs and drawings of the form are shown in FIGURES A-3 and A-4. The beam was then cast and cured following the same procedure used for the pretensioned beams.

Two weeks after casting the tendons were placed and pre-stressed. Five, twenty-six foot lengths of wire were cut and pushed individually through each duct. A small bullet shaped wooden button was fitted over the end of each wire before it was inserted to guide the wire along the duct. After all wires were inserted, the 5" x 5" x 1/2" end anchorage plates were placed over the wires and the pre-stressing operation was carried out as for the pretensioned beams.

Grout was pumped into the cable ducts through the 1/2" hole in the end plate by means of a small single action hand pump. The grout was pumped in one end of a cable duct until it emerged from the far end. The far end of the cable duct was then plugged and as much pressure as possible was applied by the grout pump. A photograph of the grout pump connected to a beam is shown in FIGURE A-5. The beam was cured for the remaining two weeks and then was placed on the load beam as described in Chapter V.



- (A) Form Sides
- (B) Wood Inserts
- (C) End Plates
- (D) Bottom Plates
- (E) Top Braces
- (F) Support Rocker
- (G) Wire Deflector
- (H) Deflector Anchor
- (I) Prestressed Wires

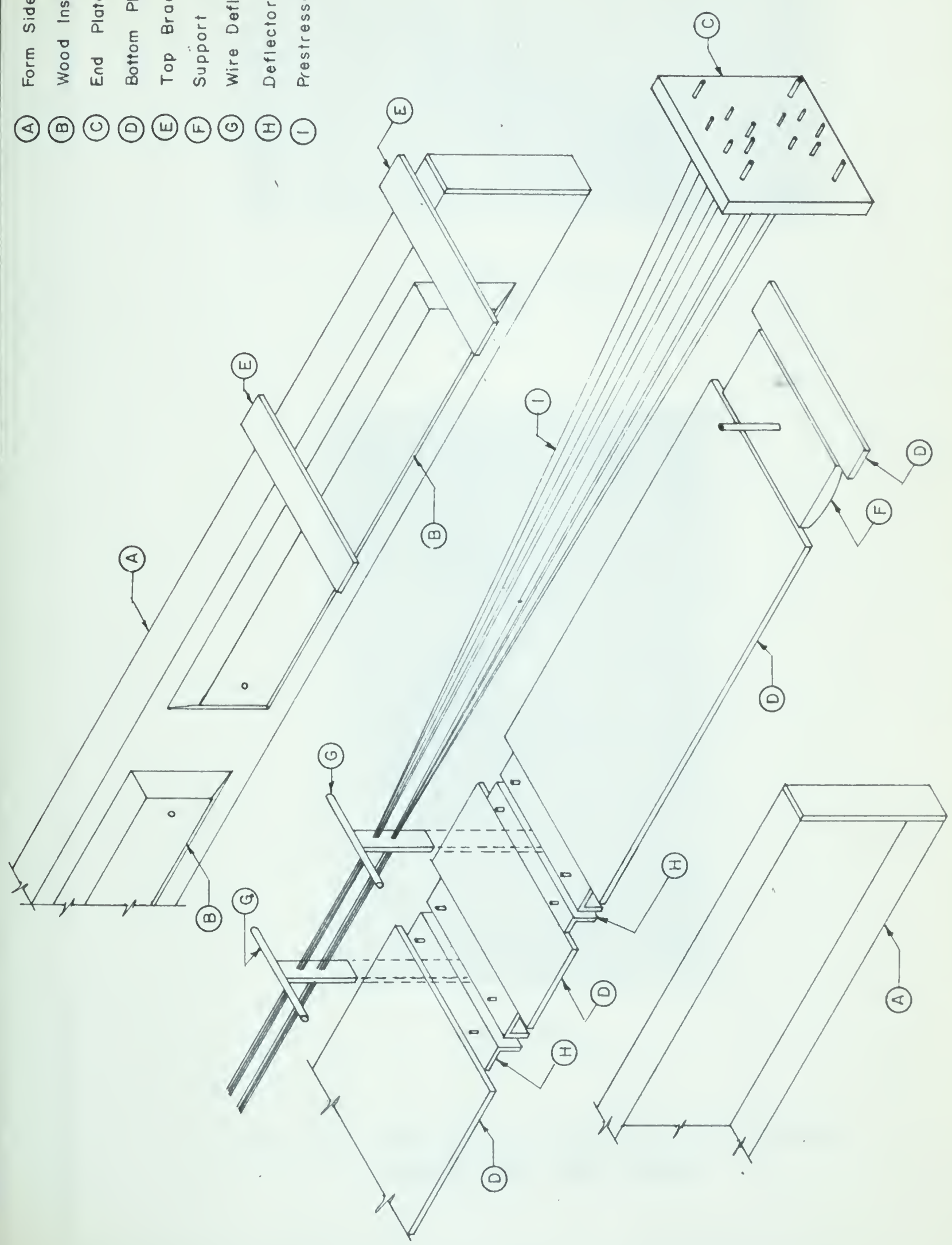
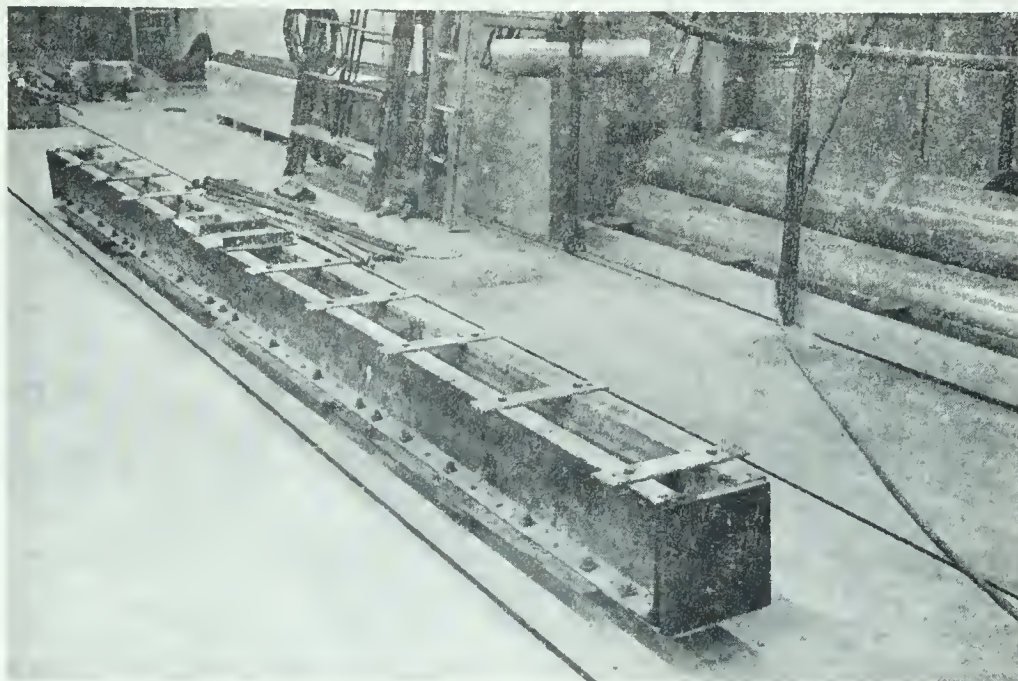


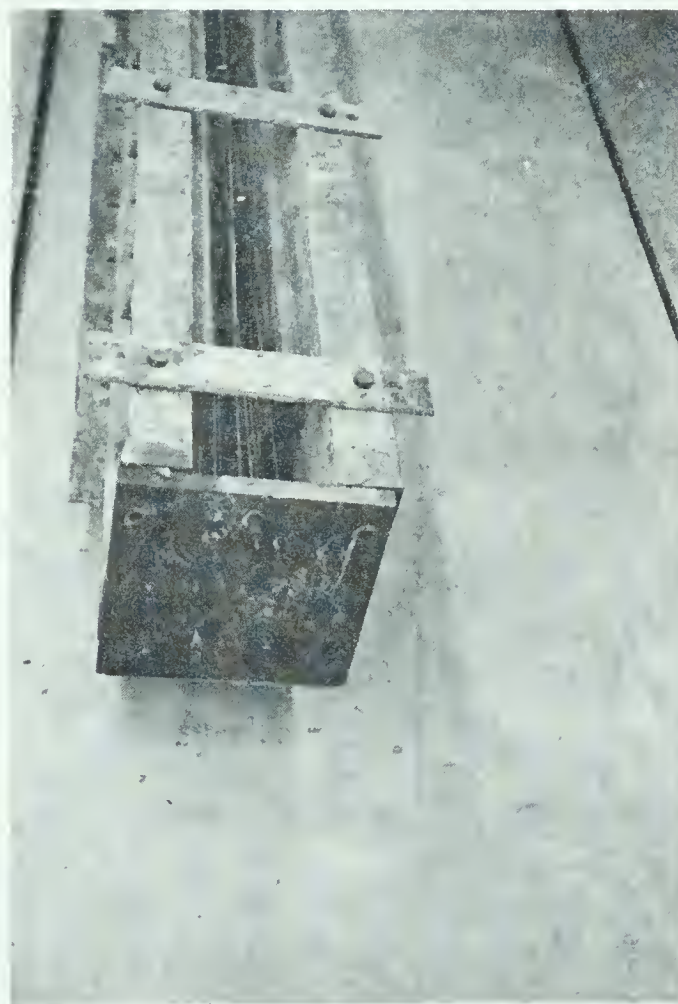
FIG. A-I FORM ASSEMBLY FOR PRETENSIONED BEAM







GENERAL VIEW



END DETAIL

FIG. A-2 PHOTOGRAPHS OF FORM ASSEMBLED  
FOR PRETENSIONED BEAM



- (A) Form Sides
- (B) Wood Inserts
- (C) End Plates
- (D) Bottom Plate
- (E) Top Brace
- (F) Cable Duct
- (G) Support Rods
- (H) Conical Duct End Forms

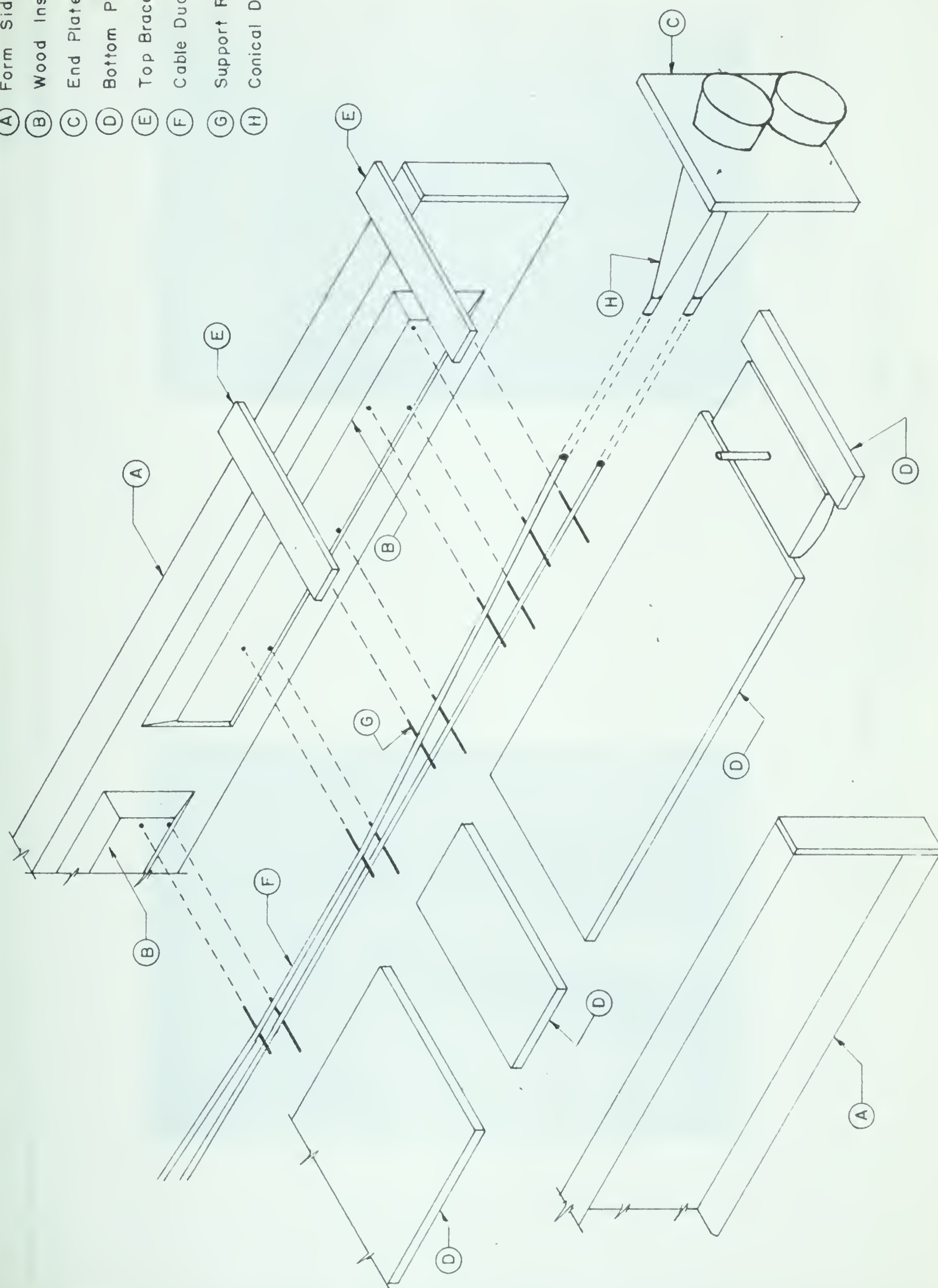


FIG. A-3 ASSEMBLY OF CASTING FORM FOR POST-TENSIONED BEAM





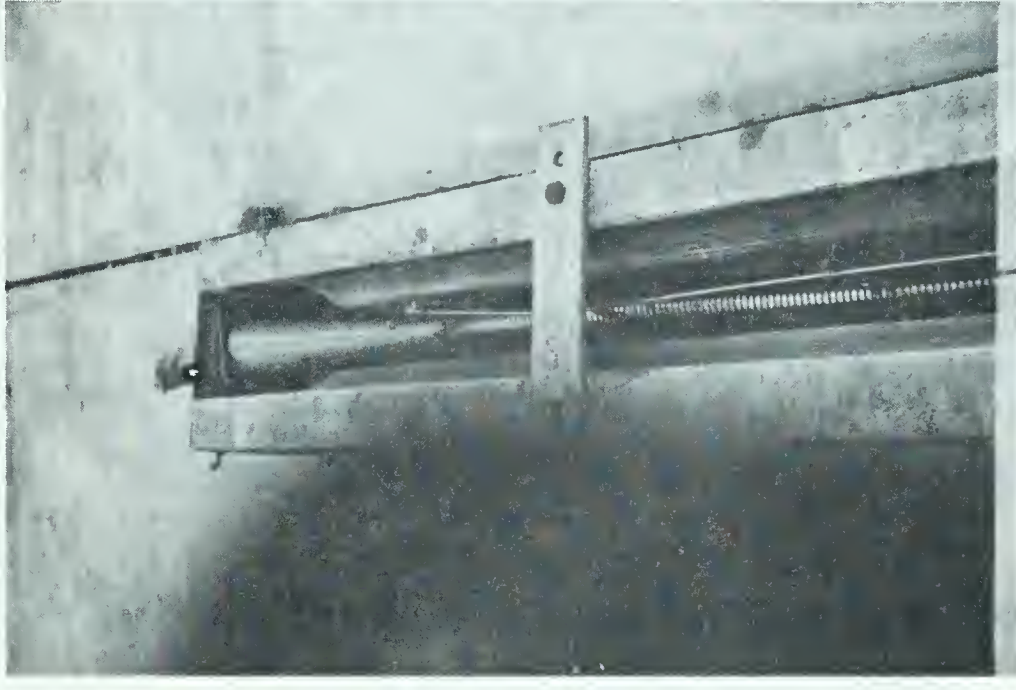
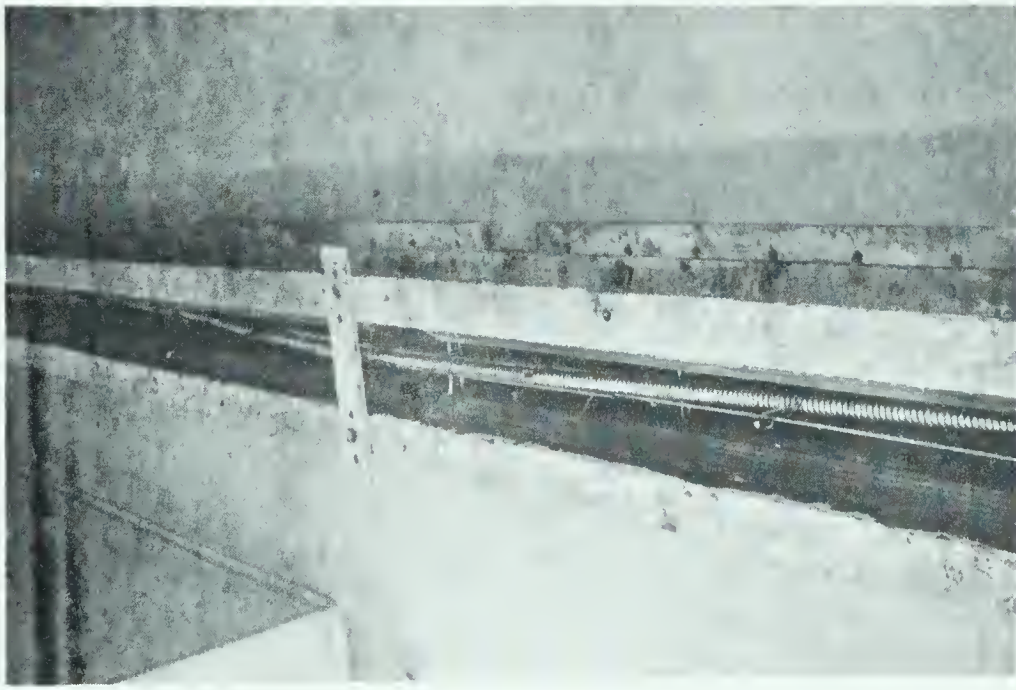


FIG. A-4 PHOTOGRAPH OF CASTING FORM FOR A  
POST-TENSIONED BEAM





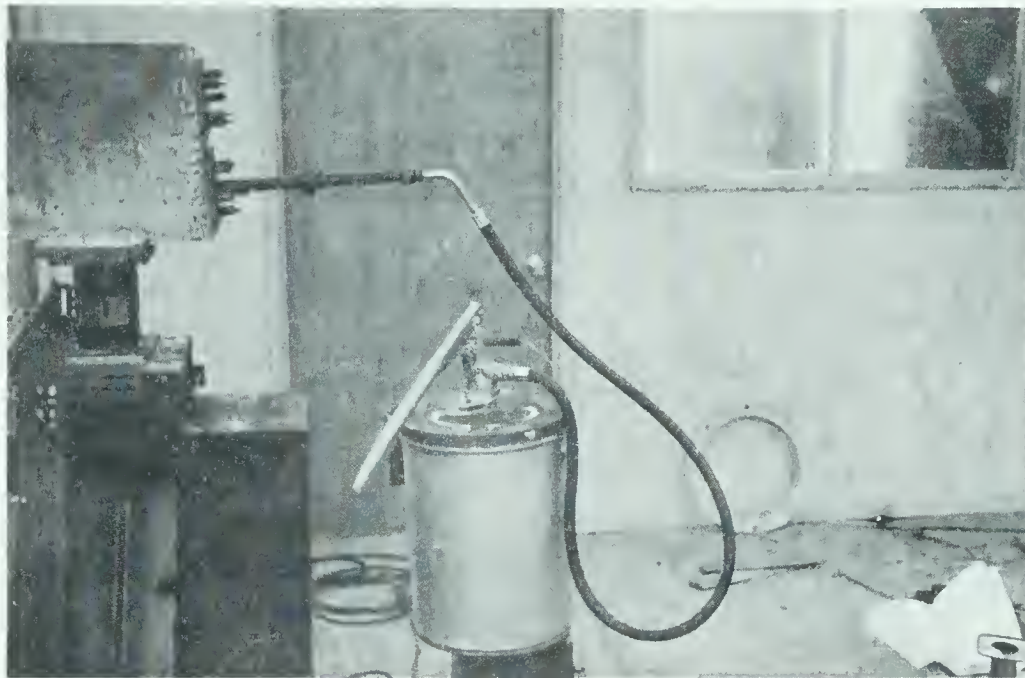


FIG. A-5 PHOTOGRAPHS SHOWING GROUTING  
OF POST-TENSIONED BEAM



APPENDIX B

CASTING FORM



## APPENDIX B

### CASTING FORM

Details of the various parts of the form are shown in FIGURES B-1, B-2, B-3 and the assembled form is shown in FIGURES A-1, A-2, A-3. Although the drawings and photographs in these figures illustrate the form and its assembly, the following points should be noted.

- (a) The form was assembled using 1/2" machine bolts.
- (b) The distance between the side channels was adjustable so that a beam 4 1/2", 6" or 7 1/2" wide by 12" deep could be cast using this form.
- (c) The 7/8" inside diameter cable duct was a 3/4" flexible aluminum conduit obtained from an electrical supplier.





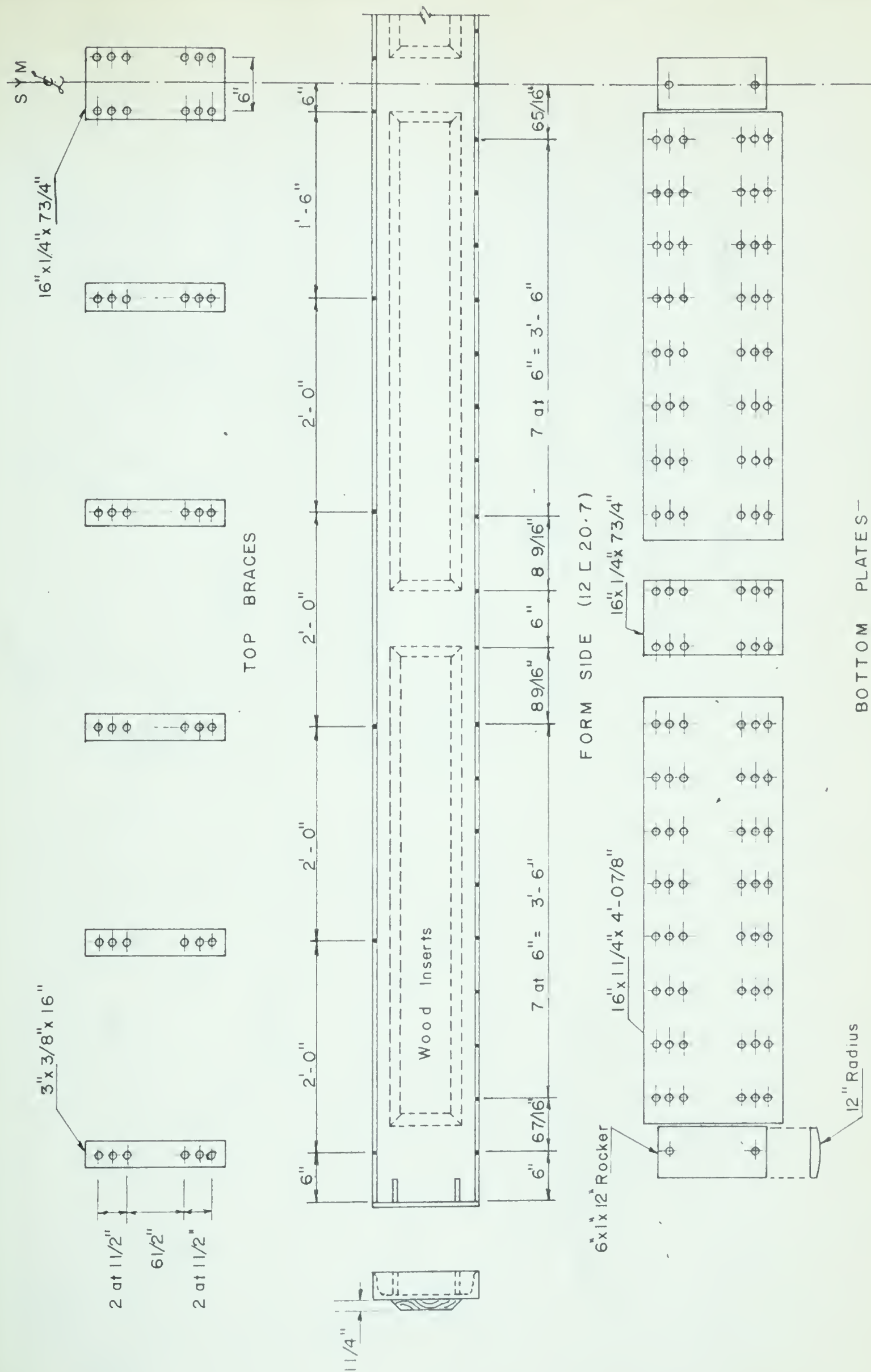


FIG. B-1 CASTING FORM PIECES



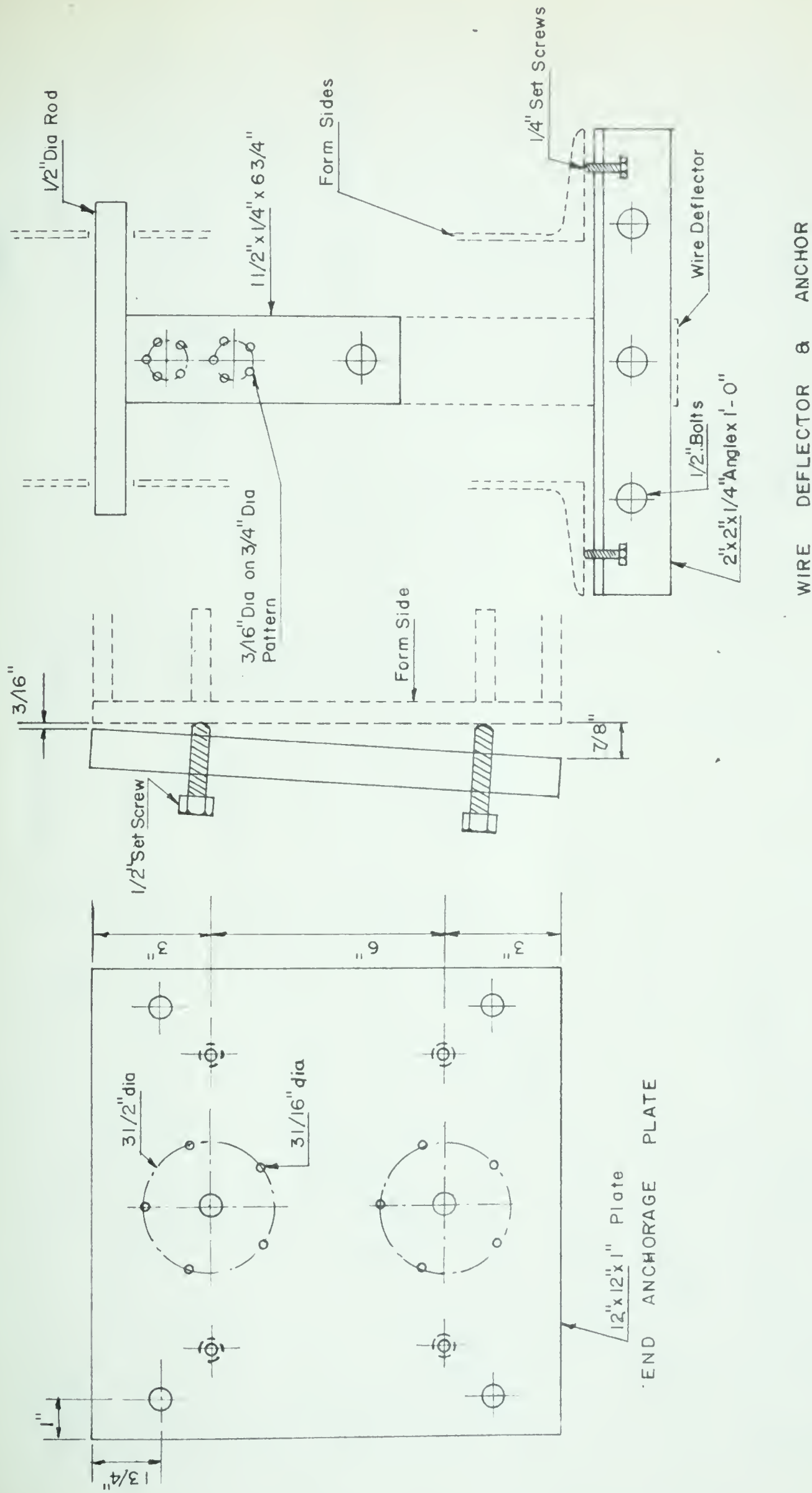
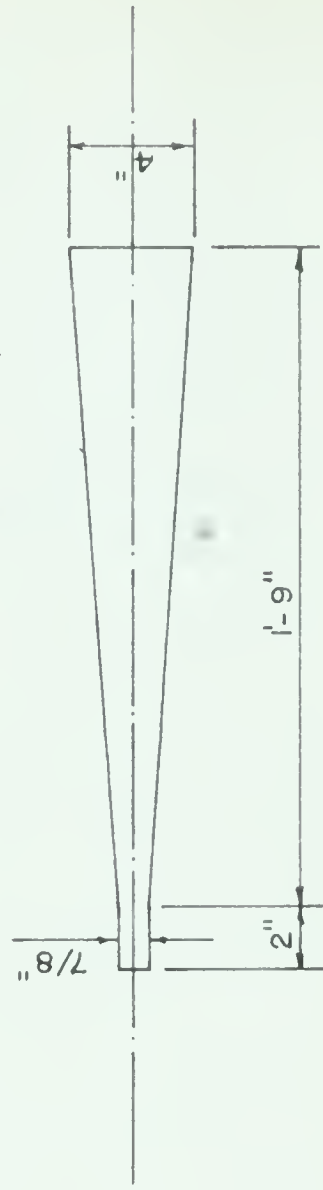
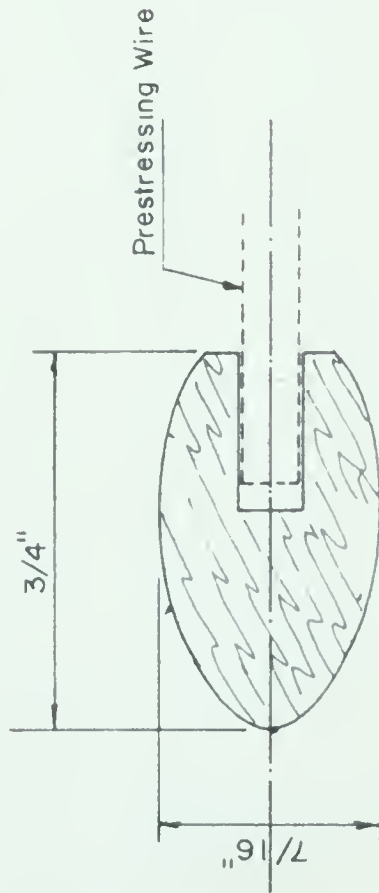
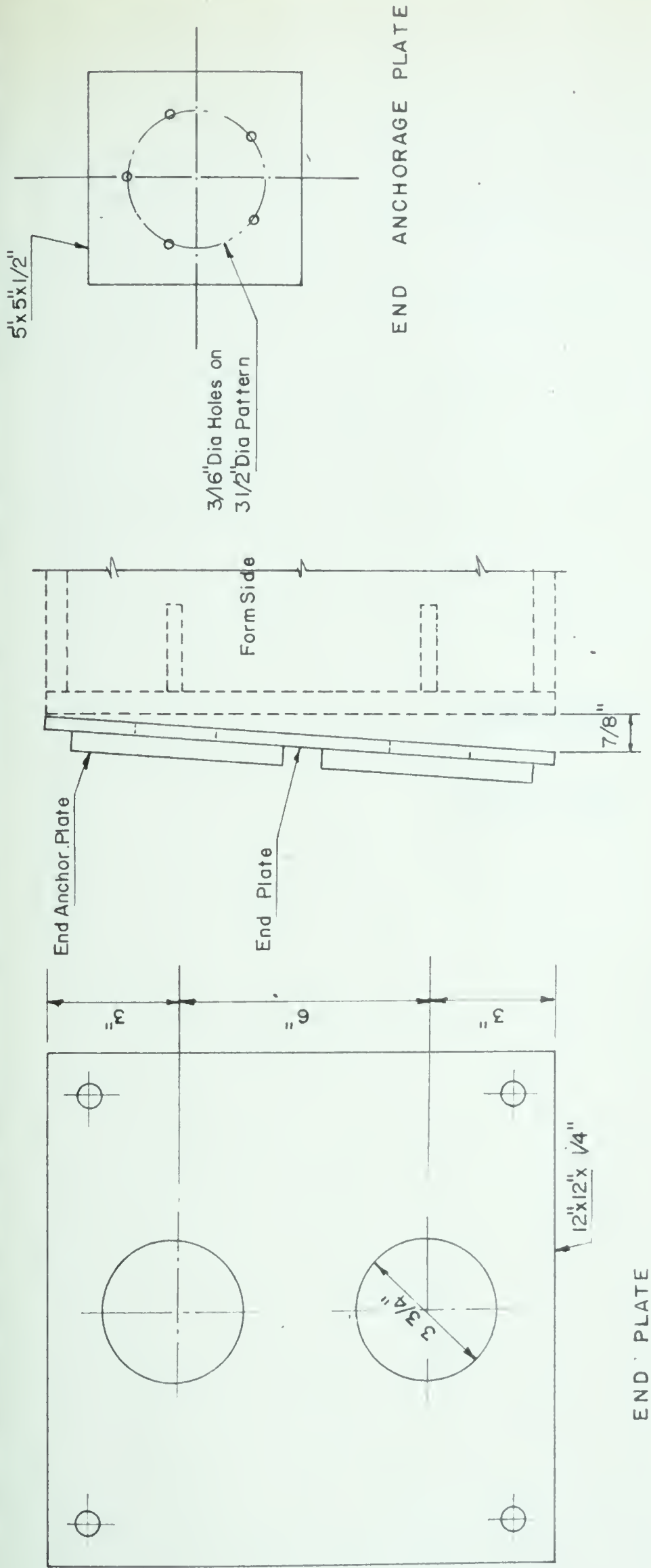


FIG. B-2 CASTING FORM PIECES FOR THE PRETENSIONED BEAM





WOODEN GUIDE BUTTON

CONICAL END DUCT FORM

FIG. B-3 CASTING FORM PIECES FOR THE POST-TENSIONED BEAM





APPENDIX C

LOADING BEAM



## APPENDIX C

### LOADING BEAM

Details of the loading beam are shown in FIGURE C-1 and C-2. It should be noted that the loading head and support points may be positioned at any location along the beam.



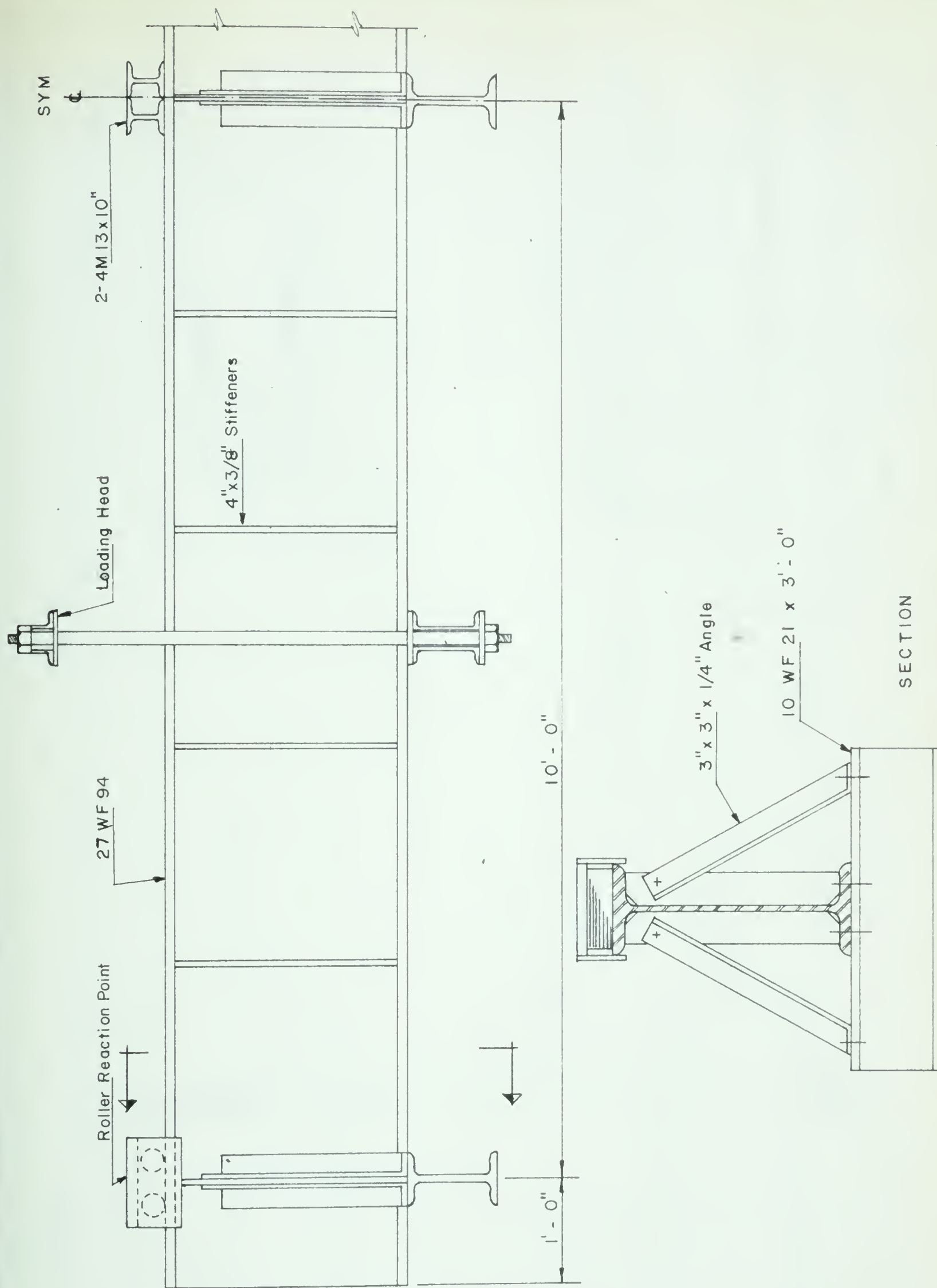


FIG. C-1 LOADING BEAM DETAILS





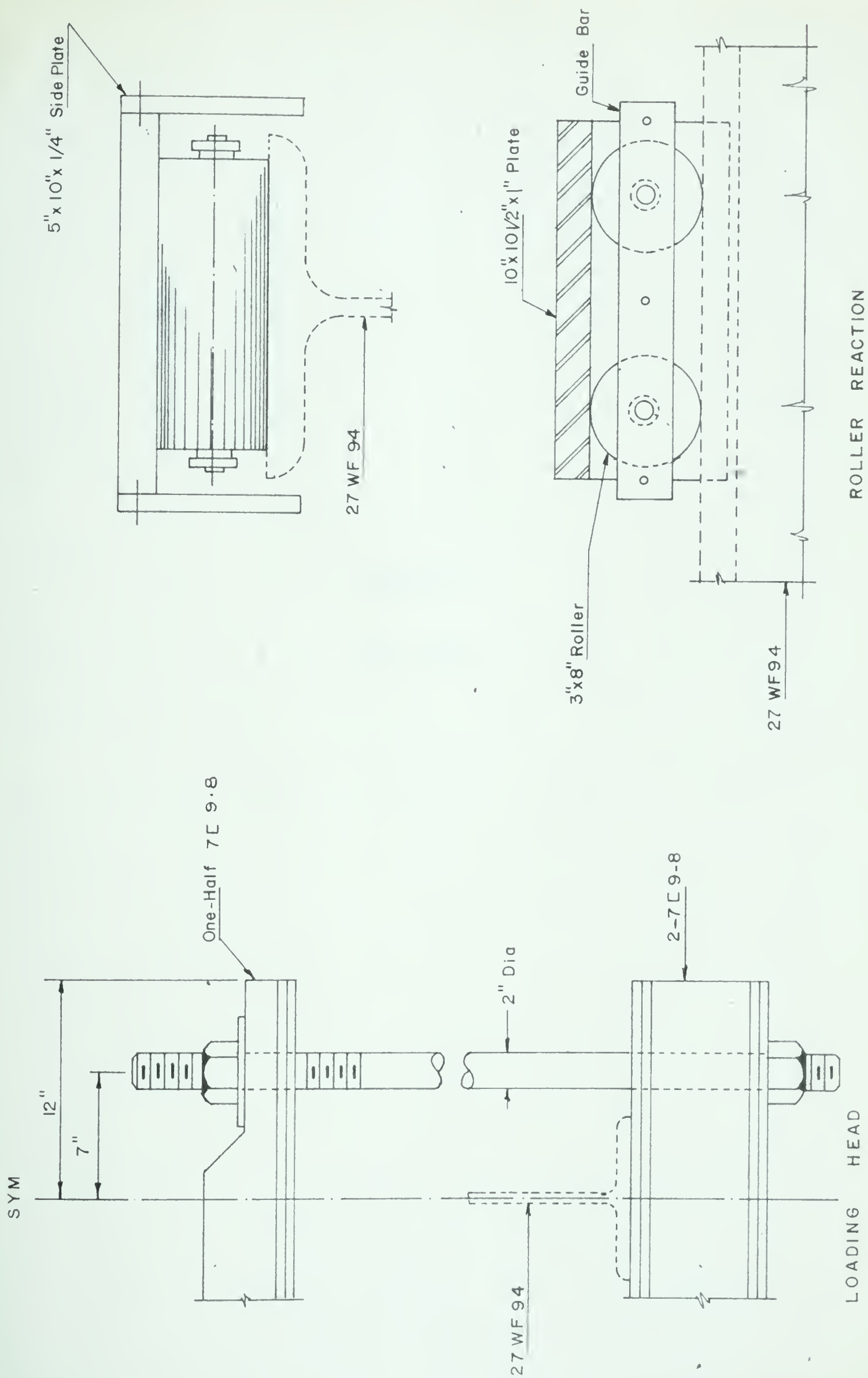


FIG. C-2 LOADING BEAM DETAILS



## APPENDIX D

### LOAD CELLS



## APPENDIX D

### LOAD CELLS

Load cell details are shown in FIGURE D-1. Each of the electrical strain gages was connected to a pair of lead wires. The strain gages were identified by the color of the lead wires. Dummy gages were mounted on a 1" x 1" x 5" steel bar.

Calibration graphs (FIGURE D-2) were obtained for the centric loading of each load cell. Readings were also taken with the load applied eccentrically to the central axis of the load cell. These readings are not shown in the calibration graphs as they were not significantly different from readings obtained from a centric load.

The accuracy of the SR-4, Type A3, 1 inch electrical strain gage is given by the manufacturer as  $\pm 5 \times 10^{-6}$  inches per inch.





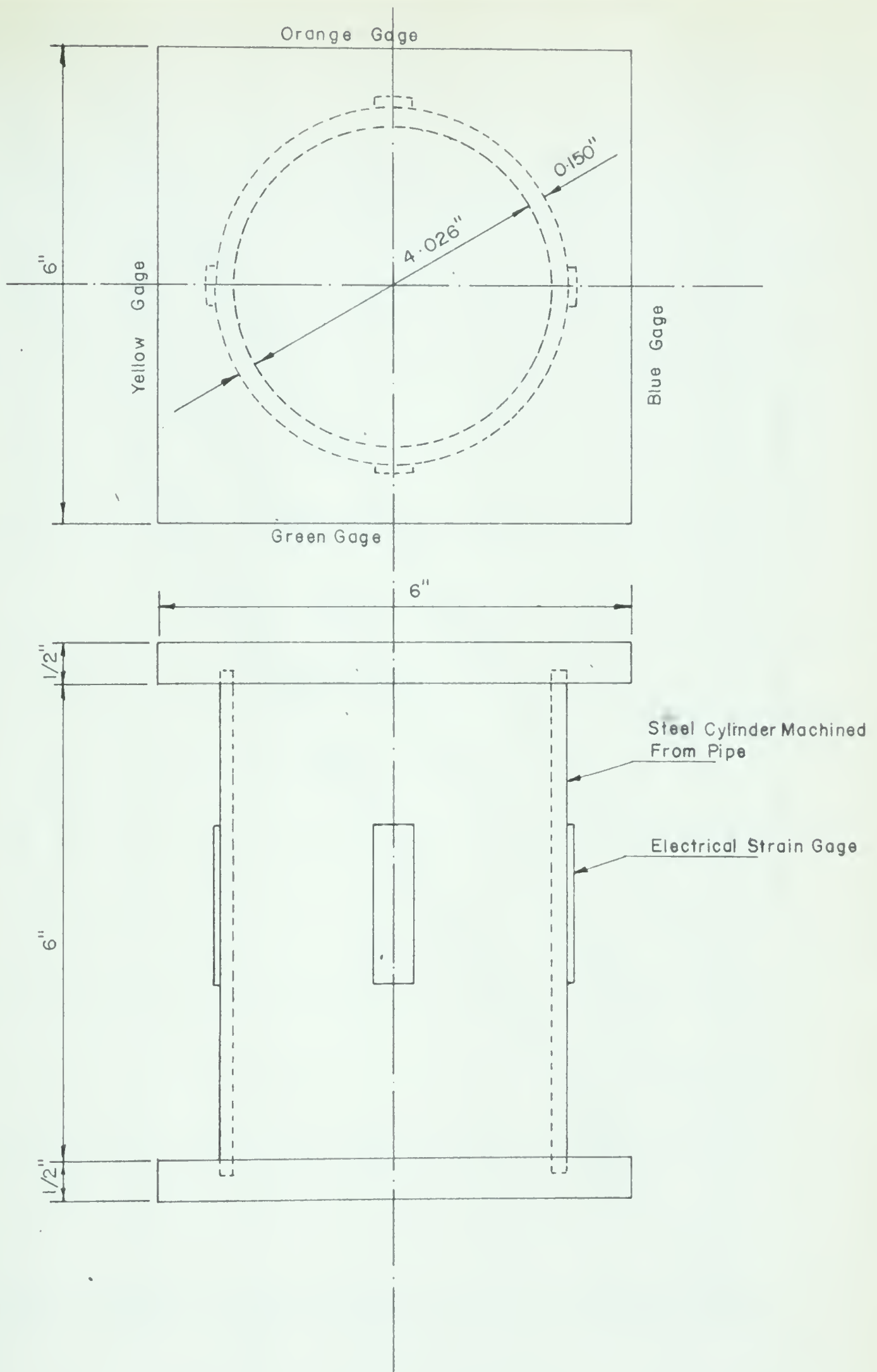


FIG. D-1 LOAD CELL



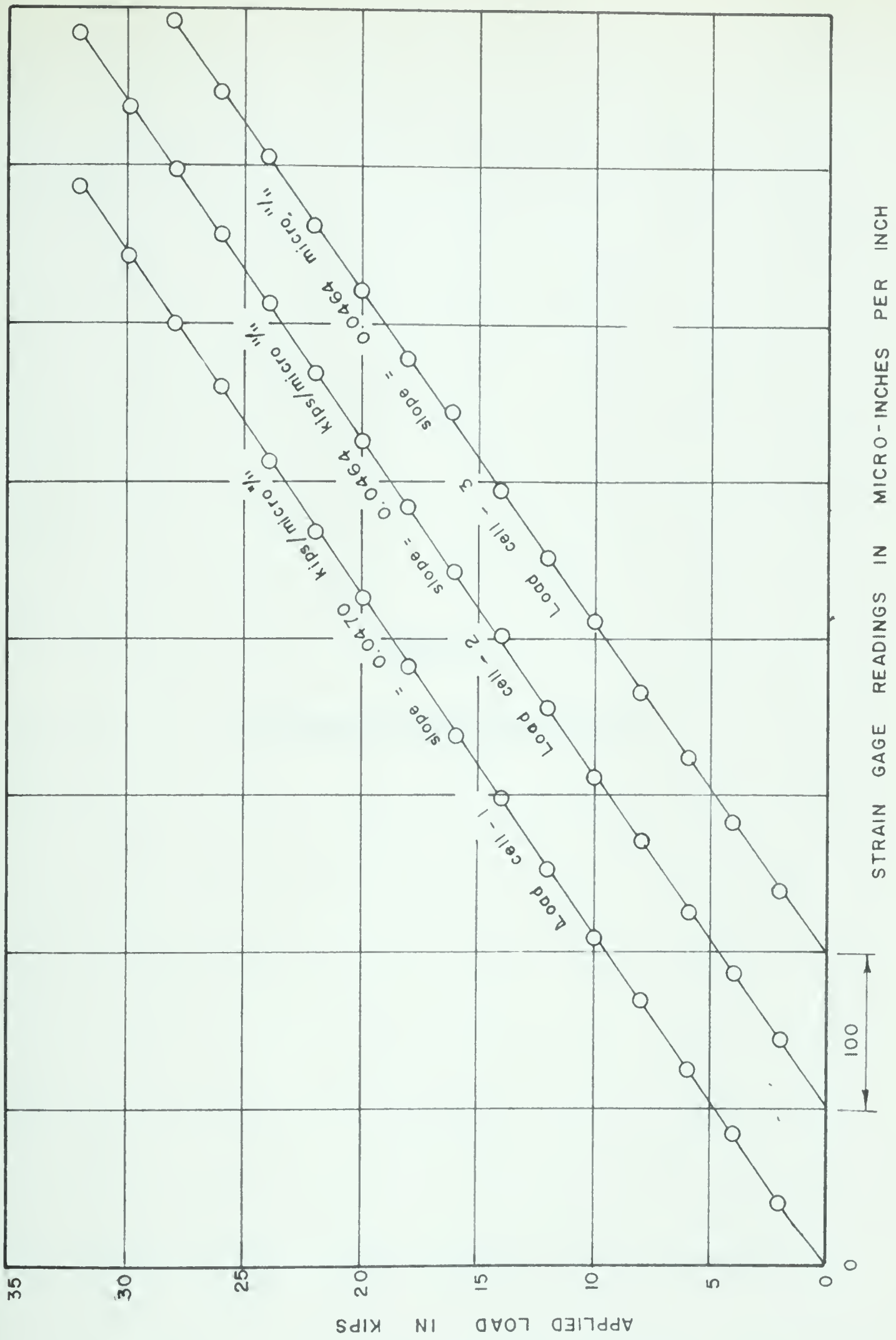


FIG. D-2 CALIBRATION GRAPH OF LOAD CELL



## APPENDIX E

### PRESTRESSING AND LOADING JACKS





## APPENDIX E

### PRESTRESSING AND LOADING JACKS

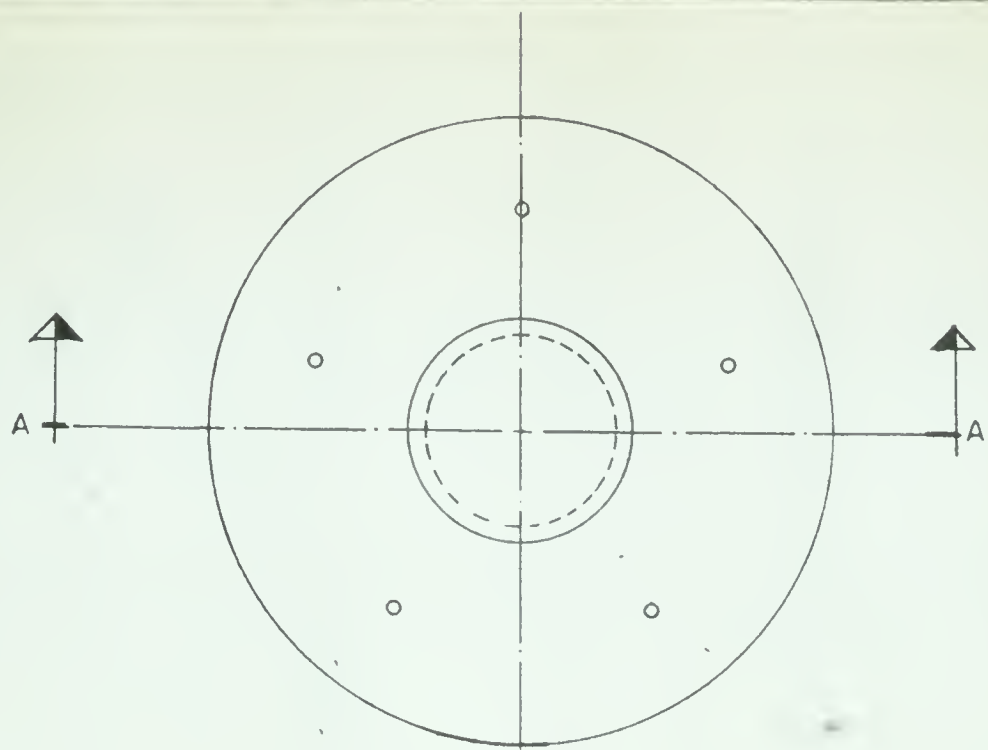
The prestressing jack was a ten ton capacity Blackhawk hydraulic jack with 12 inch extension which was activated by a Blackhawk hand pump. Head and tail pieces (FIGURE E-1) were fitted to the jack for prestressing the tendons as described in Appendix A.

The calibration graph for the jack (FIGURE E-2) was obtained using a Baldwin testing machine.

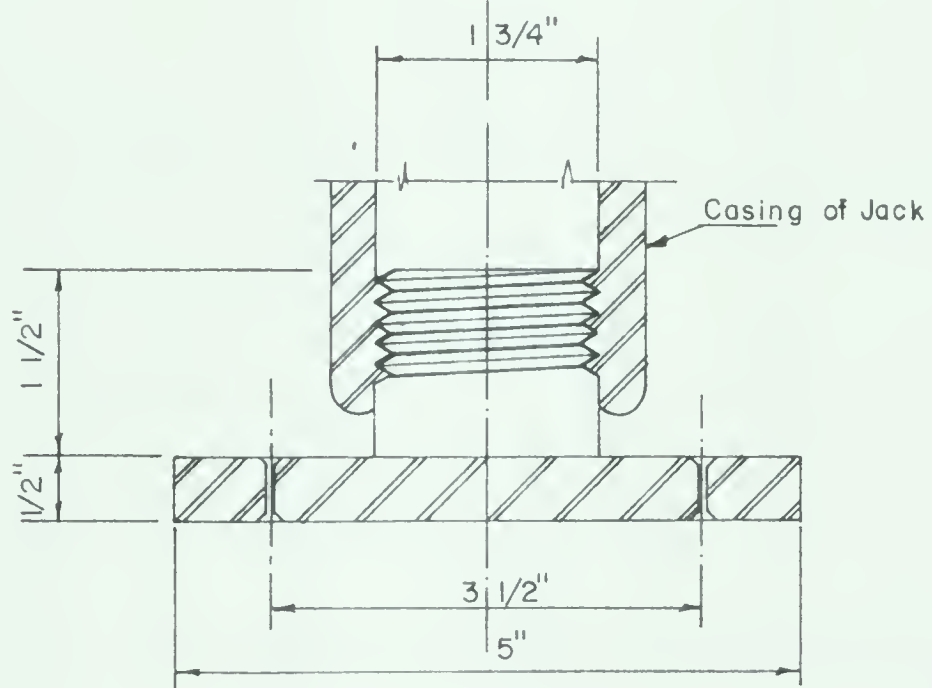
In testing the prestressed beams, the loads were applied to each midspan by a ten ton capacity Blackhawk hydraulic jack having a 12 inch extension. In applying load to the specimen the piston end of the jack was placed directly against the loading head of the loading beam, while a bearing head (FIGURE E-3) was attached to the other end of the jack and positioned on top of test specimen. The two jacks were connected to a common pump and pressure gage.

To calibrate the pressure gage, both jacks were placed together in the Baldwin testing machine at the same time and jacked against the loading head. As both jacks were of identical manufacture, it was assumed that the load applied by each was equal. The calibration readings obtained are shown in TABLE E-4.





TAIL PIECE



SECTION A - A

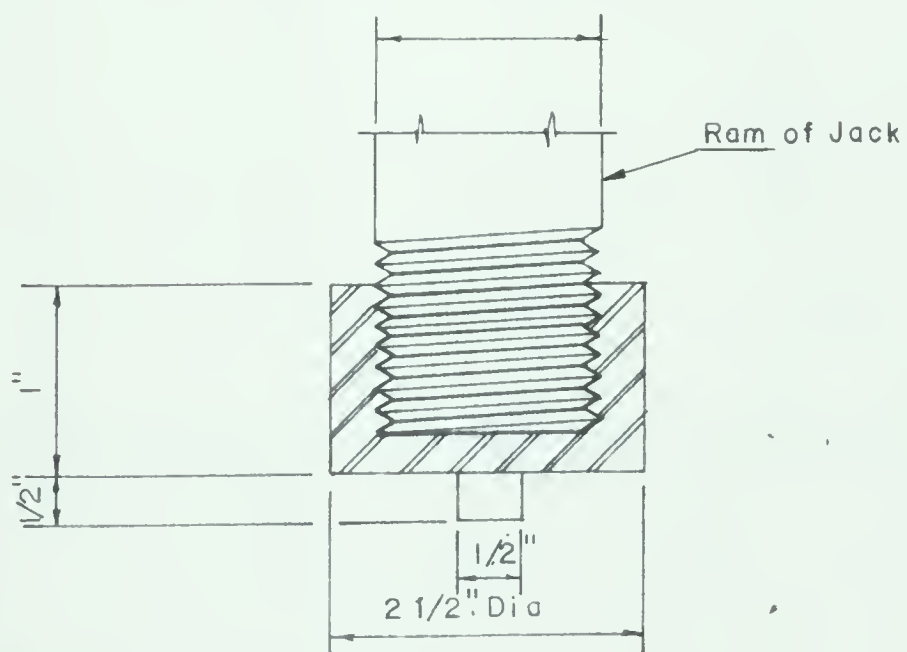
SECTION THROUGH  
HEAD PIECE

FIG. E-1 PRESTRESSING JACK ATTACHMENTS



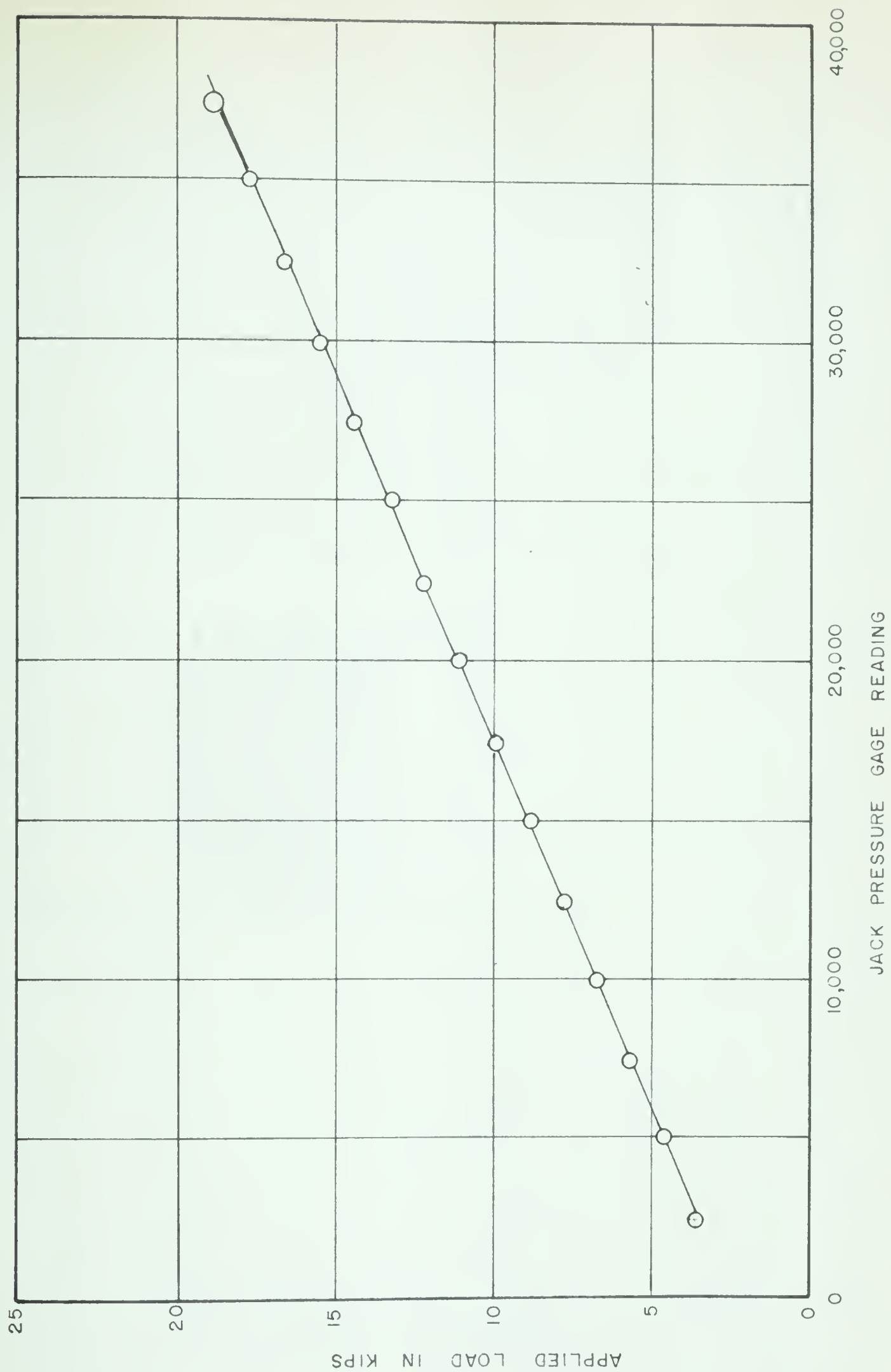


FIG. E-2 CALIBRATION GRAPH OF PRESTRESSING JACKS





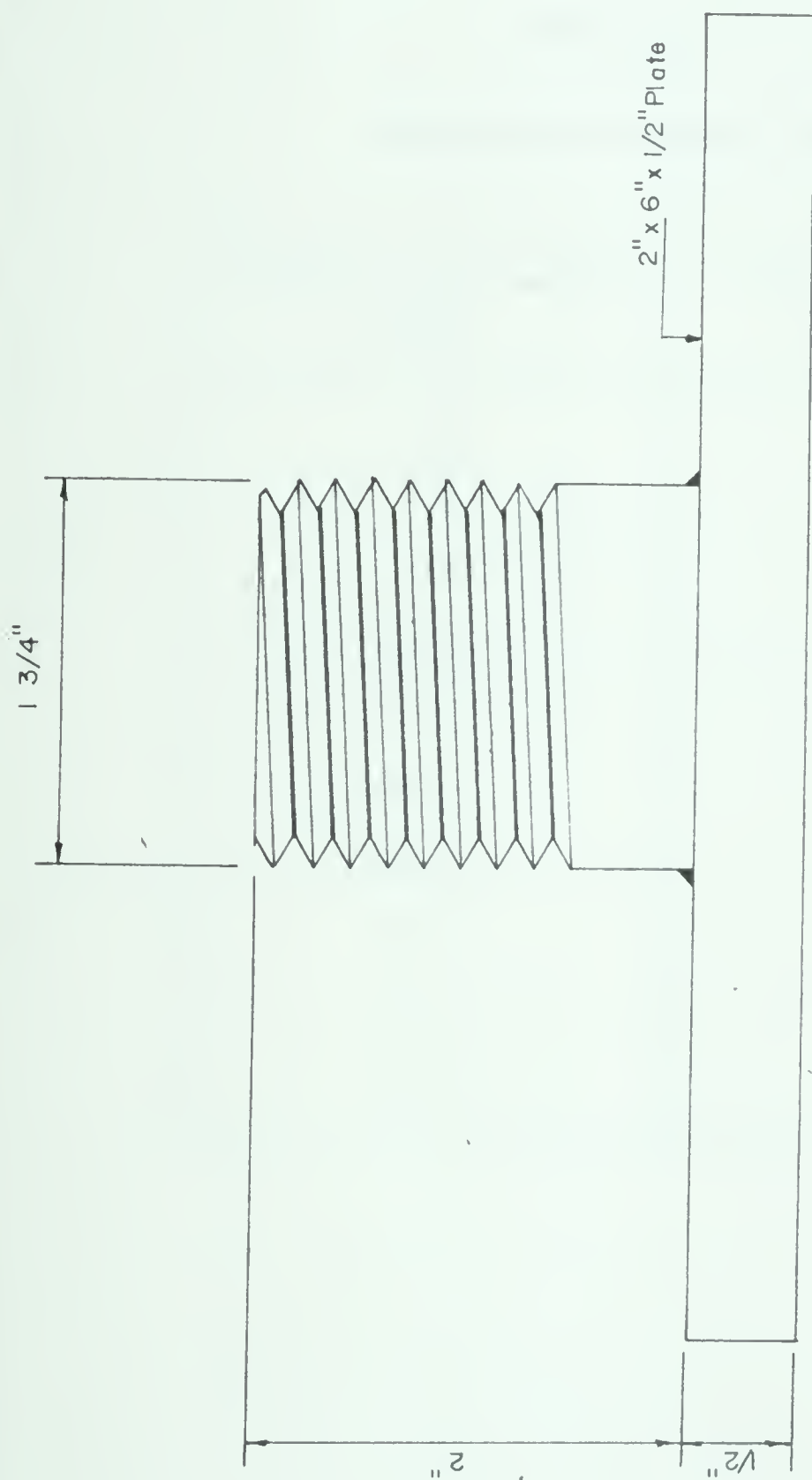


FIG. E-3 LOADING JACK ATTACHMENT



TABLE E-4

## CALIBRATION OF LOADING JACKS

Pressure gage reading (kips)	Load on one jack (kips)
2.0	1.95
4.0	3.92
6.0	5.85
8.0	7.85
10.0	9.80
12.0	11.79
14.0	13.84
16.0	15.81
18.0	17.85
20.0	19.86



## APPENDIX F

### CALCULATION OF PRESTRESS LOSSES IN THE STEEL





## APPENDIX F

### CALCULATION OF PRESTRESS LOSSES IN THE STEEL

#### (a) ANCHORAGE LOSS

The slippage of the wires that occurred when the jack pressure was released was measured as approximately 0.01 inches. The anchorage loss would therefore be:  $E_s \frac{\delta}{L} = \frac{0.01}{21 \times 12} \times 30.0 \times 10^3 = 12 \text{ k.s.i.}$  for both the pretensioned and post-tensioned beams.

#### (b) LOSS DUE TO ELASTIC STRAIN IN CONCRETE

This loss was assumed to be  $n$  times the average stress, along the beam, in the concrete at the elevation of the centroid of the steel. This average concrete stress was computed for the pretensioned beam and found equal to 650 p.s.i. The steel loss would therefore be  $n \times 650 \text{ p.s.i.} = 9 \times 650 \text{ p.s.i.} = 5.9 \text{ k.s.i.}$

As the post-tensioned beam was to be tensioned in two equal stages the steel loss was estimated as one quarter that of the pretensioned or 1.5 k.s.i.

#### (c) LOSS DUE TO CREEP OF CONCRETE

The concrete was assumed to have a coefficient of creep of 0.5(3) in the 14-day period between prestressing and testing of the beam. The loss in both beams would therefore be equal to 0.5 times the loss due to elastic strain in the pretensioned beam or  $0.5 \times 5.9 \text{ k.s.i.} = 3.0 \text{ k.s.i.}$



## (d) LOSS DUE TO SHRINKAGE OF THE CONCRETE

The concrete was assumed to shrink 0.0067 inches per inch in 28 days (3). The loss due to shrinkage in the pretensioned beam would therefore be  $0.000067 E_s = 0.000067 \times 30.0 \times 10^3 = 2.0 \text{ k.s.i.}$

## (e) FRICTION LOSS

This loss in the post-tensioned beam was determined using the simplified method in the American Concrete Institute's "Code for Prestressed Concrete"(15). Values for the curvature and wobble coefficient were assumed as  $K = 0.001$  per foot

$$\mu = 0.3$$

As the post-tensioned beam was stressed from both ends the friction losses were taken for one span only. From FIGURE 3.3 the total angular curvature is  $21.5^\circ$  or 0.367 radians. The friction loss would therefore be equal to  $f_{se} (Kl + \mu d) = 125 (0.001 \times 10 + 0.3 \times 3.76) = 15.4 \text{ k.s.i.}$  The friction loss in the pretensioned beam was assumed equal to zero.



## APPENDIX G

### CALCULATIONS FOR PREDICTING THE BEHAVIOR OF THE TEST BEAMS





## APPENDIX G

### CALCULATIONS FOR PREDICTING THE BEHAVIOR OF THE TEST BEAMS

#### (a) ASSUMPTIONS

Load-deflection and load-curvature relationships were established for a pretensioned beam assuming a cylinder strength,  $f'_c = 5600$  p.s.i. When variations in the concrete strength were appreciable, values were also calculated for the individual test beams. In order to simplify the calculations, or due to a lack of specific information, the following assumptions were made:

(1) The stress-strain relationship of sample #1 in FIGURE 6.2 was assumed to represent the stress-strain relationship of the steel.

(2) The modulus of elasticity of the concrete was assumed to be  $4.0 \times 10^3$  k.s.i.

(3) The stress distribution on the concrete in the beam was assumed to be as shown in FIGURE G-1 (12).

(4) The tensile strength was assumed to be  $f_t = 4 \sqrt{f'_c}$

(5) The modulus of rupture was assumed to be  $f_r = 6 \sqrt{f'_c}$

(6) The ultimate strain of the concrete under the bearing plate was assumed equal to 0.006.

(7) The width of the bearing plate was assumed to be 5 inches at the supports and load points.



(8) Inclined cracks were assumed to initiate 9 inches from the edge of the bearing plates.

(9) Before flexural cracking the concentrated loads and reactions were assumed to act as point loads.

(10) After flexural cracking the loads were assumed to act as two equal point loads located at each edge of the bearing plate (1).

(11) The self-weight of the beam was assumed to act as a concentrated load of 0.30 kips at each midspan.

(12) The prestress in the wires was assumed equal to 125 k.s.i. at all sections.

(13) Moments induced by movement of the support points were assumed equal to zero.

#### (b) FLEXURAL CRACKING

The modulus of rupture was  $f_r = 6 \sqrt{f'_c} = 6 \sqrt{5600} = 450$  p.s.i. and the prestressing force  $F_{se}$  was  $= A_s f_{se} = 125 \times .206 = 25.8$  kips. The flexural cracking moments were calculated and the cracking envelope shown in FIGURE G-2 was plotted. For example at midspan

$$M_{cr} = S \left( f_r + \frac{F_{se}}{A} \pm \frac{F_{se}}{S} \cdot e \right) \quad \text{Eq. (1)}$$

$$M_c = 144 \left( .450 + \frac{25.8}{72} \pm \frac{25.8 \times 3.0}{144} \right)$$

$$= 144 (.450 + .358 \pm .537)$$

$$= 194 \text{ inch kips, or } 39 \text{ inch kips}$$



The bending moment diagram at flexural cracking over the centre support is indicated by line A in FIGURE G-2. The cracking load was calculated from the bending moment diagram in FIGURE G-3(c) as follows:

$$\frac{3}{16} P_t L = M$$

$$P_t = \frac{194}{\frac{3}{16} \times 120} = 8.6 \text{ kips} \quad \text{and}$$

$$P = P_t - P_1 = 8.6 - 0.3 = 8.3 \text{ kips}$$

Similarly the bending moment diagram when flexural cracking occurred at midspan is indicated by line B in FIGURE G-2. The corresponding bending moment diagram is shown in FIGURE G-3(c) and

$$\frac{1}{6} P_t L = M$$

$$P_t = \frac{194}{\frac{1}{6} \times 120} = 9.7 \text{ kips} \quad \text{and}$$

$$P = 9.4 \text{ kips}$$

As the cylinder strengths of the concrete in the beams varied considerably, the flexural cracking loads for the individual beams were calculated and are presented in TABLE VII-1.

### (c) INCLINED CRACKING

The flexural-shear cracking value and web-shear cracking value were computed as follows:

- (1) Web-shear cracking a distance  $h/2 = 6"$  from the edge of the bearing plate at the centre support and the load point equals



$$V_s = \frac{Ib'}{Q} f_t \sqrt{\left(1 + \frac{F_{se}}{A f_t}\right)} A_{sd} f_{se} \sin \beta \quad \text{Eq. (4)}$$

$$V_s = \frac{765 \times 3.5}{87.8} \times .300 \sqrt{1 + \frac{25.8}{52.6 \times .300}} + 25.8 \times .125$$

$$V_s = 15.1 + 3.2 = 18.3 \text{ kips}$$

(2) Flexural-shear cracking 9" from the centre support and 9" from the load point towards the centre support.

$$V_f = \frac{S}{a - d} \left( f_r + \frac{F_{se}}{A} + \frac{F_{se} e}{S} \right) \quad \text{Eq. (5)}$$

$$V_f = \frac{125.5}{27.5 - 9} \left( .450 + \frac{25.8}{52.6} + \frac{25.8 \times 2.31}{127.5} \right)$$

$$V_f = 9.5 \text{ kips}$$

(c) Flexural-shear cracking 9" from the load point toward the end reaction.

$$V_f = \frac{127.5}{57.5 - 9} \left( .450 + \frac{25.8}{52.6} + \frac{25.8 \times 2.73}{127.5} \right) \quad \text{Eq. (5)}$$

$$V_f = 3.9 \text{ kips}$$

Hawkins (1) suggests the following relationship between  $V_c$ ,  $V_s$ , and  $V_f$

$$\frac{V_c}{V_s} = 1 - \frac{3}{4} \left( \frac{V_s - V_f}{V_s} \right) - \frac{1}{4} \left( \frac{V_s - V_f}{V_s} \right)^2 \quad \text{Eq. (11)}$$





From calculations of the above formula it was found that:

(1) At sections beside the centre support and beside the load point toward the centre support  $V_c = 10.8$  kips which corresponds to a load  $P = 16.2$  kips and

(2) At sections beside the load point toward the end reaction  $V_c = 5.2$  kips which corresponds to a load  $P = 15.3$  kips. For simplicity the load which produced inclined cracks at both sides of all points of maximum moment was taken as  $P = 16.2$  kips. The bending moment diagram corresponding to this load is shown in FIGURE G-2 by line C.

Similar calculations using the dimensions of the post-tensioned beams yielded

$$V_s = 16.1 \text{ kips}$$

$$V_f = 10.2 \text{ kips}$$

$$V_c = 11.0 \text{ kips}$$

$$P = 16.5 \text{ kips}$$

#### (d) ULTIMATE SHEAR-COMPRESSION FAILURE MOMENT

The method, outlined in Section 2.3 was used to compute the ultimate moment due to a shear compression failure. As this is a trial and error method only the final trial is shown as follows:

$$(1) \text{ Assume } k_u d = 1.81''$$

$$(2) \text{ Equating the horizontal forces}$$

$$f_{su} = \frac{A_c f_{cu}}{A_s} = \frac{1.81 \times 6 \times 4.38}{.208} = 227 \text{ k.s.i.}$$



- (3) From the stress-strain relationship of the reinforcement

$$\epsilon_{su} = 0.0133$$

$$\begin{aligned} (4) \quad \epsilon_{sa} &= \epsilon_{sa} - \epsilon_{se} = 0.0133 - 0.0045 \\ &= 0.0088 \end{aligned}$$

$$(5) \quad M_u = f_{su} A_s (d - k_2 k_u d)$$

$$M_u = 227 \times 0.206 (9 - .42 \times 1.81)$$

$$M_u = 387 \text{ inch kips}$$

- (6) At the initiating flexural crack

$$kd = k_u d - \frac{x}{ak_2} (d - k_2 k_u d) - \frac{x \tan \beta}{k_2} \quad \text{Eq. (9)}$$

$$kd = 1.81 - \frac{9}{27.5 \times 0.42} (8.24) - \frac{9 \times .06}{.42}$$

$$kd = 8.03 \text{ inches}$$

- (7) Referring to the simplified curvature distribution

(FIGURE 1.3(c)) and assuming the width of the bearing plate to be five inches and  $x_h = 9''$ .

$$\int \frac{\epsilon_{ca}}{(kd)_x} dx = \frac{\epsilon_{cu}}{k_u d} \times 13'' = \frac{0.006}{1.81} \times 13 = 0.0431$$

Referring to the curvature distribution in FIGURE 1.3(d)

$$\begin{aligned} \int \frac{\epsilon_{sa}}{(d - kd)} dx &= \frac{\epsilon_{sa} \times 5''}{(d - k_u d)} + \frac{\epsilon_{sa} \times 18''}{1/2 (d - kd) + (d - k_u d)} \\ &= \frac{\epsilon_{sa} \times 5}{7.79} + \frac{\epsilon_{sa} \times 18}{1/2 (0.93 + 7.79)} = 4.87 \epsilon_{sa} \end{aligned}$$



Equating the two quantities

$$\epsilon_{sa} = \frac{0.0431}{4.87} = 0.00885 \quad \text{Eq. (10)}$$

which compared favorably with the assumed value

$$\epsilon_{sa} = 0.0088$$

The moment diagram for this condition is indicated in FIGURE G-2 by line D. This moment diagram corresponds to an applied load  $P = 20.8$  kips.

#### (e) ULTIMATE FLEXURAL MOMENT

A method proposed by Warwaruk (12) was used to compute the steel stress. The stress compatibility factor  $F$  was assumed to be 0.75 and therefore  $F\epsilon_u$  was equal to  $0.75 \times 0.006 = 0.0045$ . As this was a trial and error method the last trial is shown below:

$$(1) \text{ Assume } f_{su} = 234 \text{ k.s.i.}$$

$$(2) \epsilon_{su} = \epsilon_{se} + \epsilon_{ce} + F\epsilon_u \left( \frac{f_{cu}}{0.00386 \times 230} - 1 \right)$$

$$\begin{aligned} \epsilon_{su} &= 0.0045 + 0.00018 + 0.0045 \left( \frac{4.38}{0.00386 \times 234} - 1 \right) \\ &= 0.02208 \end{aligned}$$

(3) From the stress-strain relationship of the steel at a strain of 0.02208,  $f_s = 235$  k.s.i. which agreed favorably with the assumed value  $f_{su} = 234$  k.s.i.

The depth to the neutral axis was computed by equating the horizontal forces thus

$$k_u d = \frac{A_s f_{su}}{f_{ca} b} = \frac{.206 \times 234}{4.38 \times 6} = 1.85 \text{ inches}$$





The ultimate flexural moment was computed as

$$\begin{aligned} M_u &= A_s f_{su} (d - k_2 k_u d) \\ &= .206 \times 234 (9 - 0.43 \times 1.85) \\ &= 400 \text{ inch kips} \end{aligned}$$

The moment corresponds to an applied load  $P = 21.5$  kips.

#### (f) STRAIN RELATIONSHIPS

The increase in strain in the concrete was first computed at flexural cracking and at ultimate flexural moment as follows. The cracking moment was computed in section G(b) and found to be 194 inch kips. The small tensile stresses existing at transfer were neglected and the increase in strains in the concrete immediately before cracking were

$$\epsilon_c = \frac{M_{cr}}{E_c I} = \frac{194}{4.4 \times 10^3 \times 144} = .000306$$

Similarly the increase in steel strain was computed as

$$\epsilon_{sa} = \frac{M_{cr} y_s}{E_c I} = \frac{194 \times 3}{4.0 \times 10^3 \times 864} = 0.000168$$

At ultimate flexural moment, the concrete strain is equal to  $\epsilon_{cu} = 0.006$ . The increase in strain was obtained from values previously computed in section G(c) thus

$$\epsilon_{sa} = \epsilon_{su} - \epsilon_{se} = 0.02208 - 0.00450 = 0.01758$$



The above values were plotted in FIGURE G-4 and were joined by the broken line.

The values for the increase in strains at inclined cracking ( $M = 303$  inch kips) were computed using a trial and error system and the strain relationships established for the section loaded in pure flexure (broken line in FIGURE G-4. The final trial was:

$$(1) \text{ Assume } \epsilon_{ca} = 0.0014$$

$$(2) \text{ From FIGURE G-4}$$

$$\epsilon_{sa} = 0.0034$$

$$(3) \epsilon_s = \epsilon_{sa} + \epsilon_{se} = 0.0034 + 0.0045 = 0.0079$$

$$(4) \text{ From the stress-strain relationship of the steel}$$

$$f_{se} = 183 \text{ k.s.i.}$$

$$(5) T = f_s A_s = 183 \times 0.206 = 38.1 \text{ kips.}$$

(6) From FIGURE G-1 for a concrete strain of 0.0014,  $f_{ca} = 2200$  p.s.i. and  $k_2 = 0.333$ . Equating the horizontal forces at the section gave:

$$kd = \frac{T}{f_{cu} b} = \frac{38.1}{2.2 \times 6} = 2.87 \text{ inches}$$

$$(7) M = T(d - k_2 kd)$$

$$M = 38.1 (9 - .333 \times 2.87) = 307 \text{ inch kips}$$

which compares favourably with the moment at inclined cracking of 303



inch kips initially assumed. The increase in strains at inclined cracking was therefore  $\epsilon_c = 0.0014$  and  $\epsilon_{sa} = 0.0034$ . These values were plotted in FIGURE G-4.

The strains at shear compression failure were obtained directly from computations made in section (d) and were  $\epsilon_{ca} = \epsilon_{cu} = 0.006$  and  $\epsilon_{sa} = 0.0088$ . These values were plotted in FIGURE G-4. A bold line was drawn joining the increase in strains at flexural cracking, inclined cracking, and shear-compression failure in FIGURE G-4. This line represents the predicted increase in strain relationships for the concrete beams of this investigation.

(g) MOMENT CURVATURE RELATIONSHIPS AT A MAXIMUM MOMENT SECTION

At flexural cracking the curvature computed by elastic methods is:

$$\phi_{cr} = \frac{M_{cr}}{E_c I} = \frac{194}{4,0 \times 10^3 \times 765} = 0.0000635 \text{ radians per inch.}$$

After flexural cracking, the curvature was computed as

$$\phi_{cr} = \frac{\epsilon_c}{kd}$$

The values  $\epsilon_c$  and  $kd$  were obtained directly from previous calculations. Hence at inclined cracking:

$$\phi = \frac{0.0014}{2.87} = 0.00048 \text{ radians per inch}$$

and at failure

$$\phi = \frac{0.006}{1.81} = 0.0033 \text{ radians per inch}$$



One intermediate value was also computed as follows:

(1) Assume an increase in concrete strain,  $\epsilon_c = 0.003$

(2) From FIGURE G.4

$$\epsilon_{sa} = 0.0052$$

(3)  $\epsilon_s = \epsilon_{sa} + \epsilon_{se} = 0.0052 + 0.0045$

$$\epsilon_s = 0.0097$$

(4) From the stress-strain relationship of the steel

$$f_s = 200 \text{ k.s.i.}$$

(5)  $T = A_s f_s = 200 \times 0.206 = 41.2 \text{ kips}$

(6) Equating the horizontal forces gave:

$$kd = \frac{T}{f_{ca} \times b} = \frac{41.2}{3.6 \times 6} = 1.94 \text{ inches}$$

(7)  $M = T(d - k_2 kd)$

$$= 41.6 (9 - .39 \times 1.94) = 342 \text{ inch kips.}$$

(8)  $\phi = \frac{\epsilon_c}{kd} = \frac{0.003}{1.94} = 0.00155 \text{ radians per inch}$

The above values were plotted in FIGURE G-5. The load-curvature relationships were obtained using the moment-curvature relationships shown in FIGURE G-5 and the moment-load relationships shown in FIGURE G-5. These curves were reproduced on the measured load-curvature relationships which are in Chapter 7.



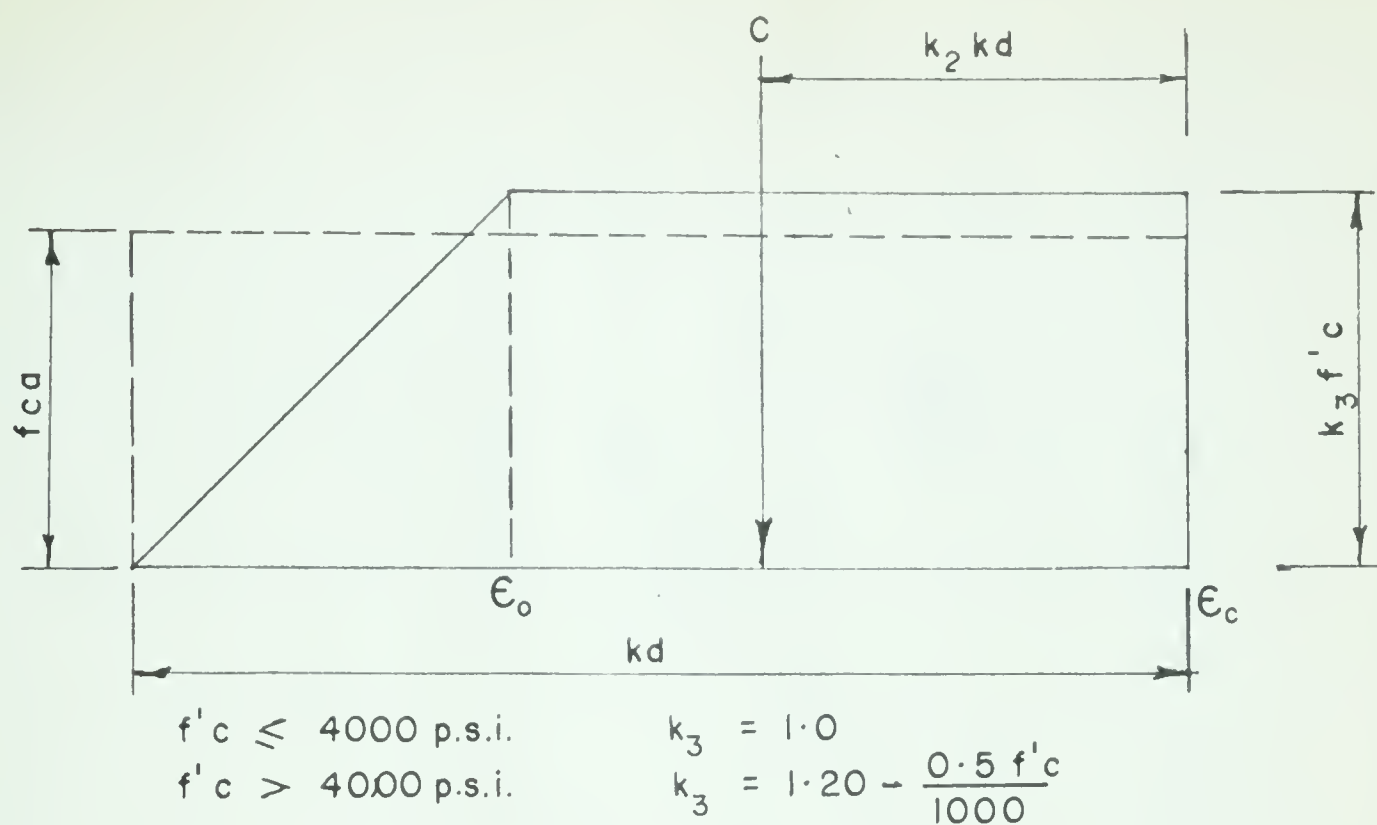


#### (h) LOAD-DEFLECTION RELATIONSHIPS

The curvature distributions shown in FIGURE G were used to compute the load-deflection relationships. In FIGURE G-6 line A represents the curvature at the first flexural crack, and is proportional to the elastic bending moment diagram. Line B is the curvature distribution at the formation of a flexural crack under the load point. This is proportional to the plastic bending moment diagram except for a concentration of curvature over the centre support. Line C and D represent the curvature at inclined cracking and ultimate load respectively. The curvatures between the load point and reactions were assumed negligible.

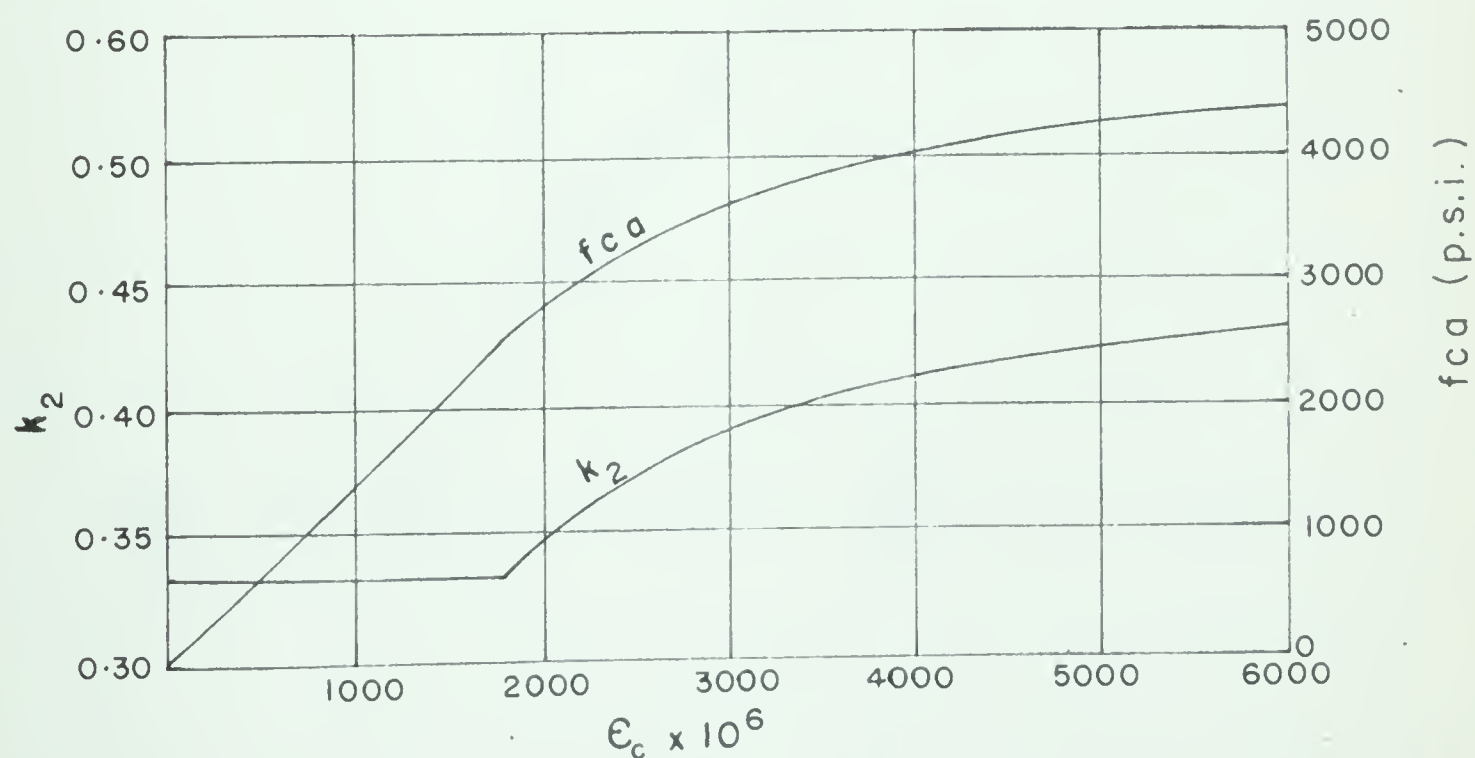
The load-deflection graph (FIGURE G-7) was computed directly from the curvature distribution diagrams. However the amount of curvature concentrations that took place over the centre reaction, between first cracking and cracking under the load point, would have been very tedious to compute. Therefore the constant slope of the load deflection curve, from zero load to the formation of the first flexural crack, was assumed to remain constant until flexural cracking occurred under the load point. The load deflection graph in FIGURE G-7 is reproduced on the actual load deflection curves in Chapter 7.





$$\epsilon_0 = \left( \frac{k_3 f'c}{4} + 500 \right) 10^{-6}$$

(b) Idealized stress distribution. (Warwaruk Ref. 12)



(a)  $k_2$  and  $f'ca$  for rectangular section when  $f'c = 5600 \text{ p.s.i.}$

FIG. G-1 IDEALIZED STRESS DISTRIBUTION FOR CONCRETE



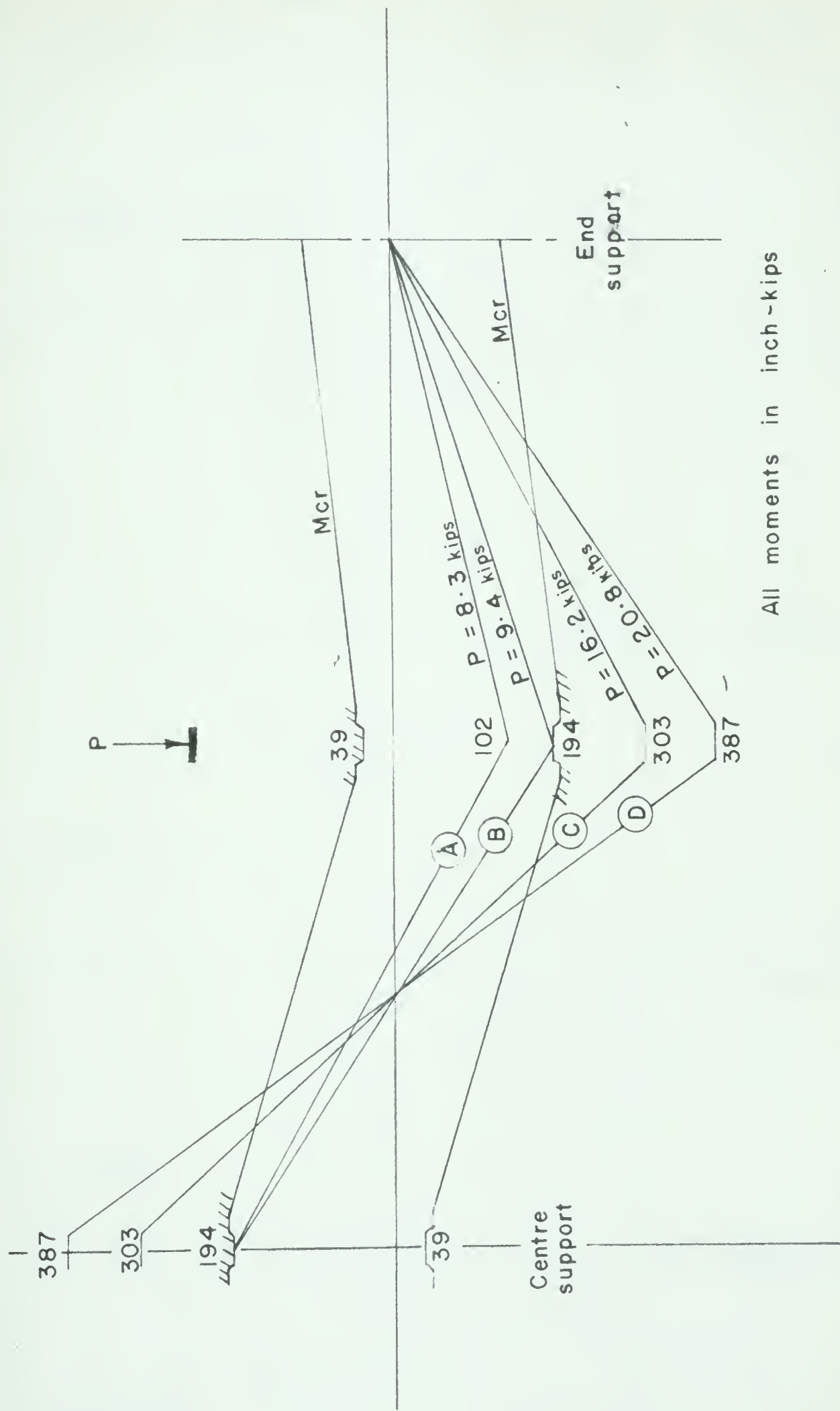


FIG. G-2 CALCULATED BENDING MOMENT DIAGRAMS AT VARIOUS STAGES OF LOADING





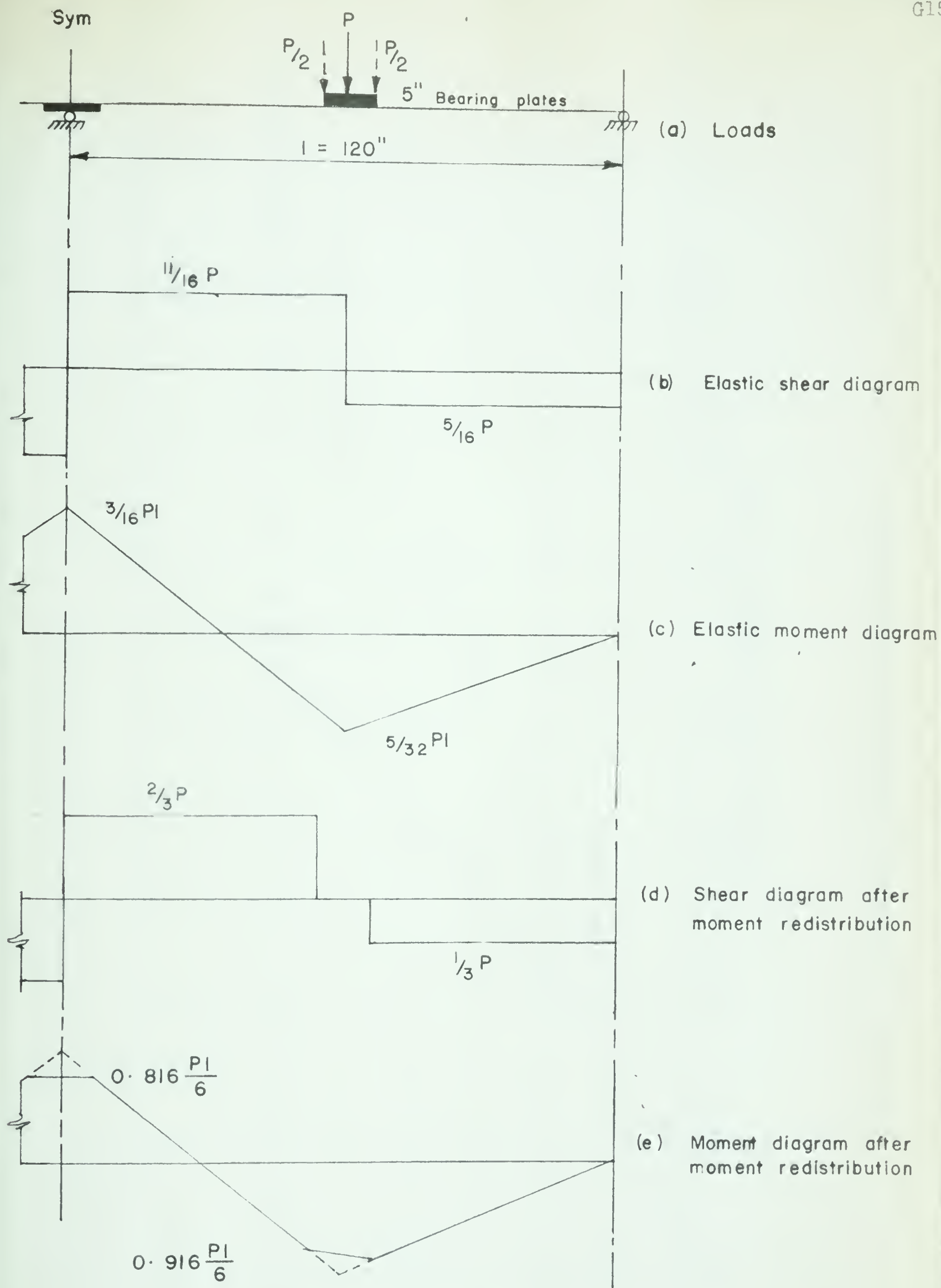


FIG. G-3 BENDING MOMENT AND SHEAR FORCE DIAGRAMS



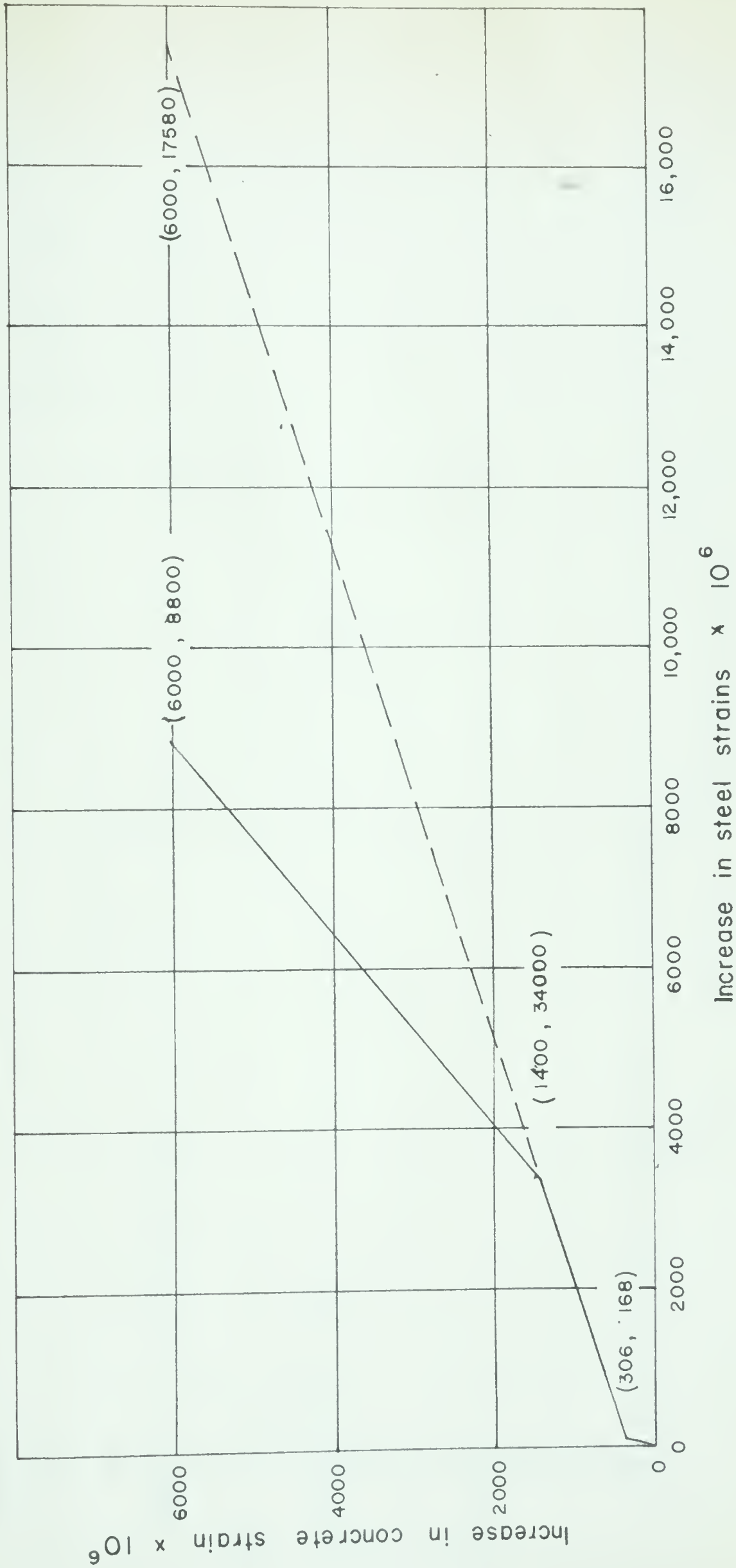


FIG. G-4 · CALCULATED STRAIN RELATIONSHIPS



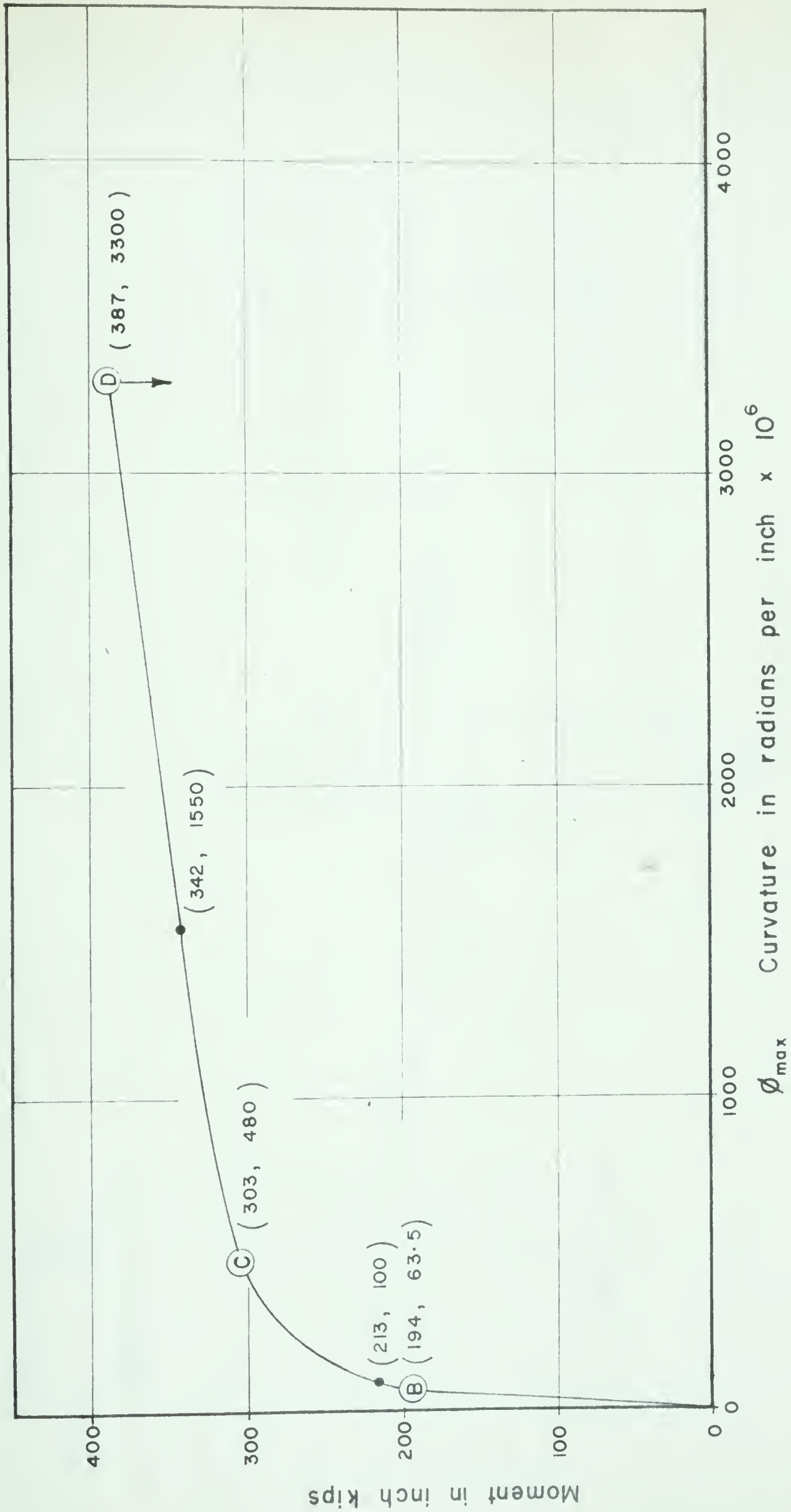


FIG. G-5 CALCULATED MOVEMENT - MAXIMUM CURVATURE RELATIONSHIP.



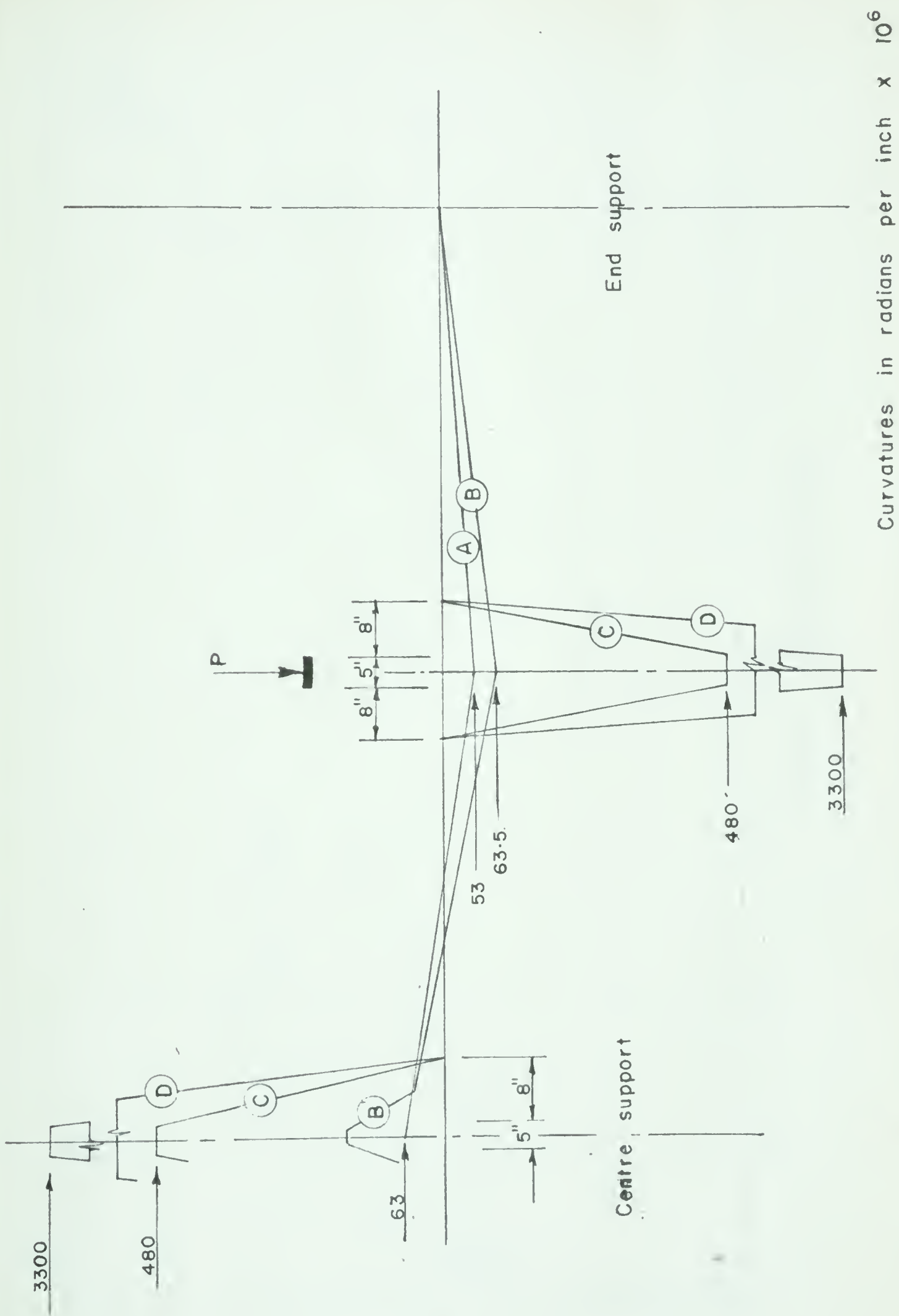


FIG. G-6 CALCULATED CURVATURE DISTRIBUTIONS AT VARIOUS STAGES OF LOADING





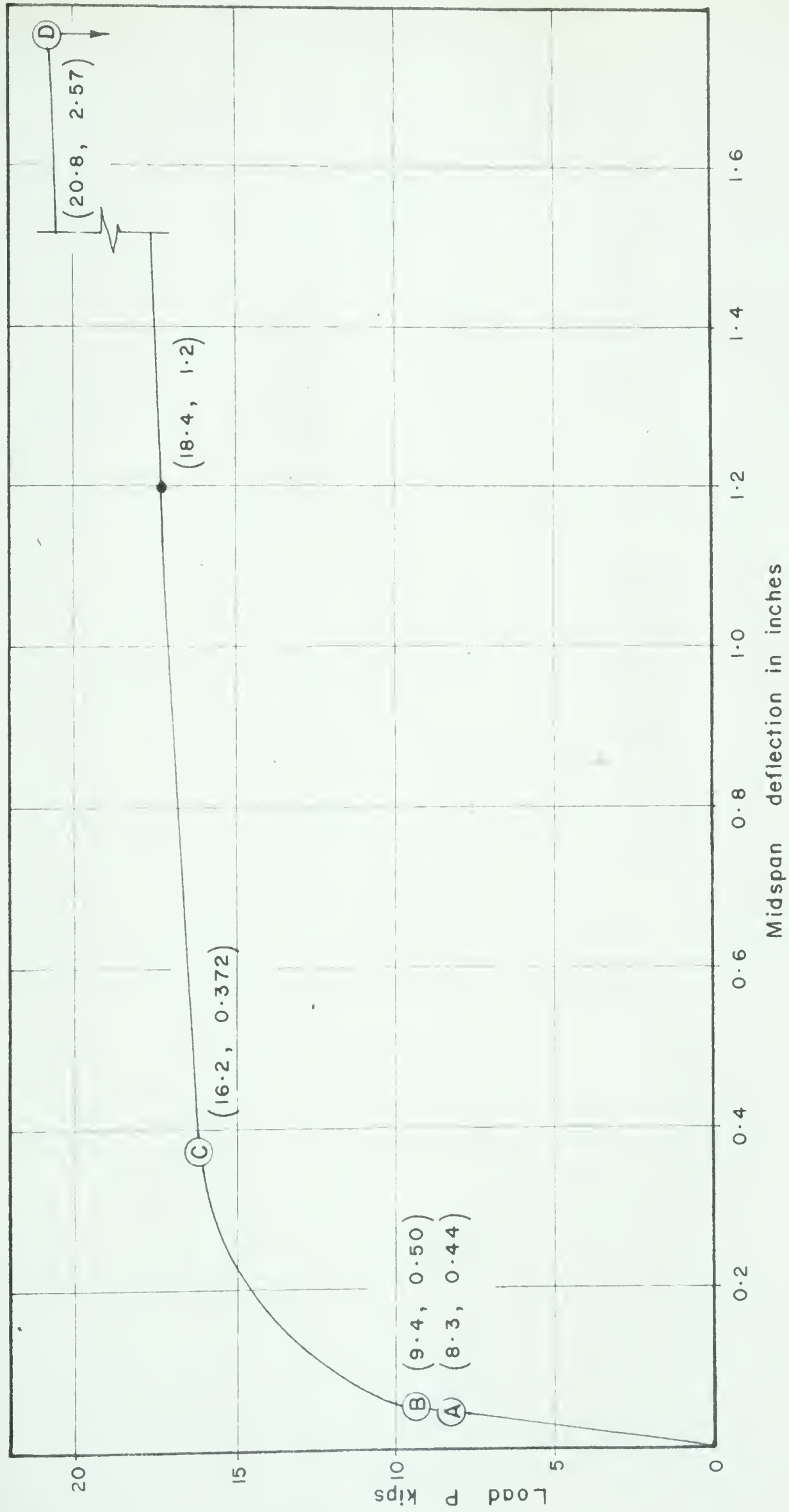


FIG. G-7 CALCULATED LOAD - DEFLECTION RELATIONSHIP







**B29828**